Genetic and Infectious Causes of Microcephaly: *NDE1* Mutations Compared to the Zika Virus

David J. Doobin

Submitted in partial fulfillment of the
requirements for the degree of
Doctor of Philosophy
under the Executive Committee
of the Graduate School of Arts and Sciences

COLUMBIA UNIVERSITY

2017

ABSTRACT

Genetic and Infectious Forms of Microcephaly: *NDE1* Mutations Compared to the Zika Virus

David J. Doobin

Brain development is an exquisitely coordinated process of progenitor cell proliferation followed by the migration of progeny to their final location in the developing brain. There are a myriad of points at which this process can be disturbed, and the examination of these perturbations help us further understand basic science, as well as epidemics sweeping through the world around us. Microcephaly, which is defined as a head circumference greater than 2 standard deviations below the mean, can occur through genetic, infectious, vascular, or metabolic etiologies, and the studies herein examine two forms by which microcephaly occurs. First, we investigate the role of the dynein regulatory protein Nde1 in the development of the neocortex, which is the outer region of the forebrain. *NDE1* mutations are associated with severe microcephaly, and we find that unlike most microcephaly genes whose products have one role in the cell cycle, Nde1 is required at three discrete points in neuronal progenitors, termed radial glia progenitors (RGPs). We initially find that Nde1 is required to recruit dynein to the nuclear envelope to allow for interkinetic nuclear migration (INM) during G2. Additionally, Nde1 helps to initiate primary cilia resorption at the G1-to-S transition. Finally, there is a necessity for Nde1 at the G2-to-M transition after the completion of INM and prior to nuclear envelope breakdown. These three distinct roles for Nde1 illustrate the breadth of functions that the protein has during RGP

proliferation, and help to explain why patients with *NDE1* mutations have such severe microcephaly.

As this work was ongoing there was a global outbreak of a new pathogen that had previously been dormant throughout Africa and Asia, only to emerge at epidemic proportions in the Western Hemisphere. This pathogen, the Zika Virus (ZIKV), is particularly alarming because of its subclinical course in adults but devastating consequences for fetal development, with the hallmark symptom being microcephaly. Using our organotypic brain slice model system, we demonstrate the ability of a variety of ZIKV isolates to infect and replicate in embryonic brain tissue. All ZIKV isolates that infect the organotypic slices lead to increases in apoptosis, though these increases are particularly pronounced in isolates from the Asian/American lineages. Notably, one isolate from a patient in Nigeria (termed 30656) does not replicate in mouse neuronal tissue, but electroporation of the 30656 ZIKV genome allows for a single cycle replication, suggesting that this isolate is unable to enter RGPs. All infectious isolates are pathogenic in early- and mid-gestation embryonic tissue, but only one isolate infects and replicates in late-gestation embryonic tissue. This was the most recently isolated sample tested, and it demonstrates a predilection for neurons, suggesting that ZIKV may be mutating as it spreads. These results provide foundational insight into the pathogenesis of ZIKV-associated microcephaly, and illustrate how studies of genetic forms of microcephaly can enhance and facilitate our understanding of infectious causes of the disease.

Table of Contents

List of Figures

Chapter 1: Introduction: Cytoplasmic Dynein and its Regulators in Neocortical Development and Disease

Chapter 2: Severe *NDE1*-Mediated Microcephaly Results from Neural Progenitor Cell Cycle Arrests at Multiple Specific Stages

Chapter 3: The Pathogenic Potential of Various Isolates of Zika Virus

Chapter 4: How Investigations of Genetic Forms of Micocephaly Can Inform Research on the Zika Virus

Acknowledgements

To the countless people who have helped me along the way, I have nothing but gratitude. To my mentor Richard Vallee, thank you for your patience, your generosity with sharing knowledge and wisdom regarding not just science but the act of performing science, and for creating an environment that fosters us as we better learn how to conduct research. The enduring legacy of the laboratory is a testament to his guidance and the climate that he creates.

To the members of the Vallee lab, who have been some of the greatest colleagues one could ask for. I would like to thank Alex Baffet and Dan Hu for indoctrinating me into the 'brain-trust' experimental group in lab and initially teaching me how to design experiments, Aurelie Carabalona for her ongoing friendship and help as we worked through experiments over the years, and Tiago Dantas for not only helping me with experimental design and execution, but teaching me everything about bringing a project from inception to publication. To Caitlin Wynne, Shahrnaz Kemal, and Sarah Weill, for their friendship and wonderful mentoring, and Shahrnaz in particular for her pioneering work with Nde1 and Ndel1. To Julie Yi, Noopur Khobrekar, Julian Scherer, Jie Zhou, Ana Maria Low-Calle, and Chiara Bertipaglia for the camaraderie and scientific discourse they provided, and to João Goncalves, for being a beacon of positivity as he carries the brain work of the Vallee lab forward. And to Amy Rosenfeld, for helping and guiding me through the turbulent waters of Zika research as the field has germinated and then exploded.

To the various mentors that I have had throughout my education who have guided me to this point: the members of my thesis committee, Franck Polleux,

Hynek Wichterle, and Gregg Gundersen, who have all expanded my ability to present and understand my work. To Mary Beth Hatten, who helped point me in the direction of the MD/PhD degree and guide my education, and Bob Stewart, Janet Alder, and Smita Thakker-Varia, all of whom exposed me to research very early on and taught me about the allure of science. And to all of the people throughout the medical school, the neurobiology graduate program, and my undergraduate training who helped sculpt me into the scientist I am today.

A multitude of thanks goes to my friends in medical school and the MD/PhD program who provided enormous support as we all struggled through these challenges together. I am very blessed to have been among such inspiring and conscientious friends, who pushed me further in the classroom, hospital, and lab. And to all of my friends outside of science, with whom I have grown so much – thank you for providing me with stability, reassurance, and the loyal support to push through my professional life and always know that I have a shoulder to rest on at the end of the day.

To my family, for their support and understanding as I continue to embark on this foreign journey. To my father and stepmother, for their unwavering commitment to my studies, explicit encouragement, and consistently going out of their way to help me through nearly every professional milestone. And to my mother, for although she does not quite understand what I am doing and may still be holding out hope that I can become an accountant, she has provided the base for all that which I am today.

Chapter 1

Introduction: Cytoplasmic Dynein and its Regulators in Neocortical Development and Disease

This chapter is modified from the following book chapter written for publication in

Dyneins: Structure, Biology, and Disease 2 Edition (Elsevier)

CYTOPLASMIC DYNEIN AND ITS REGULATORS IN NEOCORTICAL

DEVELOPMENT AND DISEASE

Authors: David J. Doobin[1,2], Richard B. Vallee[1,2]
1Department of Pathology and Cell Biology, 2Program in Neurobiology and Behavior Columbia University, New York, NY 10032, USA

ABSTRACT:

A hallmark of mammalian evolution is the establishment of the cerebral neocortex, which allows for the extremely complex level of connectivity required for many higher order cognitive functions. Recently cytoplasmic dynein and its regulatory proteins have been found to play a fundamental role in development of the neocortex. Human mutations in genes encoding cytoplasmic dynein or its regulatory factors are associated with a variety of malformations of cortical development such as lissencephaly and microcephaly. This chapter provides an introduction on what is known about the role of cytoplasmic dynein during normal neocortical development, with an emphasis on studies in rodent models. The latter part of the chapter focuses on the neuropathology associated with human mutations in dynein-related genes that result in cortical malformations, as well as genetic-forms of microcephaly beyond genes within the dynein complex.

1.1 – Neocortical Development:

The neocortex is a specialized structure of the mammalian central nervous system made up of six distinct neuronal layers located in the superficial portion of the forebrain (Glasser et al., 2016) (Figure 1.1). Eighty percent of the neurons here are excitatory and project axons to other regions of the neocortex or deep brain structures such as the thalamus, basal ganglia, cerebellum, hindbrain, or nuclei within the spinal cord (Marín and Müller, 2014). Therefore, the neocortex plays a paramount role in coordinating activity of neurons throughout the central nervous system.

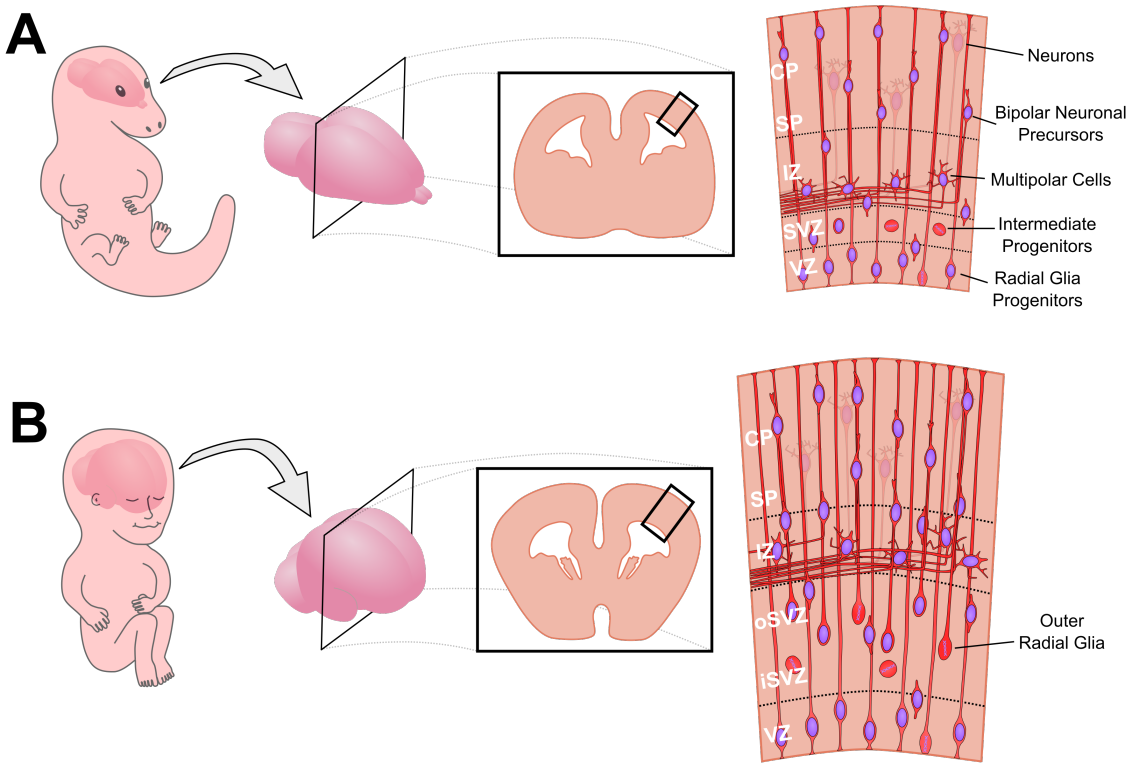

Figure 1.1: Comparison of Rodent and Human Neocortical Development: Schematic illustrating the location of the neocortex within the developing rodent and human embryos. There re are striking differences in the proliferative regions containing radial glia progenitors (RGPs). **(A)** In the rodent neocortex all RGP cell bodies are located within the ventricular zone (VZ), with some transient amplifying cells in the subventricular zone (SVZ). The intermediate zone (IZ) contains horizontally-oriented axons, while the subplate (SP) and cortical plate (CP) represent the expanding neuronal layers in which the bipolar migrating neurons accumulate. **(B)** In the developing human neocortex, the SVZ is greatly expanded into an inner (iSVZ) and outer SVZ (oSVZ). It is here that the cell bodies of the specialized outer radial glia (oRG) are found, which help greatly amplify the number of neurons generated in the primate brain. Otherwise the zones of the developing neocortex are quite similar to those in the rodent neocortex.

Development of the rodent neocortex is quite similar to that of the human neocortex (Figure 1.1), with the most noticeable differences being between the proliferative zones containing the stem cells, leading to the gross differences in the extend and size of convolutions observed in the adult human brain (Lewitus et al., 2013). Development of the neocortex begins during embryogenesis with the formation and closure of the neural tube, which begins as a single layer of pseudostratified neuroepithelial cells (Paridaen and Huttner, 2014) (Figure 1.2).

These cells are highly elongated, with an apical process that contacts the lumen of the neural tube (eventually the ventricular surface), and a basal process that extends to the extracellular matrix at the outer surface of the neural tube. The neuroepithelial cells exhibit an unusual form of proliferative behavior involving interkinetic nuclear migration (INM), in which the nucleus oscillates between the apical and basal surfaces of the neural tube in a cell cycle-dependent manner (Hu et al., 2013; Noctor et al., 2001; Sauer, 1935). Mitosis occurs at the ventricular surface. During G1 the nucleus moves basally, undergoes S phase at the apex of migration, and migrates apically back toward the ventricular surface during G2 (Figure 1.2). Notably, the neuroepithelial cells enter mitosis only after returning to the ventricular surface (Hu et al., 2013).

The neuroepithelial cells undergo multiple rounds of INM, dividing symmetrically to produce two progenitors, leading to exponential expansion of the progenitor pool. By embryonic day 9 in mice, roughly corresponding to gestation week 6 in humans, the first asymmetric neuroepithelial cell divisions occur (Kriegstein and Alvarez-Buylla, 2009). In this case one of the progeny retains its stem cell potential and its elongated morphology. The other daughter cell retracts its apical and basal processes and migrates as a postmitotic neuronal precursor towards the basal (outer) surface of the neural tube (Kriegstein and Alvarez-Buylla, 2009; Paridaen and Huttner, 2014). The arriving cells establish a transient embryonic structure known as the preplate, which consists of Cajal-Retzius cells which secrete reelin to establish a chemoattractant gradient that guides neuronal

migration, and the earliest neurons of the neocortex which send pioneering axons to target deep subcortical regions (Govek et al., 2011; Marín and Müller, 2014).

Following the period of preplate formation neuroepithelial cells are referred to as radial glia progenitors (RGPs). They retain their connections to the apical and basal surfaces, which become the respective ventricular and pial surfaces of the developing neocortex. The RGP nuclei continue to exhibit INM, though nuclear migration within the cell is now restricted to the ventricular zone (VZ), defined as the portion of the neocortex below the preplate (Kriegstein and Alvarez-Buylla, 2009; Paridaen and Huttner, 2014). As with most zones in embryonic development, the VZ is a transient region of great importance during development, though it disappears in the adult brain. The RGPs have been found to give rise to all of the cells that populate the adult neocortex, with the exception of the microglia, which arise from the bone marrow (Kriegstein and Alvarez-Buylla, 2009) The basal processes of the RGP continue to lengthen throughout embryonic brain development and serve as tracks along which postmitotic neuronal precursors migrate toward their final destinations within the neocortex (Noctor et al., 2001; 2004).

As the RGP cells continue to divide, the orientation of the cleavage plane is thought to play in important role in determining symmetric versus asymmetric division of the RGP. When the cleavage plane is oriented perpendicular to the ventricular surface the RGP division will likely be symmetric, resulting in two RGP cells (Chenn and McConnell, 1995). When the cleavage plane is oriented at an oblique angle to the ventricular surface the RGP division will likely be asymmetric,

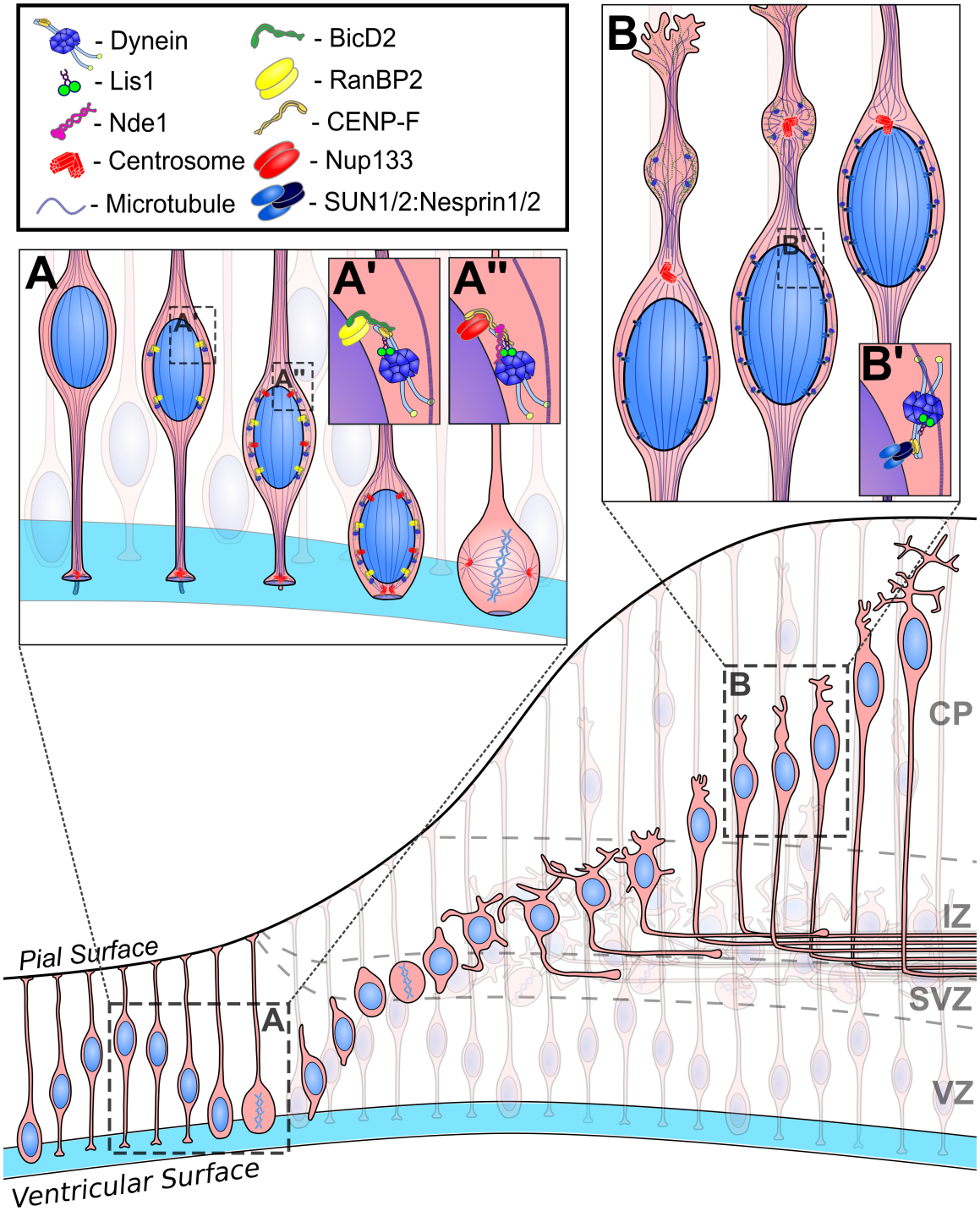

Figure 1.2: Various Roles for the Dynein Complex During Neocortical Development
The neocortex begins as a single layer of neuroepithelial progenitors that eventually divide asymmetrically, creating a postmitotic neuronal precursor and a radial glia progenitor (RGP). The nuclei of neuroepithelial cells and, the RGPs they become, oscillate in synchrony with cell cycle progression, restricting mitosis to the ventricular surface, in a behavior termed interkinetic nuclear migration (INM). The RGP nuclei only undergo INM within the ventricular zone (VZ) of the developing brain. The progeny of asymmetric RGP divisions may divide a couple of times in the subventricular zone (SVZ) as intermediate progenitors, and they then migrate into the (cont'd)

Figure 1.2 (cont'd): intermediate zone (IZ) where they adopt a multipolar morphology. Here they emit a nascent axon, and retract the remaining neurites with the exception of the neurite oriented most basally, which becomes the leading process. These neuronal precursors then migrate along basal radial glia fibers to their final destinations within the cortical plate (CP), which develops into the neocortex. **(A):** During INM there are two separate pathways by which dynein is recruited to the nuclear envelope. The first involves the nucleoporin RanBP2 binding the dynein adaptor BicD2 *(A')*, while the second involves Nup133 recruiting CENP-F to bring in Nde1, which binds dynein *(A'')*. Lis1 is present in both pathways. **(B):** During bipolar migration of the neuronal precursor dynein is required to move the centrosome and nucleus, where the SUN/Nesprin complex is thought to help anchor dynein to the nuclear envelope of the migrating bipolar cell *(B')*.

or neurogenic (Chenn and McConnell, 1995). In the development of the *Drosophila* neuroepithelium the inheritance of apically polarized Notch versus basally polarized Numb is thought to determine why oblique cleavage planes result in asymmetric divisions (Knoblich, 2010), though this mechanism and the fidelity of cleavage plane orientation to cell fate specification is less reliable during mammalian neocortical development (Lancaster and Knoblich, 2012).

After the completion of mitosis and cytokinesis the progeny of asymmetric divisions leave the VZ and migrate towards the outer pial surface of the developing brain (Noctor et al., 2004)(Figure 1.2). There are a number of behaviors these cells can undergo, however, en route. The precursors first pass through the subventricular zone (SVZ), where they can divide further as transient amplifying cells termed intermediate/basal progenitors (but it is unclear if all RGP progeny must pass through an intermediate progenitor stage) (Haubensak et al., 2004). Following these divisions the neuronal precursors continue to migrate outward and enter the intermediate zone (IZ). Here, in the lower IZ, they encounter a dense arrangement of axons oriented orthogonally to the RGP basal fibers (Figure 1.2). The neuronal precursors adopt a multipolar morphology at this point, with several processes extending transiently in all directions, and they remain in this state

anywhere from 24-48hrs (Tabata and Nakajima, 2003). One of the processes outgrows the others and becomes the nascent axon, which then typically extends in the medial or apical direction and grows along the axon tracts established by the earlier arriving neurons (de Anda et al., 2010; Polleux and Snider, 2010). A second polarization event follows as another process thickens to become the leading migratory process (Tsai et al., 2005), and the remaining transient processes retract. All together these changes are referred to as the multipolar-to-bipolar transition.

The migratory process attaches to the basal fibers of the RGPs and helps guide the neuronal precursors as they migrate radially through the IZ and into the developing cortical plate (CP), which will become the neocortex during postnatal development (Figure 1.2) (Rakic, 1972; Vallee et al., 2009). As the CP expands, the six neuronal layers are established in an inside-out manner, with earlier born neuronal precursors populating the deeper layers and later born precursors contributing to the more superficial layers (Noctor et al., 2004). Whole cell migration is sometimes referred to as "locomotion," to contrast with another form of behavior – translocation – in which the migratory process attaches to the pial surface of the brain, and then shortens to bring the nucleus closer to this region (Marín et al., 2010).

As a consequence of radial migration, neurons generated from individual RGPs are arranged in columnar radial units, which preferentially form microcircuits with each other (Gao et al., 2014; He et al., 2015; Rakic, 1988). Additionally, twenty percent of neurons in the neocortex are inhibitory interneurons, which arise from RGPs located on the ventral surface of the rostral lateral ventricle (Harwell et al.,

2015; Mayer et al., 2015). These interneuron precursors must migrate tangentially as they make their way to the neocortex (Polleux et al., 2002), where they then incorporate into the circuitry and provide important modulatory signals.

Neocortical development in higher-order mammals, such as primates and humans, differs from that of rodents most noticeably in the complexity of the proliferative regions (LaMonica et al., 2012; Lewitus et al., 2013). The primate SVZ, which in rodents contains the transit amplifying intermediate progenitors, is greatly expanded and separated into the inner and outer SVZ (Figure 1.1). The outer SVZ was recently found to contain a novel and distinct progenitor cell population known as basal radial glia (also termed outer radial glia [oRGs]) (Fietz et al., 2010; Hansen et al., 2010). oRGs are derived from the horizontal division of RGPs in the VZ (LaMonica et al., 2013a) and retain the capacity to divide symmetrically or asymmetrically, and to create different fates (LaMonica et al., 2013b). The oRGs have a unique morphology, with a basal process connecting to the pial surface, but no apical process. The presence of the oRGs is thought to greatly expand the proliferative capacity of the stem cell population of the developing neocortex, and contribute to increased neuronal production, leading to the complex gyri and sulci found in humans and other primates.

The extent to which oRGs retain the unusual subcellular behavior of RGPs remains to be fully explored. So far it has been observed that oRG nuclei exhibit a form of blebbistatin-inhibited, myosin-driven basal movement termed mitotic somal translocation, which occurs immediately prior to mitosis (Ostrem et al., 2014). The basal processes of the oRGs also contribute as guides for the neuronal precursors as

they migrate through the CP in the later stages of primate neocortical development, though the during early development the basal processes of RGPs in the VZ are still required (Nowakowski et al., 2016).

1.2 – The Role of Dynein in Radial Glia Progenitors and Interkinetic Nuclear Migration

Cytoplasmic dynein is involved in a number of independent basic aspects of neurogenesis and migration during neocortical development. One crucial role for dynein and its regulatory proteins is during interkinetic nuclear migration (INM) in radial glia progenitors (RGPs) (Tsai et al., 2005). Throughout this process the RGP centrosome remains at the apical terminus, within the endfoot of the cell, where it serves as the microtubule-organizing center (Tsai et al., 2010). This creates a highly uniform microtubule network, with microtubule minus ends located at the apical pole of the RGPs, and 93% of plus ends extending up towards the basal process (Tsai et al., 2010). The nucleus is able to utilize this arrangement of microtubules and to recruit microtubule motors at different stages of the cell cycle to drive nuclear migration in the basal and apical directions. During G1 the unconventional kinesin-3 KIF1A was found to be responsible for basal movement of the nucleus (Carabalona et al., 2016; Tsai et al., 2010), and it is not until G2 that dynein is recruited to the nuclear envelope to drive apical INM (Baffet et al., 2015).

We have found that there are two separate and sequential pathways through which dynein is recruited to the nuclear envelope during apical INM (Figure 1.2A) (Hu et al., 2013). The first pathway is anchored by the nucleoporin RanBP2, which recruits the dynein adaptor BicD2 to the nuclear envelope, which in turn recruits

Lis1 and dynein, and likely dynactin as well (Baffet et al., 2015; Hu et al., 2013). Early G2 dynein recruitment is responsible for the initial stage of apical INM, but as the nucleus approaches the ventricle, it is thought that the biophysical forces needed to overcome the increased crowding are greater (Miyata et al., 2014). Therefore more dynein is required at the nuclear envelope to complete apical INM. For this purpose a second pathway of dynein recruitment becomes active, in which the nucleoporin Nup133 binds CENP-F, which is sequestered within the nucleus until late G2 (Baffet et al., 2015; Bolhy et al., 2011; Zuccolo et al., 2007). The nuclear envelope-associated CENP-F then recruits the dynein regulatory proteins of either Nde1 or Ndel1, and Lis1, which are thought to recruit and activate enough dynein at the nuclear envelope to allow the RGP nucleus to complete apical INM, reach the ventricular surface, and enter mitosis (Figure 1.2A) (Hu et al., 2013).

These two pathways for dynein recruitment also function in cultured non-neuronal cells, including HeLa, in which dynein may facilitate nuclear envelope breakdown and initiate mitotic spindle formation, though nuclear-envelope dynein is not required for entry into mitosis (Baffet et al., 2015; Bolhy et al., 2011; Splinter et al., 2012; 2010). In the RGPs, however, dynein recruitment is required for apical INM, and apical INM is, in turn, critical for entry into mitosis at the ventricular surface. This conclusion is supported by *in utero* electroporation of shRNAs directed against several of the dynein recruitment factors (Hu et al., 2013; Tsai et al., 2005). When there is insufficient dynein at the nuclear envelope, the RGP nuclei are blocked from reaching the ventricular surface, leading to a great reduction in the mitotic index and proliferative capacity of the progenitor pool (Baffet et al., 2015;

Hu et al., 2013; Tsai et al., 2005; 2010). When the late pathway of dynein recruitment to the nuclear envelope is interfered with – such as knockdown of *Nup133* or *CENP-F* – overexpression of BicD2 will bring enough dynein to the nuclear envelope of RGPs to allow for the completion of apical INM (Hu et al., 2013).

Because apical INM only occurs during G2, we speculated that recruitment of dynein to the nuclear envelope might depend on a cell cycle kinase. Specifically, the increase in CyclinB levels during G2 results in gradual activation of cyclin-dependent kinase-1 (Cdk1) (Baffet et al., 2015). We found the early G2 pathway of dynein recruitment to be activated by Cdk1 phosphorylation of RanBP2 at 4 sites, which promotes binding of BicD2 and the additional components of the dynein complex (Baffet et al., 2015). This mechanism is conserved in RGPs and HeLa cells (Baffet et al., 2015). Pharmacological inhibition of Cdk1 in HeLa cells blocks CENP-F from ever leaving the nucleus, suggesting a role for Cdk1 in regulating the late-G2 pathway of dynein recruitment (Baffet et al., 2015). In addition to functioning during apical INM, Lis1 has also been shown to contribute to prophase nuclear envelope invagination in RGPs (Hebbar et al., 2008). Finally multiple of these dynein regulatory proteins are also critical for mitotic spindle formation and mitotic progression in RGPs (Feng and Walsh, 2004; Yingling et al., 2008).

A similar pattern of INM has been found in other developing tissues, and has been investigated in detail in the progenitor cells of the developing zebrafish retina, *Drosophila* imaginal discs, and *Cnidarian* pseudostratified ectoderm. In these tissues basal and apical INM have been found to rely heavily on myosin II (Meyer et al., 2011; Norden et al., 2009; Strzyz et al., 2015). Myosin II inhibition was found to

interfere with the basal INM in analysis of cell cohorts in mouse, at least during earlier neocortical development (Schenk et al., 2009). Using live imagine, our lab found no effect of myosin II in INM using blebbistatin and myosin IIb RNAi. Whether the observed differences in motor protein use are tissue, species, or developmental stage dependent is unknown (Tsai et al., 2010). We do note a role for dynactin during INM in zebrafish retinal epithelium, suggesting that the dynein pathway is also active in this system (Del Bene et al., 2008).

1.3 – Roles for the Dynein Pathway in Postmitotic Neuronal Precursors

Following mitosis, neuronal precursors migrate into the IZ, where dynein is required as they assume a multipolar morphology and begin axonogenesis (Figure 1.2) (Noctor et al., 2004). The multipolar-to-bipolar transition is a complex process, dependent on changes in transcription (Ohtaka-Maruyama et al., 2013), centrosome reorientation (de Anda et al., 2010; Sakakibara et al., 2013), proper outgrowth of the nascent axon (Barnes et al., 2007), RhoGTPase activity with actin remodeling (Govek et al., 2011), and N-cadherin exocytosis (Jossin and Cooper, 2011; La Fata et al., 2014). Major cytoskeletal changes must occur, including the retraction of auxiliary neurites and the formation of an enlarged process on the pial-directed side of the multipolar cell, which becomes the leading process (Tsai et al., 2007). Knockdown of dynein or a variety of its accessory proteins, including *Lis1*, *CENP-F*, and *BicD2*, impairs the multipolar-to-bipolar transition (Hu et al., 2013). The underlying mechanism for these effects is unclear, though they suggest a role for dynein in the cytoskeletal rearrangements that accompany this aspect of neuronal morphogenesis.

During the multipolar stage neuronal precursors extend and retract a variety of neurites in a very dynamic manner, one of which later becomes the axon (Tabata and Nakajima, 2003). Axonal growth then occurs and involves both extension and guidance of the axon by the exploratory movements of the growth cone (Lewis et al., 2013). Neuronal precursors can progress through the multipolar-to-bipolar transition even if axonogenesis is blocked (Barnes et al., 2007), though the majority of neuronal precursors extend a defined axon prior to beginning bipolar radial migration (Hatanaka and Yamauchi, 2012; Namba et al., 2014).

Axonogenesis, itself, involves proteins in the dynein pathway as judged by *in vitro* analysis of primary cultured neurons or *in vivo* analysis of the multipolar-to-bipolar transition in neuronal precursors. Dynein, dynactin, and Lis1 all advance into the leading edge of the growth cone, followed by microtubule extension. *Lis1* RNAi in multipolar cells within the IZ causes axons to grow at a slower rate and with more branched terminus than normal, though the axons are still oriented correctly in the IZ (Tsai et al., 2005). Work in cultured dorsal root ganglia and hippocampal neurons suggests that Lis1 and dynein are critical for growth cone remodeling and allowing microtubules to enter into the growth cone (Grabham et al., 2007). Additionally dynein and its regulatory proteins are thought to facilitate microtubule sliding to promote axon outgrowth, by anchoring to stabilized F-actin in the cortex (Baas et al., 2006; Grabham et al., 2007; Prokop, 2013). Dynein- and kinesin-dependent vesicular transport are also critical components of axonal outgrowth and maintenance (Twelvetrees et al., 2016), though these roles for dynein will not be explored at length in this introduction.

Following nascent axon specification and outgrowth, the multipolar cell in the lower IZ must assume a bipolar morphology and migrate towards its final location in the CP. As the leading process forms at the end of the multipolar-to-bipolar transition, there is an accumulation of growing microtubules into the leading process, which may help with its enlargement and stability (Sakakibara et al., 2013). The centrosome must reorient itself from the base of the growing axon to the base of the leading process (Sakakibara et al., 2013). Once the bipolar neuronal precursor forms, it must migrate in the pial direction along the basal processes of RGP fibers. The gap junction proteins connexin 26 and connexin 43 have been reported to be critical for the attachment of neuronal precursors to the radial glia (Elias et al., 2007), just as astrotactin1 is necessary for cerebellar granular cells to migrate along Bergman glial fibers in the cerebellum (Zheng et al., 1996).

During bipolar migration dynein is required at multiple stages of the saltatory migration cycle (Figure 1.2B). First, a swelling forms within the leading process distal to the nucleus and centrosome, which serves as the microtubule-organizing center in bipolar migrating cells. Dynein is enriched in the swelling prior to movement of the centrosome or nucleus (Solecki et al., 2004; 2009; Tsai et al., 2007). The centrosome advances into the swelling, likely a consequence of the anchored dynein in the swelling pulling on the microtubule network to draw the centrosome closer (Tsai et al., 2007). The microtubule array advances with the centrosome, leaving the nucleus surrounded by on ordered array of microtubules. The nucleus then advances by microtubule minus end-directed transport toward the centrosome. This behavior suggests that dynein must also be localized to the

nuclear envelope. Although nuclear envelope dynein has not been visualized as it has during INM (Hu et al., 2013), dynein localization within the entire cell body region of migrating bipolar cells suggests that there is a role for nuclear-envelope anchored dynein (Tsai et al., 2007; Zhang et al., 2009).

Interference with dynein or its regulatory proteins impedes the migration of the bipolar neuronal precursors and offers insight into a further dynein requirement during neocortical development. Strong knockdown of *Lis1* blocks the movement of both the centrosome and nucleus into the leading process, whereas weak knockdown of *Lis1* or dynein heavy chain allow for slower than usual centrosome excursions into the leading process without permitting any apparent nucleokinesis (Tsai et al., 2007).

Similar to RGPs, migrating bipolar cells could in principle employ nuclear envelope anchored dynein to accomplish nucleokinesis. In fact, the SUN domain proteins SUN1 and SUN2, which span the inner nuclear membrane, and the KASH domain proteins Nesprin1 and Nesprin2, which span the outer nuclear membrane, play roles in tethering dynein to the nuclear envelope during neuronal migration (Zhang et al., 2009). SUN1/2 and Nesprin2 are all required for bipolar migration in the neocortex, with Nesprin1 not essential for neuronal migration but functionally complementary to Nesprin2. Colocalization and immunoprecipitation studies have suggested that dynactin participates in the Nesprin complexes during bipolar migration (Zhang et al., 2009), but further work into the dynein regulatory proteins involved in this process is needed.

In contrast to the lack of a role for myosin II in during INM in embryonic rat brain (Tsai et al., 2010), myosin II has been found to contribute to nuclear advance in migrating bipolar neuronal precursors in several studies (Solecki et al., 2009; Tsai et al., 2007; Zhang et al., 2009). The myosin inhibitor blebbistatin impeded nucleokinesis, though centrosome movement into the leading process was unaffected (Tsai et al., 2007). The same effect was observed following *in utero* electroporation of myosin IIb shRNA (Tsai et al., 2007). Thus, the dynein complex plays a critical role in centrosomal advance into the leading process and subsequent nucleokinesis, with myosin II assisting during nucleokinesis. Once the migrating neuronal precursors reach their final destination in the correct layer of the neocortex, the leading process develops many elaborate protrusions and the process of dendrite formation begins (Hand et al., 2005).

1.4 – Overview of Malformations of Cortical Development Associated with Dynein Mutations:

The multiple requirements for the dynein complex during neocortical development illustrate the many opportunities for errors that can potentially impact brain development, and in the past few years there has been a great increase in the identification of human mutations in the dynein heavy chain and dynein regulatory proteins associated with malformations of cortical development (MCD). The clinical classifications for MCDs are quite complex and depend largely on neuroradiological analysis (Barkovich et al., 2012), and a variety of genetic mutations have been associated with each type of MCD (Guerrini and Dobyns, 2014). Here the focus will be given to MCDs caused by mutations in genes encoding dynein and its regulatory

proteins. We give particular attention to mutations in *LIS1* and *DYNC1H1*, encoding dynein heavy chain, that are associated with lissencephaly (smooth brain lacking gyrations) (Reiner et al., 1993; Reiner and Sapir, 2013), polymicrogyria (many smaller gyrations), pachygyria (fewer gyrations overall), and microcephaly (gross reduction in total brain size) (Scoto et al., 2015), and mutations in *NDE1* associated with severe cases of microcephaly (Alkuraya et al., 2011; Bakircioglu et al., 2011). Although many mutations in genes encoding dynein, dynactin, and BicD2 have been associated with neurological disorders such as Charcot-Marie Tooth, Spinal Muscular Atrophy, and Amyotrophic Lateral Sclerosis (Harms et al., 2012; Lipka et al., 2013; Munch et al., 2004; Oates et al., 2013), these diseases are predominantly peripheral neuropathies and likely involve roles for dynein in axonal transport (Hafezparast et al., 2003) and perhaps other neuronal functions.

1.5 – Lissencephaly Associated with *LIS1* Mutations

One of the first pieces of evidence that cytoplasmic dynein might be important during neocortical development came from patients with lissencephaly, an MCD characterized by a smooth brain lacking gyri and sulci (Reiner et al., 1993). The causative gene, *LIS1*, was identified (Reiner et al., 1993), and then shortly thereafter found to be homologous to *Aspergillus NudF,* in the cytoplasmic dynein pathway (Xiang et al., 1995). The severity of lissencephaly varies depending on which gene mutation a patient carries, and there can be variable penetrance among patients with the same genetic alterations (Guerrini et al., 2008; Haverfield et al., 2009). Clinical symptoms are often severe and include intellectual disability, epilepsy, and failure to thrive. On pathological examination the lissencephalic cortex

has an oversimplified pattern of gyri and sulci macroscopically, and a novel four-layered cortex microscopically (very severe forms of lissencephaly only have 2 layers) (Reiner and Sapir, 2013). Mutations in doublecortin (*DCX*; which is involved in the regulation of kinesin KIF1A (Carabalona et al., 2016; Liu et al., 2012)), tubulin A (*TUBA1A*), Reelin (*RLN*), and other genes have been linked to lissencephaly (Guerrini and Dobyns, 2014), though the first discovered and most common genetic causes of lissencephaly are deletions and mutations in *LIS1*.

Human mutations in *LIS1* (also known as *PAFAH1B1* for an additional role as a subunit of platelet activating factor acetylhydrolase (Hattori et al., 1994)) can range from heterozygous deletions of *LIS1* and its adjacent gene *YWHAE*, resulting in the Miller-Dieker form of lissencephaly, or intragenic deletions, duplications, substitutions, or insertions within *LIS1*, resulting in Isolated Lissencephaly Sequence. Rare instances of LIS1 mutations are associated with subcortical band heterotopia, a normal six-layered neocortex with axons below with an ectopic band of neurons closer to the ventricle, and thought of as a MCD on the same pathological spectrum as lissencephaly but with less severe pathological impairments (Haverfield et al., 2009; Pilz et al., 1998; Reiner et al., 1993; Reiner and Sapir, 2013). Given the critical role of Lis1 during neocortical development it becomes apparent how mutations in *LIS1* could contribute to lissencephaly (Bi et al., 2009; Hippenmeyer et al., 2010; Tsai et al., 2005; 2007; 2010). The organization of the four-layered lissencephalic neocortex suggests that the position of the Cajal-Retzius cells is preserved in layer 1, but the other five layers are essentially inverted from the normal neocortical organization and organized into three distinct layers, and

located in a region normally occupied only by axonal tracts (Reiner and Sapir, 2013). This suggests that postmitotic neurons in LIS1-deficient patients migrate into the IZ, but cannot successfully complete bipolar neuronal migration to reach the CP, and they build up in successive layers opposite to the normal inside-out organization of the neocortex (Saito et al., 2011). Patients with *LIS1* mutations often exhibit agenesis of the corpus callosum as well. Although this is a gross defect that can result from many causes, it may reflect the role for LIS1 in proper axon elongation and guidance during corticogenesis (Guerrini et al., 2008). Mouse models have provided evidence that neocortical development is highly sensitive to Lis1 dosage (Bi et al., 2009; Youn et al., 2009), which may explain why the effects of *LIS1* mutations are not more severe, such as resulting in blocked INM leading to microcephaly. We also suspect that this is due to the heterozygous nature of the human mutations, with residual amounts of LIS1 being sufficient for neurogenesis but impeding neuronal migration and cortical lamination.

1.6 – Malformations of Cortical Development Associated with *DYNC1H1* Mutations

Recently mutations in the cytoplasmic dynein 1 heavy chain gene, *DYNC1H1*, have also been implicated in MCDs, with features of polymicrogyria, pachygyria, and microcephaly (Figure 1.3A,C) (Fiorillo et al., 2014; Harms et al., 2012; Hertecant et al., 2016; Poirier et al., 2013; Scoto et al., 2015; Willemsen et al., 2012). Nearly all patients with *DYNC1H1* mutations have microcephaly, though in a much less severe form than microcephalies associated with *NDE1* mutations (see section 12.7 below). Patients with polymicrogyria have multiple gyri that are smaller than normal, and

the mutations in *DYNC1H1* were the first recorded cases of polymicrogyria with pachygyria, which refers to fewer gyri overall (Poirier et al., 2013). These patients can also have agenesis of the corpus callosum and basal ganglia malformations (Poirier et al., 2013). The dynein mutations are in all cases heterozygous *de novo* missense mutations (and one known deletion of 4 amino acids), the majority of which occur in the stalk, linker, or microtubule-binding domains of the protein (Figure 1.3A,C).

The patients with *DYNC1H1* mutations typically present with intellectual disability or attention deficit hyperactivity disorder (ADHD) (Scoto et al., 2015), and a subset of the patients also present with epilepsy (Willemsen et al., 2012). Unlike *LIS1* mutations which predominantly affect the posterior neocortex, *DYNC1H1* mutations tend to affect the anterior neocortex (Guerrini et al., 2008; Scoto et al., 2015). Because dynein is required for the proliferation of RGPs in the VZ, the formation and extension of the axon, and the postmitotic migration of neuronal precursors (Hu et al., 2013; Ori-McKenney and Vallee, 2011; Tsai et al., 2007), it is readily apparent how dynein heavy chain mutations might affect brain development.

DYNC1H1 mutations have classically been associated with peripheral neuropathies, but recent reports introduce clinical cases of *DYNC1H1* mutations leading to peripheral neuropathies and MCDs that were possibly overlooked earlier (Fiorillo et al., 2014; Scoto et al., 2015; Willemsen et al., 2012). Interestingly, MCDs coinciding with peripheral neuropathies are predicted from *Loa* mouse model (Legs at Odd Angles). *Loa* heterozygous mice exhibit clear retrograde axonal transport

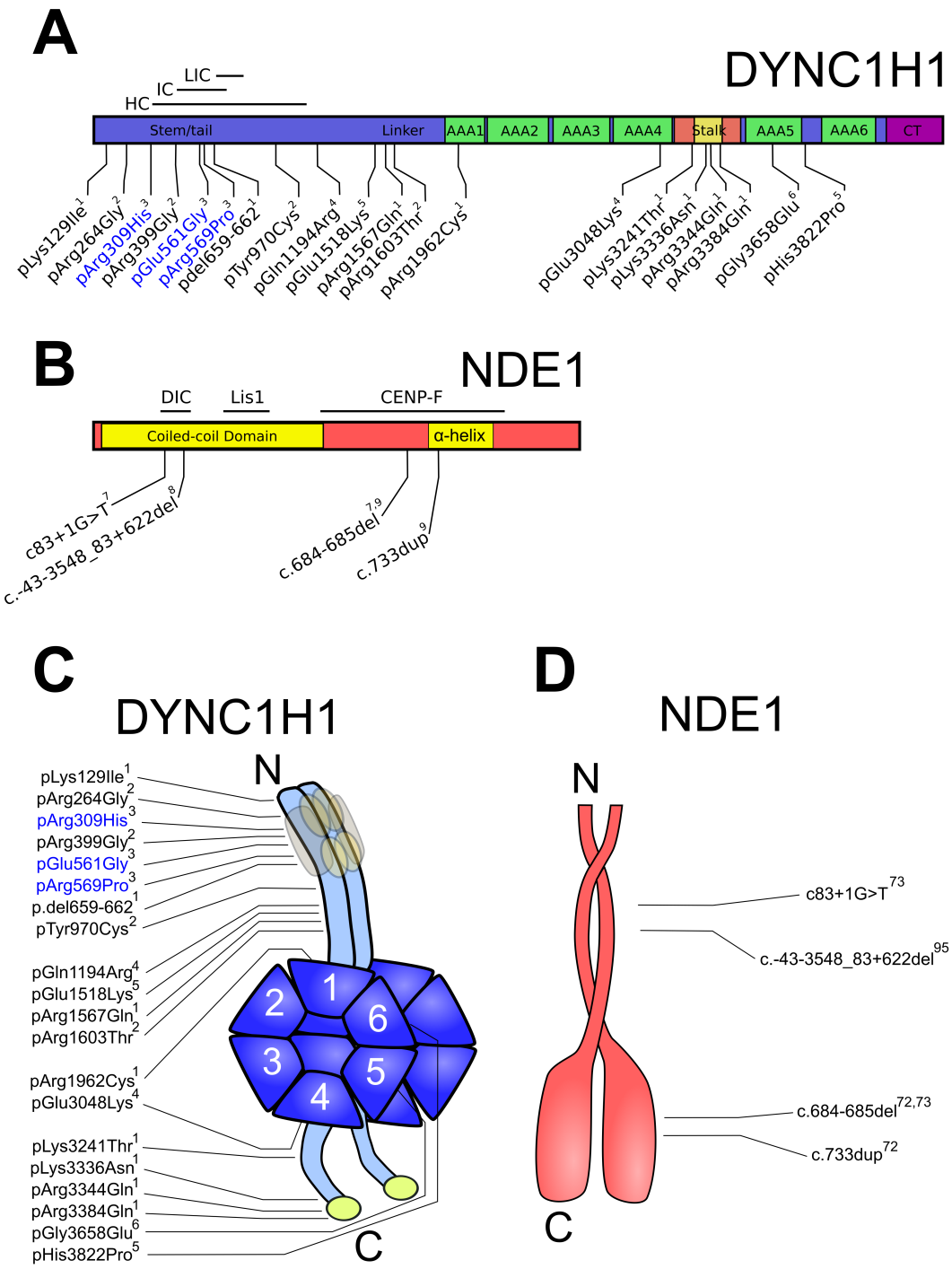

Figure 1.3: Human Mutations in *DYNC1H1* and *NDE1* Associated with Malformations in Cortical Development: Over the past few years there has been a large increase in the number of human mutations associated with malformations of cortical development identified in the *DYNC1H1* and *NDE1* genes. **(A)** Most of the *DYNC1H1* mutations lead to single amino acid substitutions, with the exception of one 4-amino acid deletion, and are denoted by the amino acid changes on the bar diagram. The scale of the diagram is proportional to the amino acid position in the protein. All patients are heterozygous for given mutations. Superscript reflects the reference

of the original studies that uncovered the mutation. Blue text indicates that the mutation was found by deep sequencing to be somatic mosaicism. **(B)** Mutations in *NDE1* associated with microcephaly. Nomenclature is that given to the mutations in the original studies. Scale of diagram is proportional to protein size. Not included is a schematic of Lis1 and the known associated human mutations, in part because of the large volume of documented mutations in *LIS1*, and the complexity of many of these mutations. **(C)** Cartoon schematic of the DYNC1H1 mutation list in (A). **(D)** Cartoon schematic of the NDE1 mutation list in (B). 1) Poirier et al., 2013; 2) Scoto et al., 2015; 3) Jamuar et al., 2014; 4) Fiorillo et al., 2014; 5) Willemsen et al., 2012; 6) Hertecant et al., 2016; 7) Bakircioglu et al., 2011; 8) Guven et al., 2012; 9) Alkuraya et al., 2011.

defects coupled with neurodegeneration (Ori-McKenney et al., 2010), and *Loa* homozygous recessive mice have profound impairments in bipolar neuronal migration and axonal extension (Ori-McKenney and Vallee, 2011).

Symptomatically, patients with *DYNC1H1* mutations leading to MCDs and peripheral neuropathies have mild cognitive impairments with or without ADHD, and provide a functional clinical link between how mutations in *DYNC1H1* can effect neocortical development plus peripheral nerve health (Fiorillo et al., 2014; Scoto et al., 2015; Willemsen et al., 2012). Additionally, an extensive recent study used deep-sequencing technology to investigate MCDs of unknown genetic origins, and found a substantial number of patients that had somatic mutations in genes already known to cause MCDs when mutated in the germline (Jamuar et al., 2014), with *LIS1* and *DYNC1H1* mutations among those found. Thus over the past few years there has been an increasingly apparent role of *DYNC1H1* mutations in causing MCDs, particularly those with atypical neuroradiology (Scoto et al., 2015).

Mutations in *DYNC1H1* and the genes encoding other regulatory proteins, such as BicD2 and dynactin, should remain high on a clinical index of suspicion for undiagnosed cases of MCDs, especially in patients with peripheral neuropathies linked to *BICD2* and *p150* mutations (Munch et al., 2004; Neveling et al., 2013; Oates

et al., 2013). Additionally, the reported substitution mutations on cytoplasmic dynein could offer new insight into the biophysical and biochemical function of the protein with great relevancy to human health.

1.7 – Genetic Forms of Microcephaly Beyond the Dynein Complex

While the above sections clearly implicate how mutations in dynein and its regulatory proteins could lead to MCDs, the vast majority of MCDs of genetic origin result from mutations in genes outside of the dynein complex (Parrini et al., 2016). The focus of this section will be on microcephaly and the validated genetic mutations associated with this MCD. Microcephaly is a neuroanatomical diagnosis of a head circumference equal or greater than 2 standard deviations below the mean (Abuelo, 2007). Since this would encompass roughly 3% of the population, distinctions are often made between the severity of microcephaly, with 2-3 standard deviations below the mean classified as borderline microcephaly, since it encompasses many individuals with normal intelligence who simply have a small head circumference (Thornton and Woods, 2009; Woods, 2004). Of individuals with microcephaly greater than 3 standard deviations below the mean, a retrospective epidemiological study of German hospitals found 41% were of unknown etiology, 29% were genetic in origin, and 27% were due to an environmental insult to the developing fetus, including toxin and infectious agent exposures (Hagen et al., 2014). The distinction is also made between primary microcephaly, which is microcephaly present at birth, and secondary microcephaly, which encompasses microcephaly cases resulting after birth where the head circumference was initially within normal limits (Pulvers et al., 2015).

Many genes have been linked to microcephaly, and nearly all of them are required for proper cell-cycle and mitotic progression of RGPs (Barkovich et al., 2012; Parrini et al., 2016). The cell cycle involvement of many of these genes is summarized in Figure 1.4. Many of the gene products, including those of *ASPM*, *WDR62*, *CENPJ*, *CDK5RAP2*, and *PCNT*, are localized to the centrosomes and/or mitotic spindle poles during mitoses (Bond et al., 2002; 2005; Désir et al., 2008; Fish et al., 2006; Griffith et al., 2008; Nicholas et al., 2010). Abnormal spindle-like microcephaly protein (ASPM, the product of the *ASPM* gene), is the most commonly mutated gene underlying autosomal recessive primary microcephaly cases. A thorough analysis of the role of Aspm in mouse models has implicated the protein in mitotic spindle alignment, with defects in Aspm leading to an increase in oblique cleavage planes (Fish et al., 2006). As discussed above, an increase in oblique cleavage planes will favor neurogenic divisions and presumably lead to a depletion of the RGP stem cell pool before adequate divisions have occurred. This increase in oblique cleavage and premature depletion of the RGP pool was seen after Aspm knockdown (Fish et al., 2006). This premature depletion of the RGP stem cell pool is thought to lead to an overall reduction in brain volume, which is one of the prevailing notions for how mutations in proteins associated with the mitotic spindle pole may lead to microcephaly. Recent work has also found that Aspm interacts directly with Wdr62 to localize other microcephaly-associated proteins, including CENPJ, CPAP, and Sas4 to the centrosome to help prevent RGP delamination from the ventricular surface (Jayaraman et al., 2016).

Gene	Additional MCDs Present	Cell Cycle Phase				Reference
		G1	DNA Repair	G2	Mitosis	
ASPM	-				X	Fish et al., 2006
WDR62	PMG				X	Nicholas et al., 2010
CENPJ	-				X	Bond et al., 2005
CDK5RAP2	PNH				X	Bond et al., 2005
MCPH1	PNH		X	x	X	Pulvers et al., 2015
PCNT	-		X	x		Griffith et al., 2008
ATR	-		X	x		Griffith et al., 2008
CEP152	-		X			Kalay et al., 2011
STIL	SGP				X	Castiel et al., 2011
PNKP	Pachy		X			Shen et al., 2010
ORC1	-		X			Bicknell et al., 2011
ORC6	-		X			Bicknell et al., 2011
CDT1	-		X			Bicknell et al., 2011
CDC6	-		X			Bicknell et al., 2011
NCAPD2	-				X	Martin et al., 2016
NCAPH	-				X	Martin et al., 2016
NCAPD3	-				X	Martin et al., 2016
TUBG	Pachy	-	-	-	-	Poirier et al., 2013
TUBA1A	PMG	-	-	-	-	Parrini et al., 2016
TUBA8	PMG	-	-	-	-	Parrini et al., 2016
TUBB3	PMG	-	-	-	-	Parrini et al., 2016
TUBB	PMG	-	-	-	-	Parrini et al., 2016

Figure 1.4: The Cell Cycle Phase Requirements for Various Microcephaly Genes: A list of primary microcephaly genes and the cell cycle stage that they are required for. Uppercase 'X' is major involvement, lowercase 'x' is minor involvement. Abbreviations for other malformations of cortical development (MCD) occurring: PMG: polymicrogyria, PNH: periventricular nodular heterotopia, Pachy: pachygyria. Figure modified from Barkovich et al., 2012.

Alternatively, a second class of genes that are associated with DNA damage repair, including *MCPH1*, *ATR*, *PCNT*, *CEP152*, *STIL*, *PNKP, ORC1, ORC6, CDT1*, and *CDC6* have been linked to primary microcephaly (Alderton et al., 2006; Bicknell et al., 2011; Castiel et al., 2011; Griffith et al., 2008; Kalay et al., 2011; Pulvers et al., 2015; Shen et al., 2010). Many of the individuals with mutation in these genes are

diagnosed with the Seckel-syndrome, which includes intrauterine growth retardation and craniofacial abnormalities with prominent primary microcephaly (Griffith et al., 2008; Kalay et al., 2011). The protein products of these genes, including ATR, MCPH1, and PCNT all interact with the Chk1 pathway, which is responsible for assessing DNA damage and preventing mitotic entry (Alderton et al., 2006; Griffith et al., 2008). ATR, for example, is responsible for phosphorylating Chk1 in response to UV induced DNA damage, and phosphorylated Chk1 then inhibits Cdc25, which prevents CyclinB/Cdk1 activation (Griffith et al., 2008). Therefore, mutations in *ATR* are thought to lead to microcephaly through inadequate DNA repair, which presumably leads to increased apoptosis later during development.

New microcephaly-associated genes are being uncovered that do not cleanly fit into the above two categories. Genes involved in chromatin condensation, such as *PHC1* (Awad et al., 2013 in Pulvers et al., 2015) and those encoding the condensin complex proteins such as *NCAPD2*, *NCAPH*, and *NCAPD3* (Martin et al., 2016) all have been linked to microcephaly when mutated in human patients. Similarly, mutations in multiple different tubulins are been found in patients with microcephaly (Parrini et al., 2016; Poirier et al., 2013). Given the heterogenous roles and requirements for tubulins during neocortical development (Chakraborti et al., 2016), the resulting microcephaly cases could result from impairments in a variety of stages of neocortical development, similar to microcephaly resulting from *DYNC1H1* mutations. Another microcephaly gene, *NDE1* (which is discussed at great length in the next section and subsequent chapter), illustrates how the gene products of these

microcephaly genes may be involved at multiple discrete steps of neurogenesis and neocortical development. Thus, impairments genes with multiple discrete roles during corticogenesis can result in particularly devastating forms of microcephaly, often with other MCDs superimposed on the microcephaly.

1.8 – *NDE1* Mutations and the Pathogenesis of Severe Microcephaly

Though *DYNC1H1* mutations are associated with microcephaly, another dynein regulatory protein has recently been found to be associated with some of the most severe genetic forms of this condition encountered clinically. Mutations in *NDE1* have been associated with multiple unrelated cases of severe microcephaly, often accompanied by lissencephaly (Alkuraya et al., 2011; Bakircioglu et al., 2011), fetal brain disruption (collapsed skull with prominent scalp rugae) (Paciorkowski et al., 2013), or hydranencephaly (gross underdevelopment of the neocortex accompanied by prominent expansion of the ventricles) (Guven et al., 2012). The lissencephaly in these patients can be so severe that only the Sylvian fissure – one of the most prominent and conserved neuroanatomical structures – remains. The mutations in *NDE1* involve premature terminations (Alkuraya et al., 2011; Bakircioglu et al., 2011), or deletions of entire chromosomal regions containing the *NDE1*-locus (Paciorkowski et al., 2013). All patients have homozygous recessive mutations (Figure 1.3B,D).

NDE1-associated microcephaly patients all exhibit extreme microcephaly, with reductions in neocortical size more severe than other genetic forms of microcephaly, such as those associated with mutations in *ASPM* or *WDR62* (Bond et al., 2002; Nicholas et al., 2010). Ventriculomegaly, which is the abnormal expansion

of the ventricular space, is also seen in all patients with *NDE1* mutations. Some patients with *NDE1*-mediated microcephaly experience seizures, whereas others have such drastic underdevelopment of neuroanatomical structures that no epilepsy occurs (Alkuraya et al., 2011; Bakircioglu et al., 2011; Guven et al., 2012; Paciorkowski et al., 2013). All patients have severe cognitive impairment and meet only minimal developmental milestones. Some of the patients develop persistent hypothermia, which suggests brainstem abnormalities, though all other organs develop normally (Paciorkowski et al., 2013), and all patients are immunocompetent.

Nde1 is highly expressed in the developing neocortex in comparison to other embryonic tissue, and its level then drops significantly after birth (Bradshaw et al., 2013). Within the developing neocortex *Nde1* expression is highest in the VZ and SVZ, which helps to explain why aberrations in Nde1 function impair neurogenesis (Feng et al., 2000). *Nde1* knockout mice displayed altered RGP mitotic spindle alignment and reduced cortical thickness – similar to mouse models for microcephaly genes such as *ASPM* and *WDR62* – though they did not recapitulate the severity of the disease seen in human patients (Feng and Walsh, 2004; Houlihan and Feng, 2014). Conditional knockout of the *Nde1* paralogue *Ndel1* resulted in neuronal migration defects with no impairments in RGP proliferation (Youn et al., 2009). There have been no recorded cases of human mutations in *NDEL1* leading to MCDs, likely because all *NDE1* mutations are penetrant only when homozygous recessive, and *Ndel1* knock out mice are embryonic lethal at the peri-implantation stage, implying that any patients with *NDEL1* mutations may die during early

embryonic development (Sasaki et al., 2005). It was not until recently that acute knockdown of both *Nde1* and *Ndel1* in the developing rodent brain revealed the cellular mechanisms by which these severe cases of microlissencephaly may occur, which is discussed at length in Chapter 2 (Doobin et al., 2016).

12.8 – Summary

In conclusion, dynein and its regulatory proteins are critical for a variety of aspects of neurogenesis and neuronal migration during neocortical development. Mutations in these genes lead to a variety of cortical malformations with clinical symptoms ranging from ADHD to crippling seizures and severe intellectual disability. Considerable progress has been made toward understanding the cellular basis for these defects, but many questions remain regarding basic mechanisms, as well as the distinct effects of specific mutations on these processes. For example, mutations in both *DYNC1H1* and *NDE1* cause microcephaly, though *NDE1*-associated microcephaly is far more severe, likely due to homozygous recessive *NDE1* mutations in patients compared to heterozygous substitution mutations in *DYNC1H1* patients. Similarly, all of the patient mutations discussed lead to cortical lamination defects, reflecting the role of the dynein complex in bipolar radial migration.

Our expanding understanding of how adaptor proteins regulate the dynein motor complex and increase its ability to carry cargo along microtubules, coupled with the knowledge of the cell biology underlying neocortical development, should help clinicians and researchers to provide improved diagnoses for patients with brain disorders, and will fuel the research into potential therapeutic options. As the

role of proper neocortical organization becomes apparent for diseases like autism (Reiner et al., 2015), and there becomes a greater appreciation for the role of somatic mutations in causing focal areas of malformed neocortex (Poduri et al., 2013), a greater understanding of the roles of dynein and its regulatory proteins during brain development will be crucial.

REFERENCES

Abuelo, D. (2007). Microcephaly syndromes. Semin Pediatr Neurol *14*, 118–127.

Alderton, G.K., Galbiati, L., Griffith, E., Surinya, K.H., Neitzel, H., Jackson, A.P., Jeggo, P.A., and O'Driscoll, M. (2006). Regulation of mitotic entry by microcephalin and its overlap with ATR signalling. Nature Cell Biology *8*, 725–733.

Alkuraya, F.S., Cai, X., Emery, C., Mochida, G.H., Al-Dosari, M.S., Felie, J.M., Hill, R.S., Barry, B.J., Partlow, J.N., Gascon, G.G., et al. (2011). Human Mutations in NDE1 Cause Extreme Microcephaly with Lissencephaly. The American Journal of Human Genetics *88*, 536–547.

Baas, P.W., Vidya Nadar, C., and Myers, K.A. (2006). Axonal transport of microtubules: the long and short of it. Traffic *7*, 490–498.

Baffet, A.D., Hu, D.J., and Vallee, R.B. (2015). Cdk1 Activates Pre-mitotic Nuclear Envelope Dynein Recruitment and Apical Nuclear Migration in Neural Stem Cells. Developmental Cell *33*, 703–716.

Bakircioglu, M., Carvalho, O.P., Khurshid, M., Cox, J.J., Tuysuz, B., Barak, T., Yilmaz, S., Caglayan, O., Dincer, A., Nicholas, A.K., et al. (2011). The Essential Role of Centrosomal NDE1 in Human Cerebral Cortex Neurogenesis. The American Journal of Human Genetics *88*, 523–535.

Barkovich, A.J., Guerrini, R., Kuzniecky, R.I., Jackson, G.D., and Dobyns, W.B. (2012). A developmental and genetic classification for malformations of cortical development: update 2012. Brain *135*, 1348–1369.

Barnes, A.P., Lilley, B.N., Pan, Y.A., Plummer, L.J., Powell, A.W., Raines, A.N., Sanes, J.R., and Polleux, F. (2007). LKB1 and SAD kinases define a pathway required for the polarization of cortical neurons. Cell *129*, 549–563.

Bi, W., Sapir, T., Shchelochkov, O.A., Zhang, F., Withers, M.A., Hunter, J.V., Levy, T., Shinder, V., Peiffer, D.A., Gunderson, K.L., et al. (2009). Increased LIS1 expression affects human and mouse brain development. Nat Genet *41*, 168–177.

Bicknell, L.S., Bongers, E.M.H.F., Leitch, A., Brown, S., Schoots, J., Harley, M.E., Aftimos, S., Al-Aama, J.Y., Bober, M., Brown, P.A.J., et al. (2011). Mutations in the pre-replication complex cause Meier-Gorlin syndrome. Nat Genet *43*, 356–359.

Bolhy, S., Bouhlel, I., Dultz, E., Nayak, T., Zuccolo, M., Gatti, X., Vallee, R., Ellenberg, J., and Doye, V. (2011). A Nup133-dependent NPC-anchored network tethers centrosomes to the nuclear envelope in prophase. The Journal of Cell Biology *192*, 855–871.

Bond, J., Roberts, E., Mochida, G.H., Hampshire, D.J., Scott, S., Askham, J.M., Springell,

K., Mahadevan, M., Crow, Y.J., Markham, A.F., et al. (2002). ASPM is a major determinant of cerebral cortical size. Nat Genet *32*, 316–320.

Bond, J., Roberts, E., Springell, K., Lizarraga, S.B., Lizarraga, S., Scott, S., Higgins, J., Hampshire, D.J., Morrison, E.E., Leal, G.F., et al. (2005). A centrosomal mechanism involving CDK5RAP2 and CENPJ controls brain size. Nat Genet *37*, 353–355.

Bradshaw, N.J., Hennah, W., and Soares, D.C. (2013). NDE1 and NDEL1: twin neurodevelopmental proteins with similar 'nature' but different 'nurture'. BioMolecular Concepts *4*, 447–464.

Carabalona, A., Hu, D.J.-K., and Vallee, R.B. (2016). KIF1A inhibition immortalizes brain stem cells but blocks BDNF-mediated neuronal migration. Nat Neurosci *19*, 253–262.

Castiel, A., Danieli, M.M., David, A., Moshkovitz, S., Aplan, P.D., Kirsch, I.R., Brandeis, M., Krämer, A., and Izraeli, S. (2011). The Stil protein regulates centrosome integrity and mitosis through suppression of Chfr. Journal of Cell Science *124*, 532–539.

Chakraborti, S., Natarajan, K., Curiel, J., Janke, C., and Liu, J. (2016). The emerging role of the tubulin code: From the tubulin molecule to neuronal function and disease. Cytoskeleton (Hoboken) *73*, 521–550.

Chenn, A., and McConnell, S.K. (1995). Cleavage orientation and the asymmetric inheritance of Notch1 immunoreactivity in mammalian neurogenesis. Cell *82*, 631–641.

de Anda, F.C., Meletis, K., Ge, X., Rei, D., and Tsai, L.H. (2010). Centrosome Motility Is Essential for Initial Axon Formation in the Neocortex. Journal of Neuroscience *30*, 10391–10406.

Del Bene, F., Wehman, A.M., Link, B.A., and Baier, H. (2008). Regulation of neurogenesis by interkinetic nuclear migration through an apical-basal notch gradient. Cell *134*, 1055–1065.

Désir, J., Cassart, M., David, P., Van Bogaert, P., and Abramowicz, M. (2008). Primary microcephaly with ASPM mutation shows simplified cortical gyration with antero-posterior gradient pre- and post-natally. Am. J. Med. Genet. A *146A*, 1439–1443.

Doobin, D.J., Kemal, S., Dantas, T.J., and Vallee, R.B. (2016). Severe NDE1-mediated microcephaly results from neural progenitor cell cycle arrests at multiple specific stages. Nature Communications *7*, 12551.

Elias, L.A.B., Wang, D.D., and Kriegstein, A.R. (2007). Gap junction adhesion is necessary for radial migration in the neocortex. Nature *448*, 901–907.

Feng, Y., Olson, E.C., Stukenberg, P.T., Flanagan, L.A., Kirschner, M.W., and Walsh, C.A.

(2000). LIS1 regulates CNS lamination by interacting with mNudE, a central component of the centrosome. Neuron *28*, 665–679.

Feng, Y., and Walsh, C.A. (2004). Mitotic spindle regulation by Nde1 controls cerebral cortical size. Neuron *44*, 279–293.

Fietz, S.A., Kelava, I., Vogt, J., Wilsch-Bräuninger, M., Stenzel, D., Fish, J.L., Corbeil, D., Riehn, A., Distler, W., Nitsch, R., et al. (2010). OSVZ progenitors of human and ferret neocortex are epithelial-like and expand by integrin signaling. Nat Neurosci *13*, 690–699.

Fiorillo, C., Moro, F., Yi, J., Weil, S., Brisca, G., Astrea, G., Severino, M., Romano, A., Battini, R., Rossi, A., et al. (2014). Novel dynein DYNC1H1 neck and motor domain mutations link distal spinal muscular atrophy and abnormal cortical development. Hum. Mutat. *35*, 298–302.

Fish, J.L., Kosodo, Y., Enard, W., Pääbo, S., and Huttner, W.B. (2006). Aspm specifically maintains symmetric proliferative divisions of neuroepithelial cells. Proc. Natl. Acad. Sci. U.S.a. *103*, 10438–10443.

Gao, P., Postiglione, M.P., Krieger, T.G., Hernandez, L., Wang, C., Han, Z., Streicher, C., Papusheva, E., Insolera, R., Chugh, K., et al. (2014). Deterministic progenitor behavior and unitary production of neurons in the neocortex. Cell *159*, 775–788.

Glasser, M.F., Coalson, T.S., Robinson, E.C., Hacker, C.D., Harwell, J., Yacoub, E., Ugurbil, K., Andersson, J., Beckmann, C.F., Jenkinson, M., et al. (2016). A multi-modal parcellation of human cerebral cortex. Nature *536*, 171–178.

Govek, E.-E., Hatten, M.E., and Van Aelst, L. (2011). The role of Rho GTPase proteins in CNS neuronal migration. Devel Neurobio *71*, 528–553.

Grabham, P.W., Seale, G.E., Bennecib, M., Goldberg, D.J., and Vallee, R.B. (2007). Cytoplasmic dynein and LIS1 are required for microtubule advance during growth cone remodeling and fast axonal outgrowth. Journal of Neuroscience *27*, 5823–5834.

Griffith, E., Walker, S., Martin, C.-A., Vagnarelli, P., Stiff, T., Vernay, B., Sanna, Al, N., Saggar, A., Hamel, B., Earnshaw, W.C., et al. (2008). Mutations in pericentrin cause Seckel syndrome with defective ATR-dependent DNA damage signaling. Nat Genet *40*, 232–236.

Guerrini, R., and Dobyns, W.B. (2014). Malformations of cortical development: clinical features and genetic causes. Lancet Neurol *13*, 710–726.

Guerrini, R., Dobyns, W.B., and Barkovich, A.J. (2008). Abnormal development of the human cerebral cortex: genetics, functional consequences and treatment options. Trends in Neurosciences *31*, 154–162.

Guven, A., Gunduz, A., Bozoglu, T.M., Yalcinkaya, C., and Tolun, A. (2012). Novel NDE1 homozygous mutation resulting in microhydranencephaly and not microlyssencephaly. Neurogenetics *13*, 189–194.

Hafezparast, M., Klocke, R., Ruhrberg, C., Marquardt, A., Ahmad-Annuar, A., Bowen, S., Lalli, G., Witherden, A.S., Hummerich, H., Nicholson, S., et al. (2003). Mutations in dynein link motor neuron degeneration to defects in retrograde transport. Science *300*, 808–812.

Hagen, von der, M., Pivarcsi, M., Liebe, J., Bernuth, von, H., Didonato, N., Hennermann, J.B., Bührer, C., Wieczorek, D., and Kaindl, A.M. (2014). Diagnostic approach to microcephaly in childhood: a two-center study and review of the literature. Dev Med Child Neurol *56*, 732–741.

Hand, R., Bortone, D., Mattar, P., Nguyen, L., Heng, J.I.-T., Guerrier, S., Boutt, E., Peters, E., Barnes, A.P., Parras, C., et al. (2005). Phosphorylation of Neurogenin2 specifies the migration properties and the dendritic morphology of pyramidal neurons in the neocortex. Neuron *48*, 45–62.

Hansen, D.V., Lui, J.H., Parker, P.R.L., and Kriegstein, A.R. (2010). Neurogenic radial glia in the outer subventricular zone of human neocortex. Nature *464*, 554–561.

Harms, M.B., Ori-McKenney, K.M., Scoto, M., Tuck, E.P., Bell, S., Ma, D, Masi, S., Allred, P., Al-Lozi, M., Reilly, M.M., et al. (2012). Mutations in the tail domain of DYNC1H1 cause dominant spinal muscular atrophy. Neurology *78*, 1714–1720.

Harwell, C.C., Fuentealba, L.C., Gonzalez-Cerrillo, A., Parker, P.R.L., Gertz, C.C., Mazzola, E., Garcia, M.T., Alvarez-Buylla, A., Cepko, C.L., and Kriegstein, A.R. (2015). Wide Dispersion and Diversity of Clonally Related Inhibitory Interneurons. Neuron *87*, 999–1007.

Hatanaka, Y., and Yamauchi, K. (2012). Excitatory Cortical Neurons with Multipolar Shape Establish Neuronal Polarity by Forming a Tangentially Oriented Axon in the Intermediate Zone. Cerebral Cortex *23*, 105–113.

Hattori, M., Adachi, H., Tsujimoto, M., Arai, H., and Inoue, K. (1994). Miller-Dieker lissencephaly gene encodes a subunit of brain platelet-activating factor acetylhydrolase [corrected]. Nature *370*, 216–218.

Haubensak, W., Attardo, A., Denk, W., and Huttner, W.B. (2004). Neurons arise in the basal neuroepithelium of the early mammalian telencephalon: a major site of neurogenesis. Proc. Natl. Acad. Sci. U.S.a. *101*, 3196–3201.

Haverfield, E.V., Whited, A.J., Petras, K.S., Dobyns, W.B., and Das, S. (2009). Intragenic deletions and duplications of the LIS1 and DCX genes: a major disease-causing mechanism in lissencephaly and subcortical band heterotopia. Eur. J. Hum. Genet. *17*, 911–918.

He, S., Li, Z., Ge, S., Yu, Y.-C., and Shi, S.-H. (2015). Inside-Out Radial Migration Facilitates Lineage-Dependent Neocortical Microcircuit Assembly. Neuron *86*, 1159–1166.

Hebbar, S., Mesngon, M.T., Guillotte, A.M., Desai, B., Ayala, R., and Smith, D.S. (2008). Lis1 and Ndel1 influence the timing of nuclear envelope breakdown in neural stem cells. The Journal of Cell Biology *182*, 1063–1071.

Hertecant, J., Komara, M., Nagi, A., Suleiman, J., Al-Gazali, L., and Ali, B.R. (2016). A novel de novo mutation in DYNC1H1 gene underlying malformation of cortical development and cataract. Meta Gene *9*, 124–127.

Hippenmeyer, S., Youn, Y.H., Moon, H.M., Miyamichi, K., Zong, H., Wynshaw-Boris, A., and Luo, L. (2010). Genetic mosaic dissection of Lis1 and Ndel1 in neuronal migration. Neuron *68*, 695–709.

Houlihan, S.L., and Feng, Y. (2014). The scaffold protein Nde1 safeguards the brain genome during S phase of early neural progenitor differentiation. eLife *3*, e03297.

Hu, D.J.-K., Baffet, A.D., Nayak, T., Akhmanova, A., Doye, V., and Vallee, R.B. (2013). Dynein recruitment to nuclear pores activates apical nuclear migration and mitotic entry in brain progenitor cells. Cell *154*, 1300–1313.

Jamuar, S.S., Lam, A.-T.N., Kircher, M., D'Gama, A.M., Wang, J., Barry, B.J., Zhang, X., Hill, R.S., Partlow, J.N., Rozzo, A., et al. (2014). Somatic mutations in cerebral cortical malformations. N. Engl. J. Med. *371*, 733–743.

Jayaraman, D., Kodani, A., Gonzalez, D.M., Mancias, J.D., Mochida, G.H., Vagnoni, C., Johnson, J., Krogan, N., Harper, J.W., Reiter, J.F., et al. (2016). Microcephaly Proteins Wdr62 and Aspm Define a Mother Centriole Complex Regulating Centriole Biogenesis, Apical Complex, and Cell Fate. Neuron *0*.

Jossin, Y., and Cooper, J.A. (2011). Reelin, Rap1 and N-cadherin orient the migration of multipolar neurons in the developing neocortex. Nat Neurosci *14*, 697–703.

Kalay, E., Yigit, G., Aslan, Y., Brown, K.E., Pohl, E., Bicknell, L.S., Kayserili, H., Li, Y., Tuysuz, B., Nürnberg, G., et al. (2011). CEP152 is a genome maintenance protein disrupted in Seckel syndrome. Nat Genet *43*, 23–26.

Knoblich, J.A. (2010). Asymmetric cell division: recent developments and their implications for tumour biology. Nat Rev Mol Cell Biol *11*, 849–860.

Kriegstein, A., and Alvarez-Buylla, A. (2009). The Glial Nature of Embryonic and Adult Neural Stem Cells. Annual Review of Neuroscience *32*, 149–184.

La Fata, G., Gärtner, A., Domínguez-Iturza, N., Dresselaers, T., Dawitz, J., Poorthuis, R.B., Averna, M., Himmelreich, U., Meredith, R.M., Achsel, T., et al. (2014). FMRP

regulates multipolar to bipolar transition affecting neuronal migration and cortical circuitry. Nat Neurosci *17*, 1693–1700.

LaMonica, B.E., Lui, J.H., Hansen, D.V., and Kriegstein, A.R. (2013a). Mitotic spindle orientation predicts outer radial glial cell generation in human neocortex. Nature Communications *4*, 1665–11.

LaMonica, B.E., Lui, J.H., Hansen, D.V., and Kriegstein, A.R. (2013b). Mitotic spindle orientation predicts outer radial glial cell generation in human neocortex. Nature Communications *4*, 1665–11.

LaMonica, B.E., Lui, J.H., Wang, X., and Kriegstein, A.R. (2012). OSVZ progenitors in the human cortex: an updated perspective on neurodevelopmental disease. Current Opinion in Neurobiology *22*, 747–753.

Lancaster, M.A., and Knoblich, J.A. (2012). Spindle orientation in mammalian cerebral cortical development. Current Opinion in Neurobiology *22*, 737–746.

Lewis, T.L., Courchet, J., and Polleux, F. (2013). Cell biology in neuroscience: Cellular and molecular mechanisms underlying axon formation, growth, and branching. The Journal of Cell Biology *202*, 837–848.

Lewitus, E., Kelava, I., and Huttner, W.B. (2013). Conical expansion of the outer subventricular zone and the role of neocortical folding in evolution and development. Front Hum Neurosci *7*, 424.

Lipka, J., Kujipers, M., Jaworski, J., and Hoogenraad, C.C. (2013). Mutations in cytoplasmic dynein and its regulators cause malformations of cortical development and neurodegenerative diseases. Biochemical Society Transactions *41*, 1605–1612.

Liu, J.S., Schubert, C.R., Fu, X., Fourniol, F.J., Jaiswal, J.K., Houdusse, A., Stultz, C.M., Moores, C.A., and Walsh, C.A. (2012). Molecular Basis for Specific Regulation of Neuronal Kinesin-3 Motors by Doublecortin Family Proteins. Molecular Cell *47*, 707–721.

Marín, O., and Müller, U. (2014). Lineage origins of GABAergic versus glutamatergic neurons in the neocortex. Current Opinion in Neurobiology *26*, 132–141.

Marín, O., Valiente, M., Ge, X., and Tsai, L.-H. (2010). Guiding neuronal cell migrations. Cold Spring Harbor Perspectives in Biology *2*, a001834.

Martin, C.-A., Murray, J.E., Carroll, P., Leitch, A., Mackenzie, K.J., Halachev, M., Fetit, A.E., Keith, C., Bicknell, L.S., Fluteau, A., et al. (2016). Mutations in genes encoding condensin complex proteins cause microcephaly through decatenation failure at mitosis. Genes Dev. *30*, 2158–2172.

Mayer, C., Jaglin, X.H., Cobbs, L.V., Bandler, R.C., Streicher, C., Cepko, C.L.,

Hippenmeyer, S., and Fishell, G. (2015). Clonally Related Forebrain Interneurons Disperse Broadly across Both Functional Areas and Structural Boundaries. Neuron *87*, 989–998.

Meyer, E.J., Ikmi, A., and Gibson, M.C. (2011). Interkinetic nuclear migration is a broadly conserved feature of cell division in pseudostratified epithelia. Curr. Biol. *21*, 485–491.

Miyata, T., Okamoto, M., Shinoda, T., and Kawaguchi, A. (2014). Interkinetic nuclear migration generates and opposes ventricular-zone crowding: insight into tissue mechanics. Front Cell Neurosci *8*, 473.

Munch, C., Sedlmeier, R., Meyer, T., Homberg, V., Sperfeld, A.D., Kurt, A., Prudlo, J., Peraus, G., Hanemann, C.O., Stumm, G., et al. (2004). Point mutations of the p150 subunit of dynactin (DCTN1) gene in ALS. Neurology *63*, 724–726.

Namba, T., Kibe, Y., Funahashi, Y., Nakamuta, S., Takano, T., Ueno, T., Shimada, A., Kozawa, S., Okamoto, M., Shimoda, Y., et al. (2014). Pioneering Axons Regulate Neuronal Polarization in the Developing Cerebral Cortex. Neuron *81*, 814–829.

Neveling, K., Martinez-Carrera, L.A., Hölker, I., Heister, A., Verrips, A., Hosseini-Barkooie, S.M., Gilissen, C., Vermeer, S., Pennings, M., Meijer, R., et al. (2013). Mutations in BICD2, which Encodes a Golgin and Important Motor Adaptor, Cause Congenital Autosomal-Dominant Spinal Muscular Atrophy. The American Journal of Human Genetics *92*, 1–9.

Nicholas, A.K., Khurshid, M., Désir, J., Carvalho, O.P., Cox, J.J., Thornton, G., Kausar, R., Ansar, M., Ahmad, W., Verloes, A., et al. (2010). WDR62 is associated with the spindle pole and is mutated in human microcephaly. Nat Genet *42*, 1010–1014.

Noctor, S.C., Flint, A.C., Weissman, T.A., Dammerman, R.S., and Kriegstein, A.R. (2001). Neurons derived from radial glial cells establish radial units in neocortex. Nature *409*, 714–720.

Noctor, S.C., Martínez-Cerdeño, V., Ivic, L., and Kriegstein, A.R. (2004). Cortical neurons arise in symmetric and asymmetric division zones and migrate through specific phases. Nat Neurosci *7*, 136–144.

Norden, C., Young, S., Link, B.A., and Harris, W.A. (2009). Actomyosin Is the Main Driver of Interkinetic Nuclear Migration in the Retina. Cell *138*, 1195–1208.

Nowakowski, T.J., Pollen, A.A., Sandoval-Espinosa, C., and Kriegstein, A.R. (2016). Transformation of the Radial Glia Scaffold Demarcates Two Stages of Human Cerebral Cortex Development. Neuron *91*, 1219–1227.

Oates, E.C., Rossor, A.M., Hafezparast, M., Gonzalez, M., Speziani, F., MacArthur, D.G., Lek, M., Cottenie, E., Scoto, M., Foley, A.R., et al. (2013). Mutations in BICD2 Cause

Dominant Congenital Spinal Muscular Atrophy and Hereditary Spastic Paraplegia. The American Journal of Human Genetics *92*, 1–9.

Ohtaka-Maruyama, C., Hirai, S., Miwa, A., Heng, J.I.-T., Shitara, H., Ishii, R., Taya, C., Kawano, H., Kasai, M., Nakajima, K., et al. (2013). RP58 regulates the multipolar-bipolar transition of newborn neurons in the developing cerebral cortex. CellReports *3*, 458–471.

Ori-McKenney, K.M., and Vallee, R.B. (2011). Neuronal migration defects in the Loa dynein mutant mouse. Neural Development *6*, 26.

Ori-McKenney, K.M., Xu, J., Gross, S.P., and Vallee, R.B. (2010). A cytoplasmic dynein tail mutation impairs motor processivity. Nature Cell Biology *12*, 1228–1234.

Ostrem, B.E.L., Lui, J.H., Gertz, C.C., and Kriegstein, A.R. (2014). Control of outer radial glial stem cell mitosis in the human brain. CellReports *8*, 656–664.

Paciorkowski, A.R., Keppler-Noreuil, K., Robinson, L., Sullivan, C., Sajan, S., Christian, S.L., Bukshpun, P., Gabriel, S.B., Gleeson, J.G., Sherr, E.H., et al. (2013). Deletion 16p13.11 uncovers NDE1 mutations on the non-deleted homolog and extends the spectrum of severe microcephaly to include fetal brain disruption. Am. J. Med. Genet. A *161A*, 1523–1530.

Paridaen, J.T., and Huttner, W.B. (2014). Neurogenesis during development of the vertebrate central nervous system. EMBO Reports *15*, 351–364.

Parrini, E., Conti, V., Dobyns, W.B., and Guerrini, R. (2016). Genetic Basis of Brain Malformations. Mol Syndromol *7*, 220–233.

Pilz, D.T., Matsumoto, N., Minnerath, S., Mills, P., Gleeson, J.G., Allen, K.M., Walsh, C.A., Barkovich, A.J., Dobyns, W.B., Ledbetter, D.H., et al. (1998). LIS1 and XLIS (DCX) mutations cause most classical lissencephaly, but different patterns of malformation. Human Molecular Genetics *7*, 2029–2037.

Poduri, A., Evrony, G.D., Cai, X., and Walsh, C.A. (2013). Somatic Mutation, Genomic Variation, and Neurological Disease. Science *341*, 1237758–1237758.

Poirier, K., Lebrun, N., Broix, L., Tian, G., Saillour, Y., Boscheron, C.E.C., Parrini, E., Valence, S., Saint Pierre, B., Oger, M., et al. (2013). Mutations in TUBG1, DYNC1H1, KIF5C and KIF2A cause malformations of cortical development and microcephaly. Nat Genet *45*, 639–647.

Polleux, F., and Snider, W. (2010). Initiating and Growing an Axon. Cold Spring Harbor Perspectives in Biology *2*, a001925–a001925.

Polleux, F., Whitford, K.L., Dijkhuizen, P.A., Vitalis, T., and Ghosh, A. (2002). Control of cortical interneuron migration by neurotrophins and PI3-kinase signaling. 1–14.

Prokop, A. (2013). The intricate relationship between microtubules and their associated motor proteins during axon growth and maintenance. Neural Development *8*, 17.

Pulvers, J.N., Journiac, N., Arai, Y., and Nardelli, J. (2015). MCPH1: a window into brain development and evolution. Front Cell Neurosci *9*, 92.

Rakic, P. (1972). Mode of cell migration to the superficial layers of fetal monkey neocortex. J. Comp. Neurol. *145*, 61–83.

Rakic, P. (1988). Specification of cerebral cortical areas. Science *241*, 170–176.

Reiner, O., Carrozzo, R., Shen, Y., Wehnert, M., Faustinella, F., Dobyns, W.B., Caskey, C.T., and Ledbetter, D.H. (1993). Isolation of a Miller-Dieker lissencephaly gene containing G protein beta-subunit-like repeats. Nature *364*, 717–721.

Reiner, O., and Sapir, T. (2013). LIS1 functions in normal development and disease. Current Opinion in Neurobiology *23*, 951–956.

Reiner, O., Karzbrun, E., Kshirsagar, A., and Kaibuchi, K. (2015). Regulation of neuronal migration, an emerging topic in autism spectrum disorders. J. Neurochem. *136*, 440–456.

Saito, T., Hanai, S., Takashima, S., Nakagawa, E., Okazaki, S., Inoue, T., Miyata, R., Hoshino, K., Akashi, T., Sasaki, M., et al. (2011). Neocortical layer formation of human developing brains and lissencephalies: consideration of layer-specific marker expression. Cereb. Cortex *21*, 588–596.

Sakakibara, A., Sato, T., Ando, R., Noguchi, N., Masaoka, M., and Miyata, T. (2013). Dynamics of Centrosome Translocation and Microtubule Organization in Neocortical Neurons during Distinct Modes of Polarization. Cerebral Cortex.

Sasaki, S., Mori, D., Toyo-oka, K., Chen, A., Garrett-Beal, L., Muramatsu, M., Miyagawa, S., Hiraiwa, N., Yoshiki, A., Wynshaw-Boris, A., et al. (2005). Complete loss of Ndel1 results in neuronal migration defects and early embryonic lethality. Molecular and Cellular Biology *25*, 7812–7827.

Sauer, F.C. (1935). Mitosis in the neural tube. Journal of Comparative Neurology *62*, 377–405.

Schenk, J., Wilsch-Bräuninger, M., Calegari, F., and Huttner, W.B. (2009). Myosin II is required for interkinetic nuclear migration of neural progenitors. Proc. Natl. Acad. Sci. U.S.a. *106*, 16487–16492.

Scoto, M., Rossor, A.M., Harms, M.B., Cirak, S., Calissano, M., Robb, S., Manzur, A.Y., Martínez Arroyo, A., Rodriguez Sanz, A., Mansour, S., et al. (2015). Novel mutations expand the clinical spectrum of DYNC1H1-associated spinal muscular atrophy.

Neurology *84*, 668–679.

Shen, J., Gilmore, E.C., Marshall, C.A., Haddadin, M., Reynolds, J.J., Eyaid, W., Bodell, A., Barry, B., Gleason, D., Allen, K., et al. (2010). Mutations in PNKP cause microcephaly, seizures and defects in DNA repair. Nat Genet *42*, 245–249.

Solecki, D.J., Model, L., Gaetz, J., Kapoor, T.M., and Hatten, M.E. (2004). Par6α signaling controls glial-guided neuronal migration. Nat Neurosci *7*, 1195–1203.

Solecki, D.J., Trivedi, N., Govek, E.-E., Kerekes, R.A., Gleason, S.S., and Hatten, M.E. (2009). Myosin II motors and F-actin dynamics drive the coordinated movement of the centrosome and soma during CNS glial-guided neuronal migration. Neuron *63*, 63–80.

Splinter, D., Razafsky, D.S., Schlager, M.A., Serra-Marques, A., Grigoriev, I., Demmers, J., Keijzer, N., Jiang, K., Poser, I., Hyman, A.A., et al. (2012). BICD2, dynactin, and LIS1 cooperate in regulating dynein recruitment to cellular structures. Molecular Biology of the Cell *23*, 4226–4241.

Splinter, D., Tanenbaum, M.E., Lindqvist, A., Jaarsma, D., Flotho, A., Yu, K.L., Grigoriev, I., Engelsma, D., Haasdijk, E.D., Keijzer, N., et al. (2010). Bicaudal D2, dynein, and kinesin-1 associate with nuclear pore complexes and regulate centrosome and nuclear positioning during mitotic entry. PLoS Biol *8*, e1000350.

Strzyz, P.J., Lee, H.O., Sidhaye, J., Weber, I.P., Leung, L.C., and Norden, C. (2015). Interkinetic nuclear migration is centrosome independent and ensures apical cell division to maintain tissue integrity. Developmental Cell *32*, 203–219.

Tabata, H., and Nakajima, K. (2003). Multipolar migration: the third mode of radial neuronal migration in the developing cerebral cortex. Journal of Neuroscience *23*, 9996–10001.

Thornton, G.K., and Woods, C.G. (2009). Primary microcephaly: do all roads lead to Rome? Trends Genet. *25*, 501–510.

Tsai, J.W., Chen, Y., Kriegstein, A.R., and Vallee, R.B. (2005). LIS1 RNA interference blocks neural stem cell division, morphogenesis, and motility at multiple stages. The Journal of Cell Biology *170*, 935–945.

Tsai, J.-W., Bremner, K.H., and Vallee, R.B. (2007). Dual subcellular roles for LIS1 and dynein in radial neuronal migration in live brain tissue. Nat Neurosci *10*, 970–979.

Tsai, J.-W., Lian, W.-N., Kemal, S., Kriegstein, A.R., and Vallee, R.B. (2010). Kinesin 3 and cytoplasmic dynein mediate interkinetic nuclear migration in neural stem cells. Nat Neuro *13*, 1463–1471.

Twelvetrees, A.E., Pernigo, S., Sanger, A., Guedes-Dias, P., Schiavo, G., Steiner, R.A.,

Dodding, M.P., and Holzbaur, E.L.F. (2016). The Dynamic Localization of Cytoplasmic Dynein in Neurons Is Driven by Kinesin-1. Neuron 1–17.

Vallee, R.B., Seale, G.E., and Tsai, J.-W. (2009). Emerging roles for myosin II and cytoplasmic dynein in migrating neurons and growth cones. Trends in Cell Biology *19*, 347–355.

Willemsen, M.H., Vissers, L.E.L., Willemsen, M.A.A.P., van Bon, B.W.M., Kroes, T., de Ligt, J., de Vries, B.B., Schoots, J., Lugtenberg, D., Hamel, B.C.J., et al. (2012). Mutations in DYNC1H1 cause severe intellectual disability with neuronal migration defects. Journal of Medical Genetics *49*, 179–183.

Woods, C.G. (2004). Human microcephaly. Current Opinion in Neurobiology *14*, 112–117.

Xiang, X., Osmani, A.H., Osmani, S.A., Xin, M., and Morris, N.R. (1995). NudF, a nuclear migration gene in Aspergillus nidulans, is similar to the human LIS-1 gene required for neuronal migration. Molecular Biology of the Cell *6*, 297–310.

Yingling, J., Youn, Y.H., Darling, D., Toyo-oka, K., Pramparo, T., Hirotsune, S., and Wynshaw-Boris, A. (2008). Neuroepithelial stem cell proliferation requires LIS1 for precise spindle orientation and symmetric division. Cell *132*, 474–486.

Youn, Y.H., Pramparo, T., Hirotsune, S., and Wynshaw-Boris, A. (2009). Distinct dose-dependent cortical neuronal migration and neurite extension defects in Lis1 and Ndel1 mutant mice. Journal of Neuroscience *29*, 15520–15530.

Zhang, X., Lei, K., Yuan, X., Wu, X., Zhuang, Y., Xu, T., Xu, R., and Han, M. (2009). SUN1/2 and Syne/Nesprin-1/2 Complexes Connect Centrosome to the Nucleus during Neurogenesis and Neuronal Migration in Mice. Neuron *64*, 173–187.

Zheng, C., Heintz, N., and Hatten, M.E. (1996). CNS gene encoding astrotactin, which supports neuronal migration along glial fibers. Science *272*, 417–419.

Zuccolo, M., Alves, A., Galy, V., Bolhy, S., Formstecher, E., Racine, V., Sibarita, J.-B., Fukagawa, T., Shiekhattar, R., Yen, T., et al. (2007). The human Nup107–160 nuclear pore subcomplex contributes to proper kinetochore functions. The EMBO Journal *26*, 1853–1864.

Contributions: DJD wrote the initial draft, RBV and DJD edited. Figures drawn by DJD. Section 1.7 and Figure 1.4 were not included in the chapter for publication.

Acknowledgements: We thank Tiago Dantas, Aurelie Carabalona, and João Goncalves for their critical reading of this manuscript.

Chapter 2

Severe *NDE1*-Mediated Microcephaly Results from Neural Progenitor Cell Cycle Arrests at Multiple Specific Stages

This chapter was modified and expanded from the original work published as:

Doobin DJ, Kemal S, Dantas TJ, Vallee RB. (2016) Severe NDE1 Mediated Microcephaly Results from Neural Progenitor Cell Cycle Arrest at Multiple Specific Stages. *Nature Communications*, 7:12551.

Nomenclature note: 'Nde1' and 'Ndel1' are referred to in throughout this chapter as 'NDE1' and 'NDEL1' to help ease the reader in distinguishing the two words. We are not explicitly referring to the human forms of the NDE1 and NDEL1 proteins by capitalizing the whole word.

ABSTRACT

Microcephaly is a cortical malformation disorder characterized by an abnormally small brain. Recent studies have revealed severe cases of microcephaly resulting from human mutations in the *NDE1* gene, which is involved in the regulation of cytoplasmic dynein. Here, using *in utero* electroporation of NDE1 shRNA in embryonic rat brains, we observe cell cycle arrest of proliferating neural progenitors at three distinct stages: during apical interkinetic nuclear migration, at the G2-to-M transition, and in regulation of primary cilia at the G1-to-S transition. RNAi against the NDE1 paralog NDEL1 has no such effects. However, NDEL1 overexpression can functionally compensate for NDE1, except at the G2-to-M transition, revealing a unique NDE1 role. In contrast, NDE1 and NDEL1 RNAi have comparable effects on postmitotic neuronal migration. These results reveal that the severity of *NDE1*-associated microcephaly results not from defects in mitosis, but rather the inability of neural progenitors to ever reach this stage.

INTRODUCTION

Autosomal-recessive primary microcephaly (MCPH) is a severe developmental condition characterized by small brain size and a substantial reduction in neuronal number (Barkovich et al., 2012). The cerebral cortex is most prominently affected. Laminar organization is often normal, though microcephaly can occasionally be accompanied by lissencephaly or other organization defects (Alkuraya et al., 2011; Barkovich et al., 2012). A number of microcephaly genes have been identified, including *ASPM*, *microcephalin*/*BRIT1*, *CDK5RAP2*/*Cep215*, *CENPJ*/*CPAP*, *SIL*/*STIL*, *WDR62*, and *NDE1* (Bond et al., 2002; Nicholas et al., 2010; Thornton and Woods, 2009). Several of these genes are associated with centrosome and/or mitotic function, suggesting that errors in neural progenitor cell proliferation contribute to disease pathology.

NDE1 was an early candidate gene for microcephaly as judged from mouse studies (Feng and Walsh, 2004), and has subsequently been implicated in a particularly severe form of microcephaly and microlissencephaly in human patients (Alkuraya et al., 2011; Bakircioglu et al., 2011; Guven et al., 2012; Lipka et al., 2013; Paciorkowski et al., 2013). NDE1 and its paralog, NDEL1, exhibit clear homology to *Aspergillus* NudE (Nuclear Distribution E) (Efimov and Morris, 2000), and function along with LIS1 in cytoplasmic dynein regulation (Huang et al., 2012; McKenney et al., 2010; Niethammer et al., 2000; Sasaki et al., 2000). The *NDE1* null mouse was reported to exhibit ectopic mitotic divisions accompanied by altered mitotic spindle orientation (Feng and Walsh, 2004). Roles for NDE1 and NDEL1 in mitosis have been borne out by analysis of non-neuronal cells *in vitro* (Liang et al., 2007; Stehman

et al., 2007; Vergnolle and Taylor, 2007; Yan et al., 2003). However, human *NDE1*-associated microcephaly is much more severe than that involving mitotic spindle assembly genes, such as *ASPM* and *WDR62* (Bond et al., 2002; Nicholas et al., 2010). This observation suggests that NDE1 might be involved in more than one aspect of neural progenitor proliferation. Additionally, patients with *NDE1* mutations often exhibit microcephaly with lissencephalic features (Alkuraya et al., 2011; Bakircioglu et al., 2011), suggesting potential roles for NDE1 during subsequent neuronal migration.

Mammalian neocortical development begins with the expansion of neuroepithelial cells within the neural tube, followed by formation of the layered neocortex (Kriegstein and Alvarez-Buylla, 2009; Paridaen and Huttner, 2014). The apical-most region, which is adjacent to lateral ventricle and defined as the ventricular zone (VZ), is populated by the soma of radial glia progenitor (RGP) cells (Noctor et al., 2004). These serve as stem cells, responsible for the production of all excitatory cortical neurons, most glial cells, and adult stem cells (Gao et al., 2014; Kriegstein and Alvarez-Buylla, 2009). RGP cells are highly elongated, with their apical and basal processes spanning the entire thickness of the developing neocortex. A hallmark of RGP cell behavior is the cell cycle-linked oscillatory movement of the nucleus of RGP cells, termed interkinetic nuclear migration (INM) (Sauer, 1935). RGP mitosis occurs exclusively at the ventricle (Hu et al., 2013). The RGP nucleus then migrates basally during G1, progresses through S-phase in the upper portion of the VZ, and then migrates apically during G2 toward the ventricle where the next mitotic division occurs (Dantas et al., 2016). Mitosis can be

symmetric, resulting in self-renewal of the neural progenitor pool, or asymmetric, leading to one neural progenitor and either a post-mitotic neuron or intermediate progenitor, each of which migrate away from the ventricle.

Our own studies revealed that knockdown of genes involved in apical INM prevent RGP nuclei from reaching the ventricle and undergoing mitosis (Baffet et al., 2015; Cappello et al., 2011; Carabalona et al., 2016; Hu et al., 2013; Tsai et al., 2005; 2007; 2010). We found that apical migration is mediated by cytoplasmic dynein anchored to the nuclear envelope during G2, which carries the nucleus along a polarized microtubule network emanating from the apically anchored centrosome (Hu et al., 2013; Tsai et al., 2010). Dynein is recruited to the nuclear envelope by two G2-specific nuclear pore mediated mechanisms in a Cdk1-dependant manner (Baffet et al., 2015). The first mechanism is activated during early G2 and involves BicD2 binding to the nucleoporin RanBP2 (Splinter et al., 2010), whereas the second mechanism is activated during late G2 and depends on CENP-F binding the nucleoporin Nup133 (Baffet et al., 2015; Bolhy et al., 2011). Based on the restriction of nuclear-envelope NDE1/NDEL1 signal to late-G2 in HeLa cells (Baffet et al., 2015), we envision that either NDE1, NDEL1, or both, might contribute to late apical nuclear migration in the developing brain, though this possibility has not been tested.

Both NDE1 and NDEL1 mRNAs and protein have been detected throughout the developing neocortex (Allen Developing Mouse Brain Atlas, http://developingmouse.brain-map.org/) (Feng et al., 2000; Niethammer et al., 2000). However, NDE1 is more highly expressed in areas of high proliferation, such

as the VZ, whereas the highest levels of NDEL1 mRNA were detected in the cortical plate (CP), where neuronal migration takes place (Allen Developing Mouse Brain Atlas, http://developingmouse.brain-map.org/). NDEL1 has not been implicated in microcephaly, but rather in later aspects of neuronal migration in animal models (Niethammer et al., 2000; Sasaki et al., 2000). These observations are consistent either with the different expression patterns for NDE1 and NDEL1 in the developing brain, or with differences in their function. Some evidence for NDEL1-specific roles has been reported in cultured cells (Shmueli et al., 2009), but the relative contributions of the two genes to neocortical development remains to be explored (Bradshaw et al., 2013).

The current study was initiated to determine which NDE1 roles contribute most significantly to the extreme form of microcephaly seen in human patients. Additionally we investigated potential roles for NDEL1 during neocortical development, and tested the degree to which these two proteins can functionally compensate for one another. Through use of RNA interference (RNAi) against each paralog we find that both NDE1 and NDEL1 contribute to postmitotic neuronal migration. However, NDE1 inhibition alone causes a complete block of apical INM, contributing to a large reduction in mitotic index with no evidence for ectopic mitoses. We also find a potent block to G1-to-S transition associated with primary cilia over-elongation upon the co-depletion of NDE1 and NDEL1. Interestingly, NDEL1 expression rescues most, but not all, of NDE1 functions, the latter effect identifying a NDE1-specific function, after INM completion, at a novel premitotic state. These results identify multiple new potential causes for microcephaly, and

provide a basis for understanding the distinct pathogenic potential of NDE1 *versus* NDEL1.

RESULTS

Common and Distinct Effects of NDE1 and NDEL1 RNAi

To address the specific roles of NDE1 or NDEL1 during neocortical development, we used *in utero* electroporation of embryonic day 16 (E16) rat brain to introduce plasmids expressing GFP alone or in combination with NDE1 or NDEL1 shRNAs. Reduction of protein levels (Figure 2.1A) and mRNA levels (Figure 2.1B) were confirmed in rat C6 glioma cells. Relative to control, NDE1 knockdown caused a nearly complete loss of transfected neurons from reaching the CP, which instead accumulated in the lower intermediate zone (IZ) and subventricular zone (SVZ) (Figure 2.2A-B). NDEL1 knockdown also prevented cells from reaching the CP, though some cells were observed in the upper IZ, and there was again a large relative accumulation in the lower IZ and SVZ (Figure 2.2A-B). The effects of dual NDE1/NDEL1 knockdown were similar to those for NDE1 and NDEL1 alone (Figure 2.2A-B).

To test the role of NDE1 compared to NDEL1 in RGP cells we performed live imaging of brain slice preparations. Control RGPs exhibited normal apical nuclear migration, followed by mitosis at the ventricular surface, and subsequent basal migration (Figure 2.3A, Supplementary Movie 1). In marked contrast, NDE1 knockdown severely inhibited INM. Although the RGP cells could initiate apical INM, the nuclei failed to migrate beyond the final 10μm, never reaching the

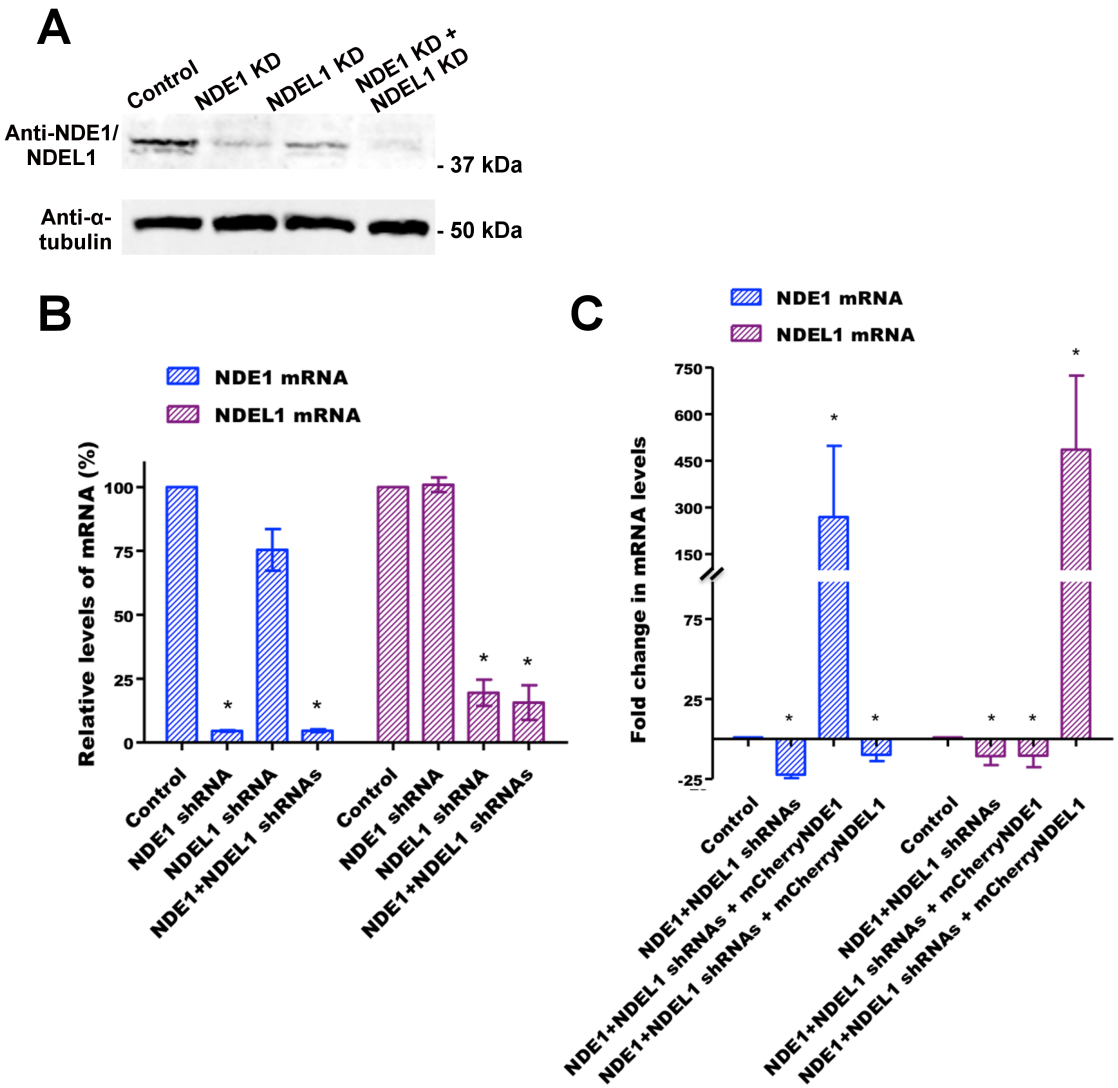

Figure 2.1: Confirmation of shRNA knockdown efficiency (A) Lysate from C6 rat glioma cells transfected with control or shRNA constructs 72 hours prior to lysing confirms successful knockdown of NDE1 and NDEL1 by western blot. **(B)** mRNA levels from C6 cell lysate were used to measure NDE1 and NDEL1 shRNA efficiency. NDE1 shRNA reduced the levels of NDE1 mRNA to <20% of the original. **(C)** Rescue of NDE1 and NDEL1 mRNA levels by RNAi-insensitive cDNA of either NDE1 or NDEL1. Data presented as mean ± SEM. Statistical analyses performed using Kruskall-Wallis with Dunn's multiple comparison test. * for $p<0.05$

ventricular surface and entering mitosis (Figure 2.3A, Supplementary Movie 2). This behavior is consistent with a block in late apical nuclear migration during INM, as we have observed with knockdown of Nup133 or CENP-F(Hu et al., 2013). NDEL1 knockdown, in contrast, had no discernable effect on INM (Figure 2.3A, Supplementary Movie 3). Intriguingly, the double knockdown of both NDE1 and

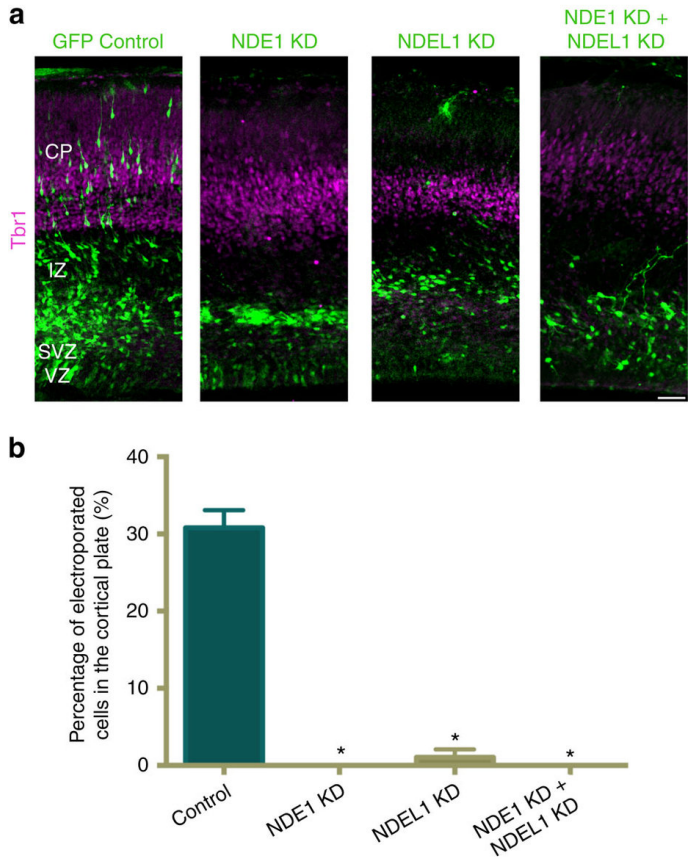

Figure 2.2: Effects of NDE1 and NDEL1 RNAi on neuronal migration into the cortical plate. (A) Representative images of embryonic day 20 (E20) rat neocortex with a control empty-vector expressing GFP alone, or shRNAs to NDE1, NDEL1, or both genes along with a GFP reporter. Sections were stained for Tbr1 to mark neurons in the cortical plate (CP). Scale bar, 50μm. Confirmation of RNAi knockdown can be found in Supplementary Figure 1. **(B)** Quantification of the fraction of electroporated cells in each respective zone of the neocortex across NDE1, NDEL1, or combined RNAi conditions 4 days post-electroporation at E16. All knockdown conditions nearly eliminated any cells from reaching the CP, in comparison to control neurons. Data presented as mean ± SEM, two-way ANOVA with Tukey's multiple comparison tests used to compare each neocortical region across the conditions. * for $p<0.05$, $n=3$ embryonic brains from different mothers.

NDEL1 prevented the vast majority of RGP nuclei from initiating apical INM (Figure 2.3A; Supplementary Movie 4). By live imaging there was no evidence for increased apoptotic events among any of the knockdowns (Supplementary Movies 1-4).

Consistent with these results, fixed tissue analysis revealed that NDE1 knockdown caused a significant accumulation of RGP soma at 10-15μm from the ventricle (Figures 2.3B-D). However, NDE1/NDEL1 double knockdown caused an accumulation of RGP soma further than 30μm from the ventricle (Figure 2.3B-D). While there is a small but significant difference in the RGP somal distributions between control and NDEL1 knockdown (Figure 2.3C), this is not reflected when the groups of somal distances are examined at prescribed distances (Figure 2.3D).

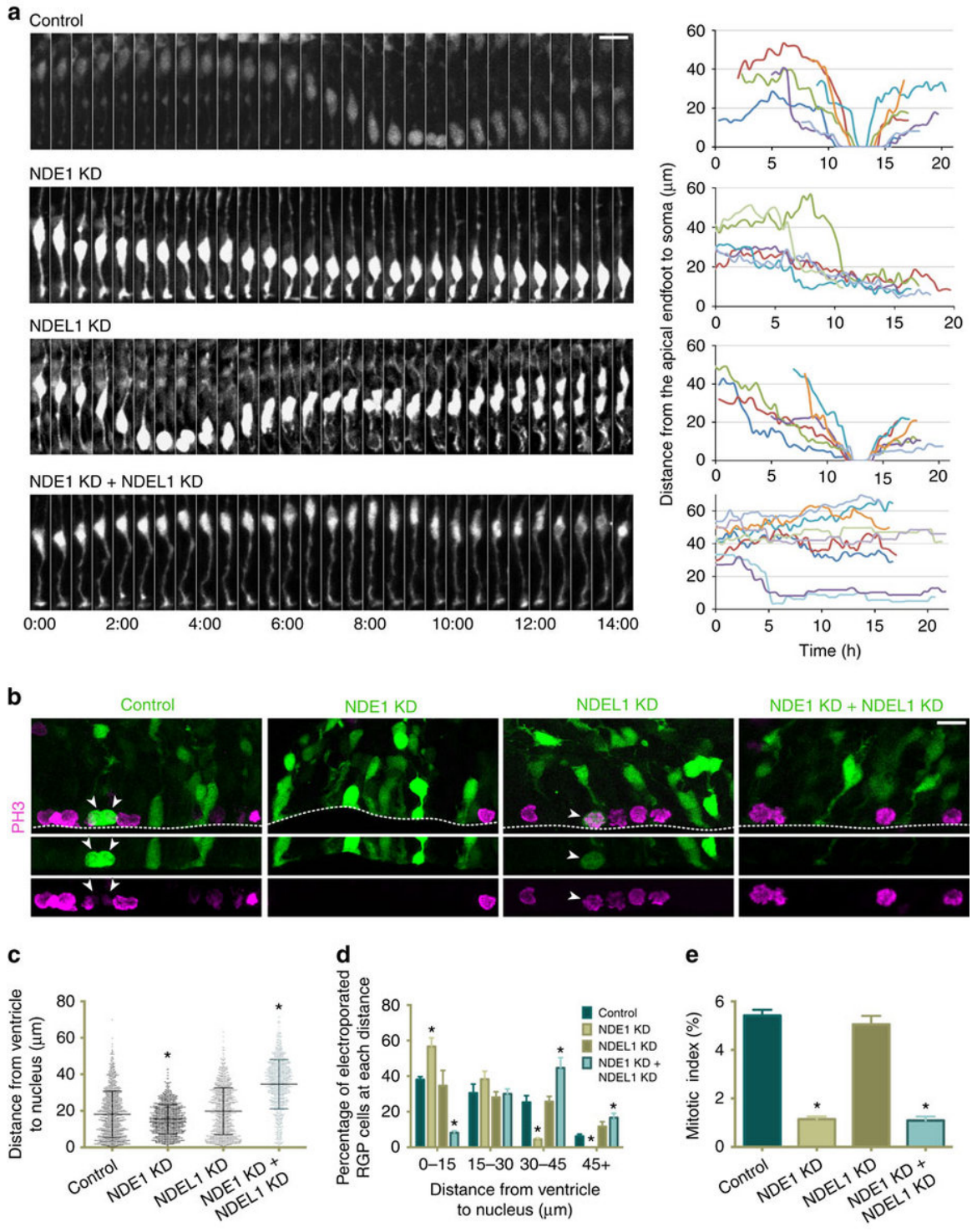

Figure 2.3: NDE1 knockdown, but not NDEL1 knockdown, blocks apical nuclear migration and potently reduces the mitotic index: (A) Live-imaging montage of GFP-expressing RGP cells at E19 with a control empty vector expressing GFP alone, or shRNAs to NDE1, NDEL1, or both genes along with a GFP reporter. Representative tracings from multiple RGP cells for each condition are shown at right. Montage panels are shown at 30 minute intervals. Full movies can be found in Supplementary Material (see Supplementary Movies 1-4). **(B)** Representative images of the VZ from the

electroporated brains stained for the mitotic marker phosphohistone-H3 (PH3). Arrowheads mark soma of PH3+/GFP+ RGP cells. Dashed line represents the ventricular surface. **(C-D)** Measurements of the distance between the bottom of the nucleus and the ventricular surface, corresponding to the apical process length, across the various conditions. NDE1 knockdown shifted the apical process length distribution towards shorter distances (C), with a significant accumulation of RGPs with an apical process of 0-15μm (D). NDE1/NDEL1 double knockdown, however, shifted the apical process length distribution to larger distances (C), with a significant accumulation of RGPs with an apical process of 30-45μm (D). Each dot represents an individual apical process length measurement for one electroporated RGP cell. **(E)** Effect of RNAi on RGP cell mitotic index, measured as the number of electroporated RGP cells positive for PH3 divided by the total number of electroporated RGP cells. All mitotic figures of RGP cells were located at the ventricular surface, and NDE1 knockdown, as well as NDE1/NDEL1 double knockdown, each caused a strong reduction in the mitotic index. Data presented as scatterplot in (C) with bars representing the median ± the interquartile range, and as mean ± SEM in (D) and (E). Kolmogorov-Smirnov test for non-parametric distributions used in (C) (* for $p<0.05$, n=1012-1073 RGP cells). Unpaired t-test used in (D) and (E) (* for $p<0.05$, n=3 embryonic brains from different mothers). Scale bar, 10μm.

Our results, together, indicate that knockdown of either NDE1 or NDEL1 inhibits postmitotic neuronal migration. NDE1 knockdown – but not NDEL1 knockdown - blocks the latter stage of apical INM. Nonetheless, combined NDE1 and NDEL1 knockdown arrests RGP nuclei much further away from the ventricular surface than is observed for NDE1 knockdown alone, suggesting an unexpected synergistic function of the knockdown at a potentially earlier stage of the cell cycle.

Cell Cycle Effects of NDE1 and NDEL1 RNAi

To address this issue, and to determine how changes to INM progression may affect RGP cell proliferation and neurogenesis, we examined the effects of NDE1 and NDEL1 RNAi on cell cycle progression. By preventing nuclear migration to the ventricular surface of the developing brain, we predicted that NDE1 knockdown, but not NDEL1 knockdown, would prevent RGP cells from dividing, identifying a potential NDE1-specific microcephaly mechanism. To test for effects on mitosis, we stained sections from electroporated brains for phosphohistone-H3 (PH3) to mark mitotic cells. We observed a severe reduction in the mitotic index in both the NDE1 knockdown and NDE1/NDEL1 double knockdown conditions (Figure 2.3E), but no

effect from NDEL1 knockdown alone (Figure 2.3E). We note that all mitotic events in control electroporated RGPs occurred at the ventricular surface. Importantly, we observed no examples of mitotic divisions of RGP cells away from the ventricular surface under any of the knockdown conditions.

The severe effect of NDE1/NDEL1 double knockdown on the distance of arrested RGP soma from the ventricle (Figure 2.3B-D) led us to test whether these cells arrest at an earlier cell cycle stage. Staining for the G1 marker CyclinD1 revealed modest or undetectable increases, respectively, in the number of positive RGP nuclei in the NDE1 or NDEL1 shRNA conditions (Figure 2.4A). However, combined NDE1/NDEL1 knockdown doubled the number of CyclinD1-positive cells (Figure 2.4A), consistent with a potent G1 accumulation. To test this possibility further, we stained sections for bromodeoxyuridine (BrdU) following a 30 min *in vivo* pulse, which revealed a steep drop in S-phase cells in NDE1 and NDE1/NDEL1 double knockdown conditions (Figure 2.4B). Staining for Geminin – a S/G2 marker – indicated a significant increase in G2 cells in the NDE1 knockdown condition, while there was a sharp decrease in G2 cells in the NDE1/NDEL1 knockdown, as predicted by CyclinD1 data and live imaging (Figure 2.5A-B). Additional staining for the proliferation marker Ki67 revealed no difference in the fraction of positive RGP cells between conditions (Figure 2.6A-B). Together, these results indicate a synergistic effect of NDE1/NDEL1 double knockdown on preventing G1-to-S transition, with no evidence of cell cycle exit.

To confirm that these knockdowns are indeed inducing a cell cycle arrest, and not merely a delay in cell cycle progression, we performed a series of BrdU

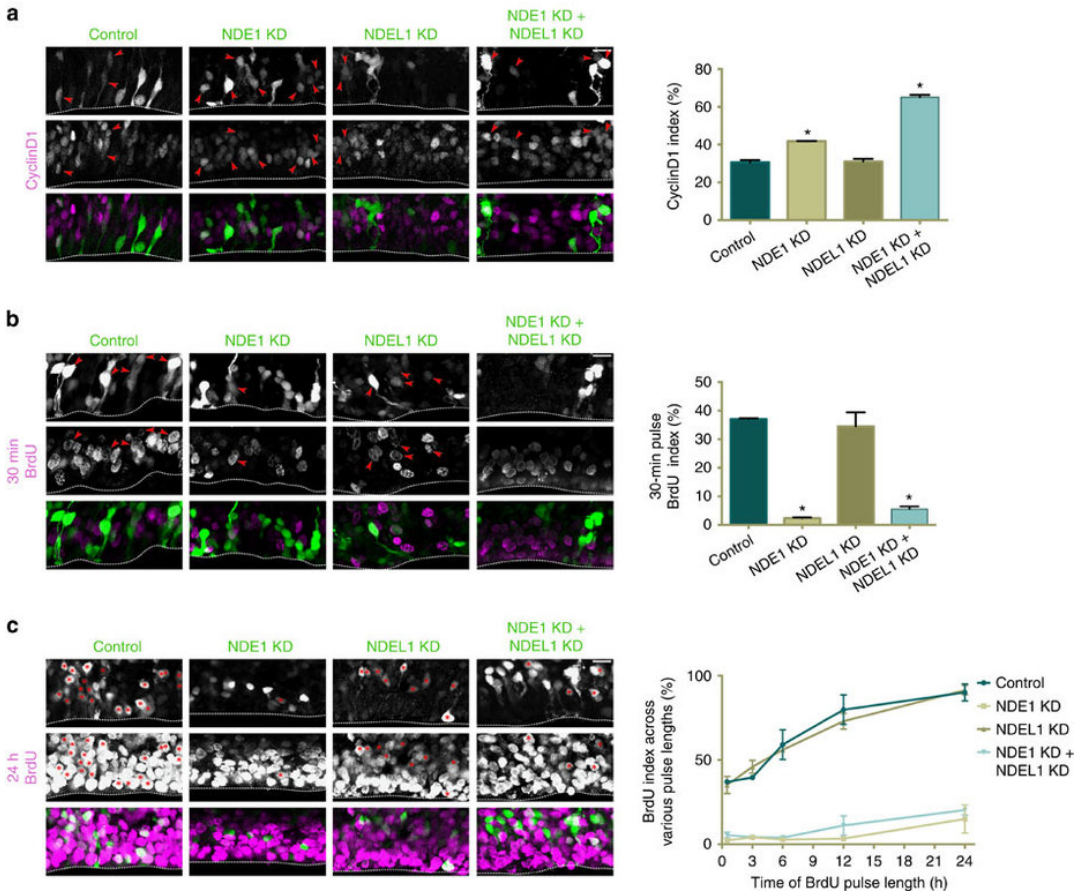

Figure 2.4: Double knockdown of NDE1/NDEL1 arrests cells at the G1-to-S transition with over-elongated primary cilia: E16 rat embryonic brains were electroporated with shRNAs for the various conditions and examined at E19. CyclinD1 staining was used to mark G1 cells, a 30-minute pulse of BrdU used to mark S-phase cells, and BrdU pulses of varying length were used to distinguish RGPs that are arrested during the cell cycle from those actively cycling. The CyclinD1 and BrdU indices used in quantification were calculated as the amount of electroporated radial glia progenitors (RGPs) positive for either marker divided by the total number of electroporated RGP cells. **(A)** NDE1 knockdown caused a small but significant increase in CyclinD1-positive RGP cells, and the NDE1/NDEL1 double knockdown caused an even more substantial doubling of CyclinD1-positive RGP cells. There was no apparent difference between NDEL1 knockdown and control conditions. CylinD1-positive RGP cells tended to have soma located further away from the ventricular surface. Arrowheads mark electroporated RGP nuclei positive for CyclinD1. **(B)** NDE1 and NDE1/NDEL1 double knockdown caused a reciprocal and severe decrease in BrdU labelled RGP cells. Again there was no significant difference between NDEL1 knockdown and control conditions. Arrowheads mark electroporated RGP nuclei positive for BrdU. **(C)** BrdU pulses of varying length revealed an increase in BrdU incorporation among control RGPs and NDEL1 knockdown RGPs, in contrast to the very minimal increase in BrdU incorporation over 24 hours in the NDE1 and NDE1/NDEL1 knockdown conditions. Unpaired *t*-tests comparing knockdown conditions at each hour revealed no significant difference between control and NDEL1 knockdown, or NDE1 and NDE1/NDEL1 knockdown, while those two pairings were significantly different at every time point observed. The initial BrdU index for the 30 minute time point was reused from Figure 3B. Asterisks mark electroporated RGP cells positive for BrdU. Data are presented as mean ± SEM. Unpaired *t*-tests used to compare conditions, * for $p<0.05$, $n=3$ embryonic brains from different mothers. Scale bar, 10μm in (A), (B), and (C). See Supplementary Figures 2 and 3 for further information regarding proliferation status cell cycle of knockdown RGP cells. Dashed line indicates ventricle surface.

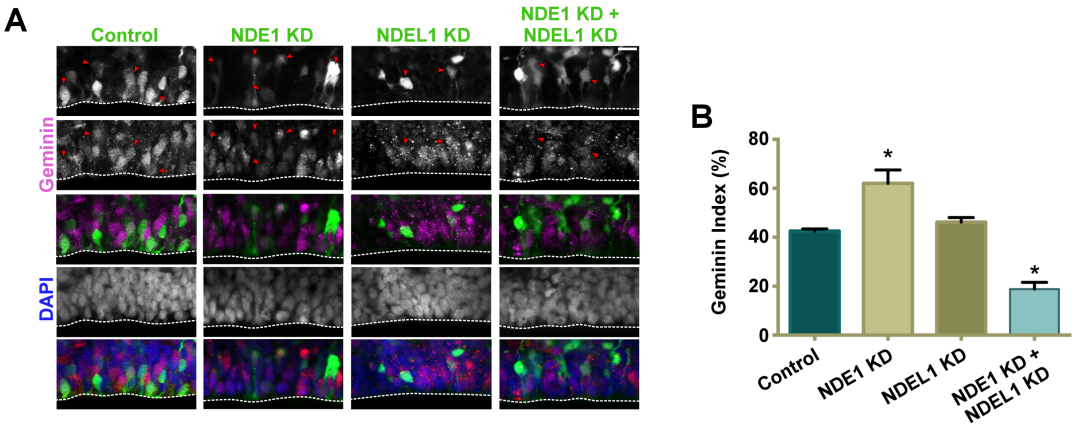

Figure 2.5: The effects of NDE1 and NDEL1 knockdowns on RGPs in G2: E16 rat embryonic brains were electroporated with shRNAs to the various conditions described below. All analysis was done at E19. **(A)** Representative images of RGP cells across the various specified conditions stained for the S/G2 marker Geminin. **(B)** Quantification of the Geminin index across conditions, defined at the ratio of electroporated RGP cells positive for Geminin divided by the total number of electroporated RGP cells. There was a significant increase in Geminin labeling between the NDE1 KD and control conditions, and a significant decrease between the NDE1/NDEL1 KD and control conditions. Data are presented as mean ± SEM. Unpaired t-tests used to compare conditions, * for p< 0.05, n=3 embryonic brains from different mothers. Scale bar, 10μm in (A).

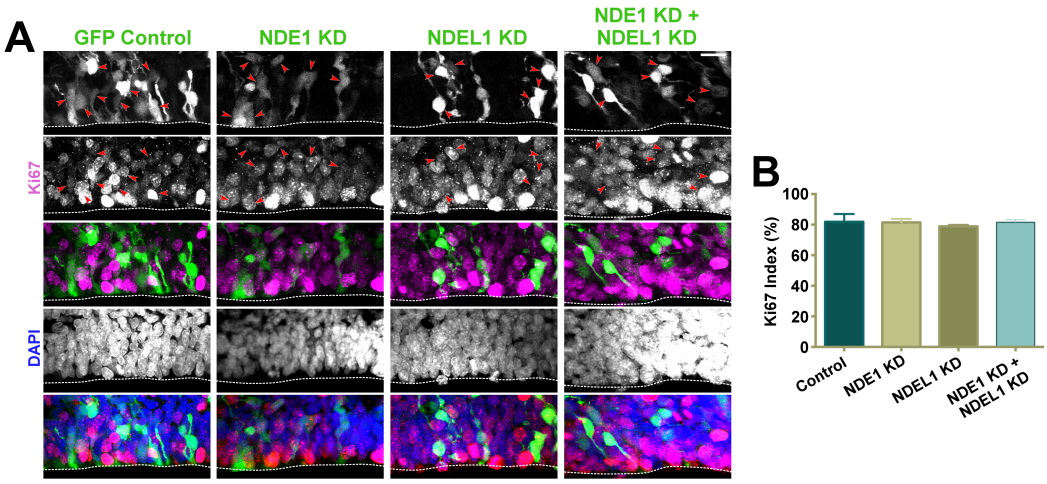

Figure 2.6: The effects of NDE1 and NDEL1 knockdowns on actively proliferating RGPs: E16 rat embryonic brains were electroporated with shRNAs to the various conditions described below. All analysis was done at E19. **(A)** Representative images of RGP cells across the various specified conditions stained for the proliferation marker Ki67. **(B)** Quantification of the Ki67 index across conditions, defined as the ratio of electroporated RGP cells positive for Ki67 divided by the total number of electroporated RGP cells. No significant differences were found between conditions. For all panels, RGP cells were identified on the basis of morphology and the possession of apical process. Arrowheads mark double labeled RGP cells. Scale bar, 10μm. 2-channel composite is presented with electroporation signal in green and immunocytochemical signal in magenta. 3-channel composite is presented with electroporation signal in green, immunocytochemical signal in red, and DAPI in blue. Data presented as mean ± SEM. Unpaired t-test used for comparisons, * for p< 0.05, n=3 embryonic brains from different mothers. Data are presented as mean ± SEM. Unpaired t-tests used to compare conditions, n=3 embryonic brains from different mothers. Scale bar, 10μm in (A).

pulses of varying durations. Intraperitoneal injections of BrdU every 3 hours, for up to 24 hours, revealed that nearly 100% of RGPs electroporated with control vector or NDEL1 knockdown were BrdU positive (Figure 2.4C). In striking contrast, we saw only a small increase in the fraction of BrdU incorporating cells over longer pulse lengths in the NDE1 knockdown and NDE1/NDEL1 double knockdown conditions (Figure 2.4C). Furthermore, this small increase is likely to result from the necessity of beginning BrdU pulses earlier (only 48 hours after electroporation), when the shRNA knockdown is just starting to take effect.

In order to further understand the G1-to-S arrest seen in the NDE1/NDEL1 double knockdown condition, we began to consider cellular processes necessary at this transition. NDE1 has been reported to be involved in primary cilia resorption in cultured non-neuronal cells, with NDE1 knockdown resulting in ciliary over-elongation (Kim et al., 2011). Proper initiation of ciliary resorption was required, in turn, for G0- or G1-to-S-phase progression in proliferating ciliated cells (Jackson, 2011; Kim et al., 2011; Li et al., 2011). To test whether the G1 accumulation we see in NDE1/NDEL1 double knockdown might reflect a related mechanism, we co-electroporated control and shRNA-encoding plasmids with the ciliary marker Arl13B-mCherry, which reliably labels primary cilia (Bangs et al., 2015; Paridaen et al., 2013) (Supplementary Fig. 2.7A), and examined primary cilia length. NDE1 knockdown caused moderate elongation of RGP cell primary cilia (Figure 2.7A-B). In contrast, the combined NDE1/NDEL1 knockdown caused a doubling of primary cilia length compared to controls (Figure 2.7A-B). The NDE1/NDEL1 double knockdown also had the greatest effect on increasing primary cilia length in cultured retinal

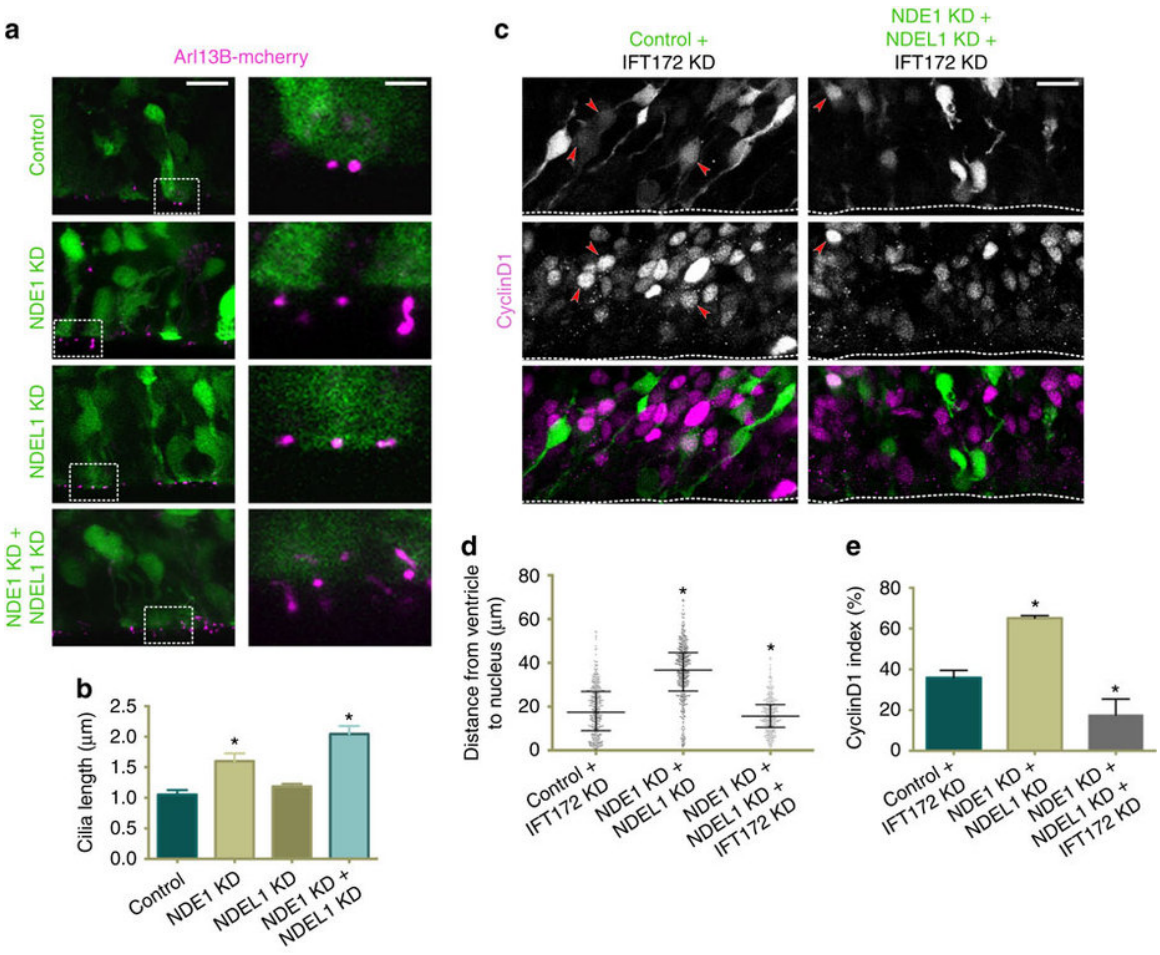

Figure 2.7: The G1-to-S arrest of radial glia progenitors in the NDE1/NDEL1 double knockdown condition involves disruptions in the regulation of primary cilia length: E16 rat embryonic brains were electroporated with the ciliary membrane marker Arl13B and shRNAs to the various conditions described below. All analysis was done at E19. **(A-B)** NDE1 knockdown resulted in a significant increase in primary cilia length among electroporated radial glia progenitors (RGPs), though the NDE1/NDEL1 knockdown caused an even greater doubling of primary cilia length. NDEL1 knockdown resulted in no change from control RGP cilia length. **(C-E)** Inhibition of primary cilia assembly by knockdown of the intraflagellar transport protein IFT172 rescued the CyclinD1 accumulation seen in the NDE1/NDEL1 double knockdown (E). Furthermore, the distribution of apical process lengths of the NDE1/NDEL1/IFT172 triple knockdown more closely mirrored the NDE1 knockdown alone (Figure 2C). Arrowheads mark electroporated RGP cells positive for CyclinD1. Dashed line indicates ventricle surface. Data are presented as mean ± SEM. Unpaired *t*-tests used to compare conditions (B, E), Kolmogorov-Smirnov test used for non-parametric distributions (D), * for $p<0.05$, $n=3$ embryonic brains from different mothers. Scale bar, 10µm in (A, C), and 2.5µm in insert panels for (A). Also see Supplementary Figures 4 and 5.

epithelia cells (Figure 2.8), confirming the synergistic effect of NDE1 and NDEL1 knockdown in this process. To test for a causative role of the primary cilia in the G1-to-S transition arrest, we utilized knockdown of IFT172 – a component of the

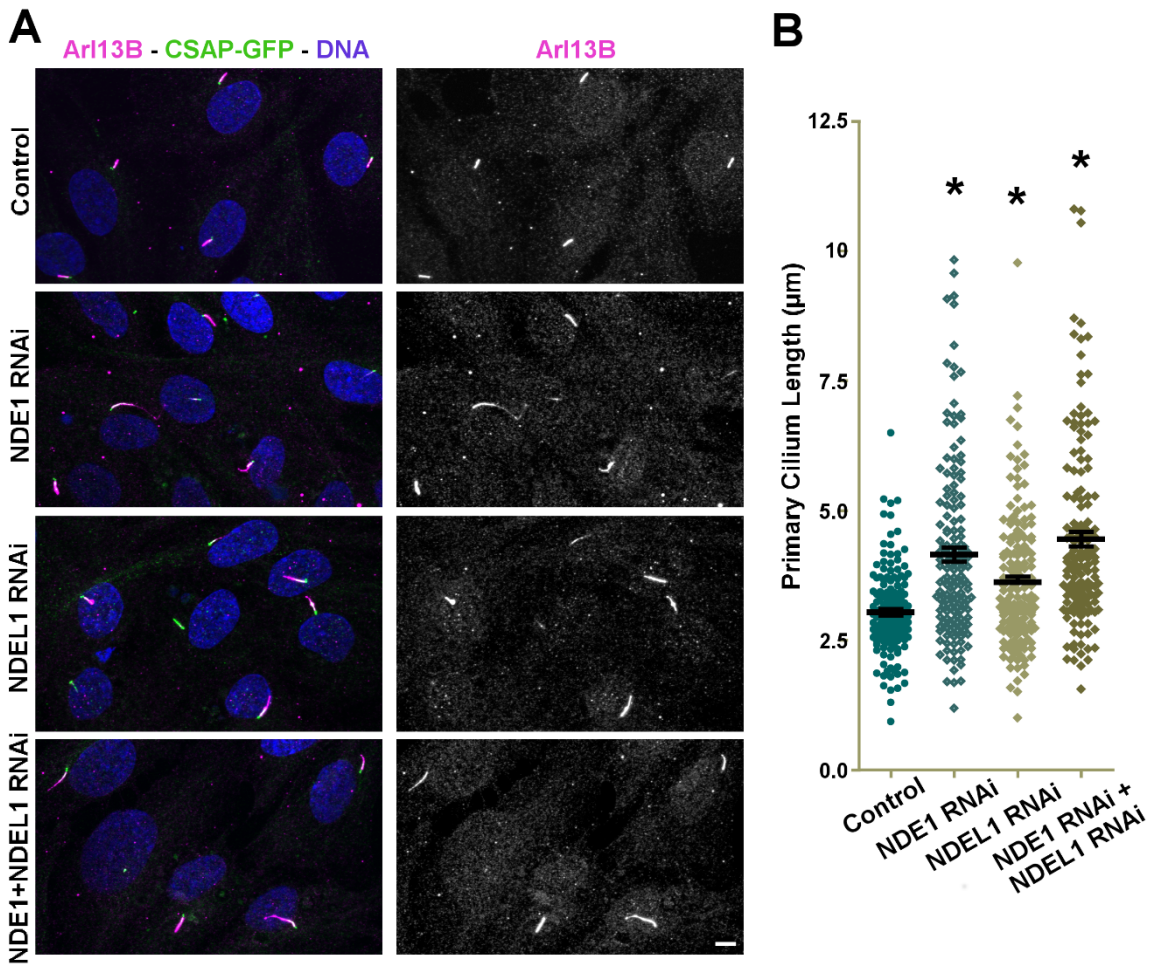

Figure 2.8: NDE1, NDEL1, or knockdown of both proteins leads to increased primary cilia length in human cells. (A) Immunofluorescence micrographs of serum-starved control and RNAi treated hTERT- RPE1-GFP-CSAP cells stained as labeled. Scale bar, 5µm. **(B)** Primary cilia length in control and RNAi conditions as labeled. RPE1 cells (n=3x50). Error bars represent ± SEM. Statistical analyses performed using Kruskall-Wallis with Dunn's multiple comparison test, $p<0.05$, values labeled with *.

anterograde IFT (intraflagellar transport) complex critical for primary cilia assembly (Ezratty et al., 2011) – to inhibit ciliogenesis in RGPs (Figure 2.9A-B). Whereas IFT172 knockdown itself had little effect on the fraction of RGPs in G1, it rescued the G1-to-S block seen in NDE1/NDEL1 double knockdown, as judged by the decrease in the number of CyclinD1 positive RGPs (Figure 2.7C,E). Furthermore, analysis of soma position revealed that the majority of RGPs displayed an INM phenotype similar to NDE1 knockdown alone, suggesting that RGPs now progressed

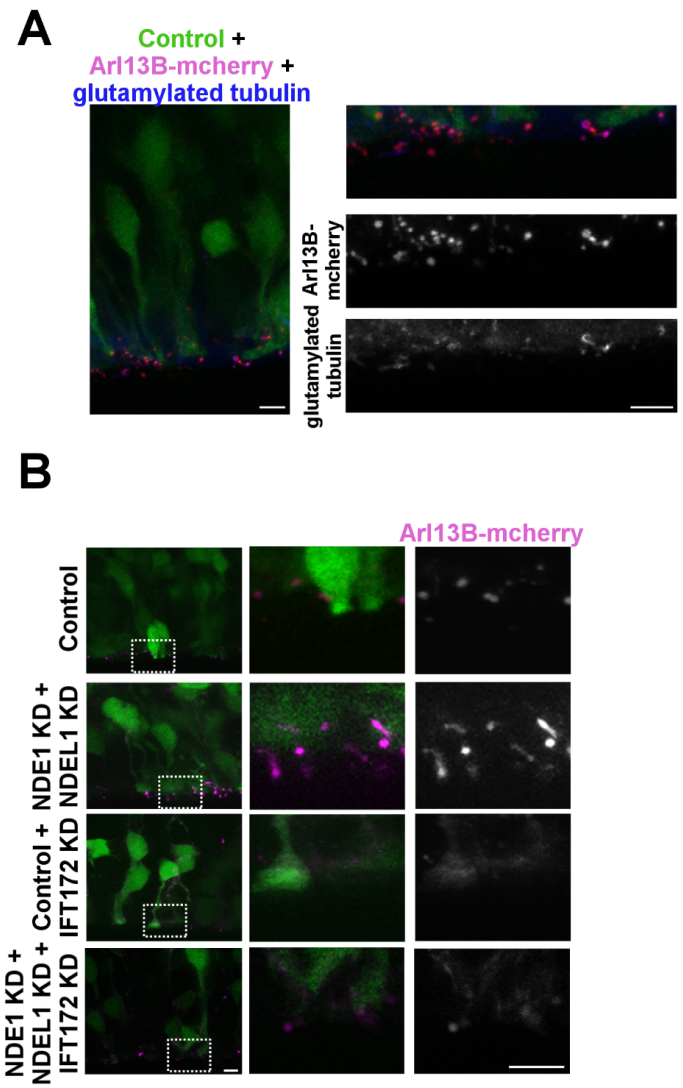

Figure 2.9: IFT172 knockdown overcomes the deregulation of primary cilia length seen upon NDE1/NDEL1 double knockdown: E16 rat embryonic brains were electroporated with the ciliary membrane marker Arl13B and shRNAs to the various conditions described below. All analysis was done at E19. **(A)** Control staining of brain slices expressing GFP empty vector and Arl13B-mCherry (magenta) with glutamylated tubulin - a ciliary axoneme and basal body marker. **(B)** Inhibition of primary cilia assembly by knockdown of the intraflagellar transport protein IFT172, decreases the occurrence of elongated primary cilia in the NDE1/NDEL1 double knockdown. Scale bars represent 5μm.

through G1 into S-phase and were arrested during apical INM in G2 (Figure 2.7C-D). These results further support the necessity of either NDE1 or NDEL1 in initiating resorption of the primary cilia to allow for transition from G1 into S-phase.

Staining for NDE1/NDEL1 in RGP cells revealed some perinuclear staining that overlapped with the intermediate chain of dynein (Figure 2.10A). This perinuclear staining was around RGP cells as marked by Pax6, and was more common around RGP nuclei located closer to the ventricular surface (Figure 2.10B). *En face* staining also revealed that the NDE1/NDEL1 immunohistochemial signal

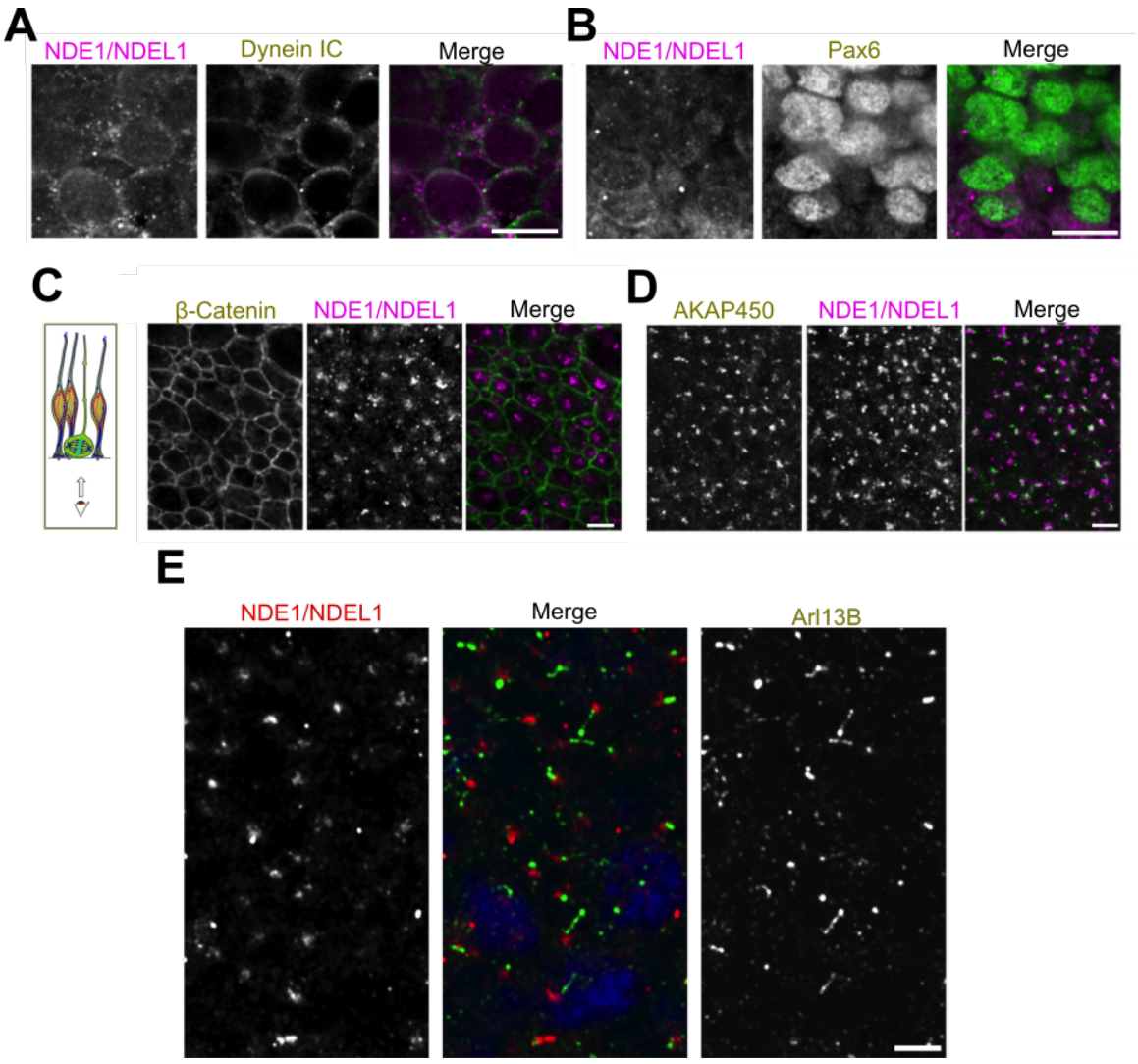

Figure 2.10: NDE1/NDEL1 Staining in Radial Glia: An antibody that recognizes both NDE1 and NDEL1 was used to localize endogenous protein in radial glia progenitor (RGP) cells at embryonic day 19. **(A-B)** Perinuclear NDE1/NDEL1 signal overlaps with dynein intermediate chain, surrounding Pax6 positive RGP cells. **(C)** NDE1/NDEL1 signal localizes in the middle of RGP endfeet when viewed by *en face* imaging, the edges of which are marked by ß-Catenin. **(D)** This NDE1/NDEL1 signal colocalized with the pericentriolar matrix marker AKAP450. **(E)** Though the NDE1/NDEL1 immunohistochemical signal localized to the pericentriolar matrix at the base of the cilia, it did not colocalize with Arl13B, which marks the primary cilia proper. Scale bar is 10µm in (A,B) and 2µm in (C,D), and 1µm in (E).

was centrally located in the RGP endfoot and overlapped with the pericentriolar matrix (Figure 2.10C-D). Interestingly, though NDE1/NDEL1 signal was very strong at the pericentriolar matrix at the base of the primary cilia, there was no NDE1/NDEL1 staining within the primary cilia itself, as marked by Arl13B (Figure

2.10E). These results suggest that there is a pool of NDE1 at the nuclear envelope during late-G2 dynein recruitment, and a substantial pool around the centrosome but not within the primary cilia itself.

Cross Rescue Reveals Shared and Unique Functions

To define the relative functions of NDE1 and NDEL1 further, in addition to ensuring RNAi specificity, we performed rescue experiments using RNAi-resistant NDE1 and NDEL1 tagged with mCherry (Figure 2.1C). NDE1 or NDEL1 overexpression each largely rescued the neuronal migration defect seen in knockdown of either NDE1 or NDEL1 (Figure 2.11A-C). Although NDEL1 overexpression only partially rescued the neuronal migration defect seen in NDE1 knockdown, these results suggest that each paralog alone is sufficient for postmitotic migration. Live-imaging of RGP cells further revealed that RNAi-resistant NDE1 fully rescued NDE1 RNAi-inhibited apical INM, mitosis, and subsequent basal migration (Figure 2.12A, Supplementary Movies 5 and 6). In addition, fixed imaging results demonstrated full rescue of somal positioning (Figure 2.12B-C) as well as mitotic index (Figure 2.12D), both in NDE1 RNAi and NDE1/NDEL1 double knockdown cells (Figure 2.12E-G). These results indicate that NDE1 alone is sufficient for INM and cell-cycle progression.

We also tested for functional complementation of the two paralogs by overexpressing NDEL1 in NDE1 knockdown, and NDE1 in NDEL1 knockdown RGPs. Live imaging revealed that NDEL1 overexpression fully rescues apical INM, but, surprisingly, the nuclei remained at the ventricle for hours without entering mitosis (Figure 2.13A, Supplementary Movie 7). Fixed imaging confirmed the distribution of

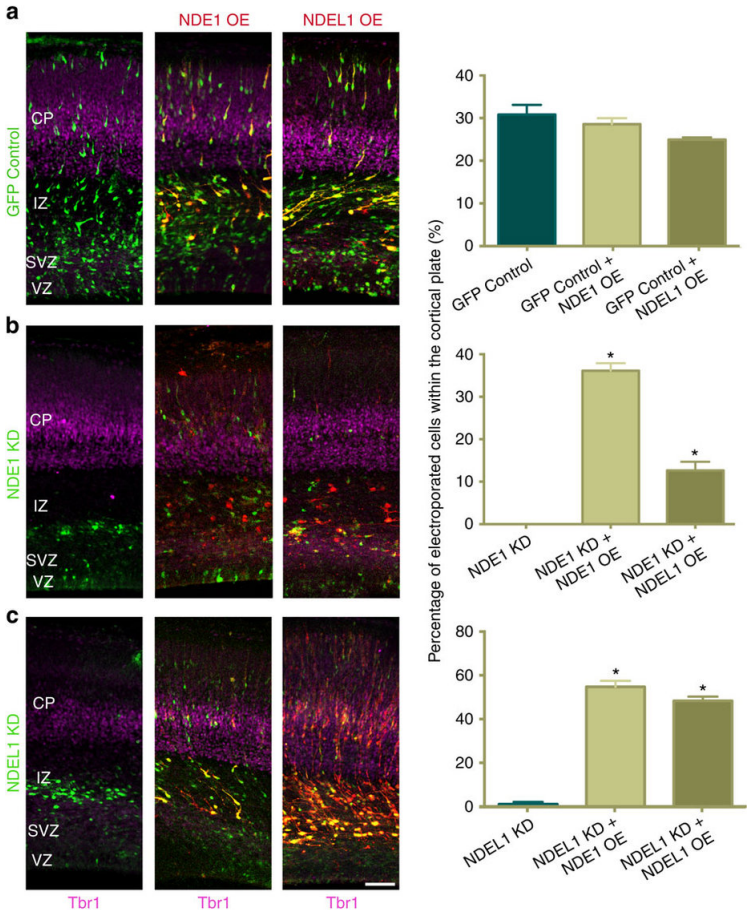

Figure 2.11: NDE1 or NDEL1 overexpression can largely rescue the neuronal migration defects seen after knockdown of either protein: To test for RNAi rescue and functional complementation, embryonic rat brains were co-electroporated at E16 with shRNA to the various conditions with cDNA encoding RNAi-resistant proteins for self-rescue, and standard cDNA for cross-rescue. All analyses were done at E20. Quantification of the amount of electroporated cells migrating into the cortical plate (CP) is shown at right. **(A)** Overexpression of NDE1 and NDEL1 produced no significant change in the amount of neurons migrating into the CP. **(B)** NDE1 knockdown with overexpression of RNAi-resistant NDE1 rescued neuronal migration into the CP. Overexpression of NDEL1 during NDE1 knockdown partially rescued neuronal migration into the CP. **(C)** Overexpression of RNAi-resistant NDEL1 or NDE1 with NDEL1 knockdown rescued the neuronal migration into the CP, even increasing the fraction of electroporated cells in the CP. Data presented as mean ± SEM, and unpaired *t*-tests used for all comparisons, * for $p<0.05$, $n=3$ embryonic brains from different mothers. Scale bars, 50μm.

RGP soma was radically altered by NDEL1 overexpression in NDE1 knockdown RGPs, with nearly all RGP nuclei located adjacent to the ventricle (Figure 2.13B-C). Surprisingly, a similar effect on somal distribution was seen with NDEL1 overexpression alone in wild type rat brain (Figure 2.13B-C).

NDE1 and NDEL1 are known to be critical during the progression of mitosis in non-neuronal cells, with inhibition of either paralog resulting in prometaphase-metaphase arrest (Liang et al., 2007; Stehman et al., 2007; Vergnolle and Taylor, 2007). Therefore it was surprising that RGP cells overexpressing NDEL1 alone, or in

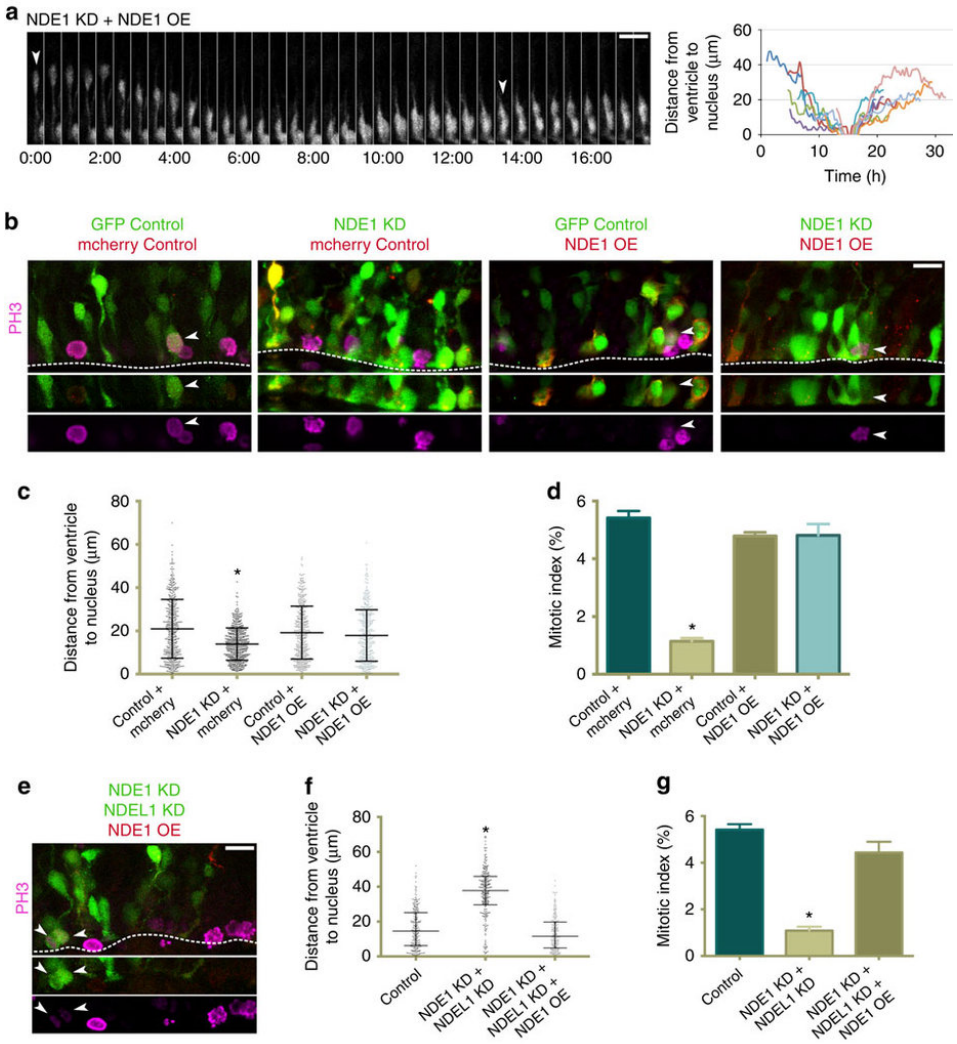

Figure 2.12: RNAi-resistant NDE1 overexpression rescues all defects seen in radial glia progenitors across knockdown conditions: RNAi-resistant NDE1 was co-electroporated into embryonic rat brains with a GFP control empty vector or along with NDE1 shRNA or NDE1 and NDEL1 shRNAs at E16, and analyzed at E20. **(A)** Restoration of apical interkinetic nuclear migration, mitosis, and subsequent basal migration of progeny measured by live imaging. Arrowhead marks the radial glia progenitor (RGP) of interest. Montage panels are shown at 30 minute intervals. Full movie can be found in Supplementary Material (see Supplementary Movie 5), as well as an additional movie that more clearly displays the 2 daughter cell progeny (Supplementary Movie 6). **(B)** Representative images of RGPs stained for PH3 within the VZ in various specified co-expression conditions. Arrowheads mark mitotic electroporated RGPs. Dashed line indicates ventricular surface. **(C)** Soma position of RGPs with RNAi-resistant NDE1 overexpressed during NDE1 knockdown indicates that the somal positioning distribution is rescued. **(D)** Overexpression of RNAi-resistant NDE1 with NDE1 knockdown also rescues the mitotic index. **(E)** Representative image of NDE1/NDEL1 double knockdown with overexpression of RNAi-NDE1, stained for PH3. Arrowheads mark mitotic electroporated RGPs. Dashed line indicates the ventricular surface. **(F-G)** Overexpression of RNAi-resistant NDE1 with double NDE1/NDEL1 knockdown rescues the distribution of RGP nuclei in the VZ (F) and restores the mitotic index of RGP cells (G) Data presented as scatterplot in (C) and (F) with bars representing the median ± the interquartile range, and as mean ± SEM in (D) and (G). Kolmogorov-Smirnov test for non-parametric distributions used in (C) (* for $p<0.05$, n=428-474 RGP cells in [C] and n=224-260 RGP cells in [F]). Unpaired t-test used in (D) and (G) (* for $p<0.05$, n=3 embryonic brains from different mothers). Scale bars, 10μm.

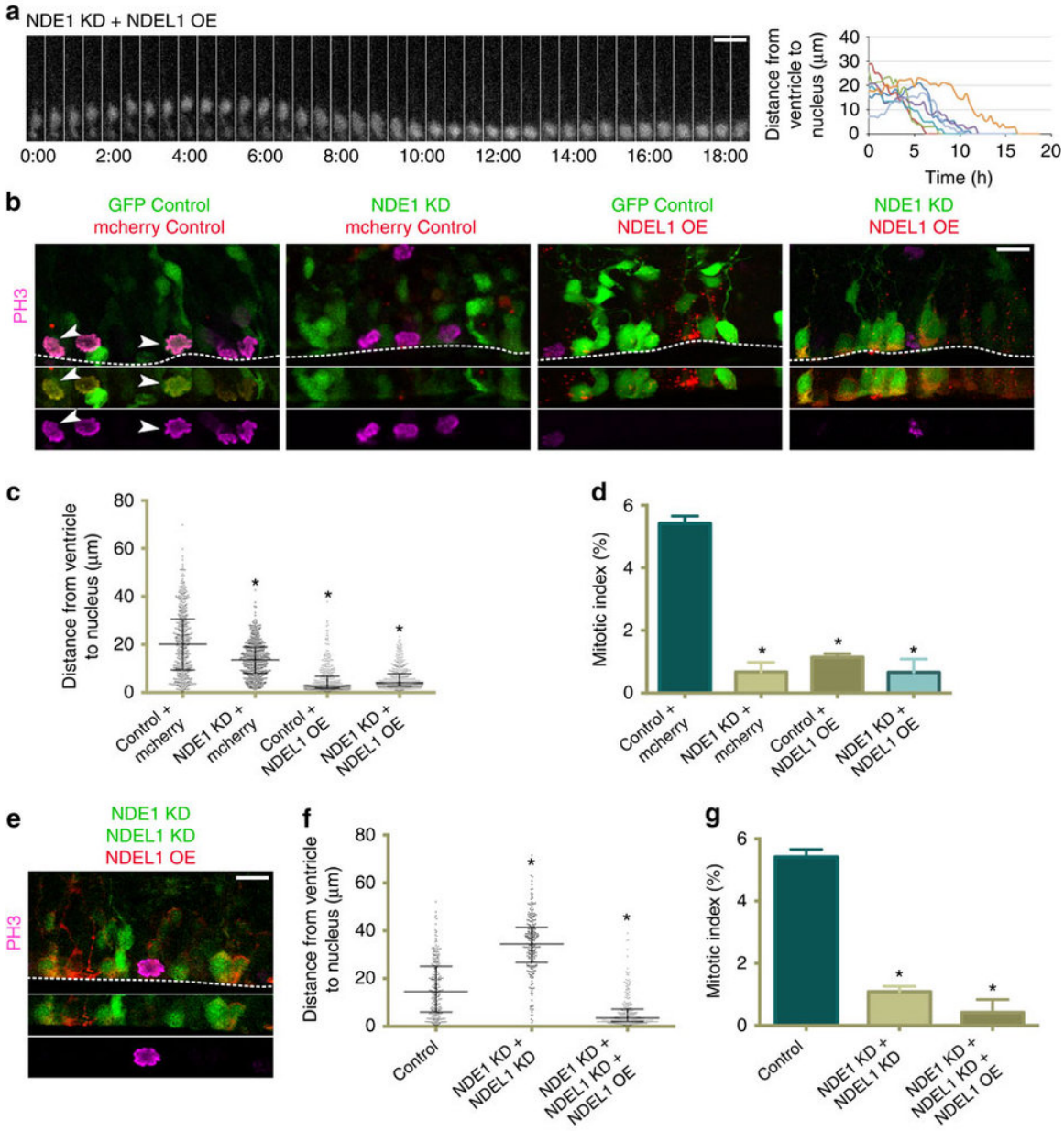

Figure 2.13: NDEL1 overexpression rescues apical nuclear migration in NDE1 deficient radial glia progenitors, but does not rescue entry into mitosis: cDNA for NDEL1 was co-electroporated into embryonic rat brains with a GFP control empty vector or along with NDE1 shRNA or NDE1 and NDEL1 shRNAs at E16, and analyzed at E20. **(A)** NDEL1 overexpression rescues apical interkinetic nuclear migration in radial glia progenitors (RGPs) where NDE1 has been knocked down, but these cells accumulate at the ventricular surface after apical INM, where they remain for hours without any evidence of mitosis. Montage panels are shown at 30 minute intervals. Full movie can be found in Supplementary Material (see Supplementary Movie 7). **(B)** Representative images of NDEL1 overexpression on both a wild type and NDE1 RNAi background reveals an accumulation of the majority of RGP nuclei at the ventricular surface in a PH3 negative state. Arrowheads mark electroporated cells in mitosis. Dashed line represents the ventricular surface. **(C)** NDEL1 overexpression causes nearly all RGP soma to accumulate at the ventricular surface regardless of whether NDEL1 is overexpressed on a wild type or NDE1 RNAi background.

(D) Even though NDEL1 overexpression caused an accumulation of RGP soma at the ventricular surface, the mitotic index remained reduced to a level similar to NDE1 knockdown alone. **(E)** Representative image of RNAi-resistant NDEL1 overexpression with NDE1/NDEL1 double knockdown in RGP cells stained for PH3. Dashed line represents the ventricular surface. **(F-G)** RNAi-resistant NDEL1 overexpression with NDE1/NDEL1 double knockdown caused an accumulation of RGP soma at the ventricular surface similar to overexpression of NDEL1 on a wild type or NDE1 deficient background (F), and once again failed to rescue the mitotic index (G) Data presented as scatterplot in (C) and (F) with bars representing the median ± the interquartile range, and as mean ± SEM in (D) and (G). Kolmogorov-Smirnov test for non-parametric distributions used in (C) (* for $p<0.05$, n=405-475 RGP cells in [C] and n=245-272 RGP cells in [F]). Unpaired t-test used in (D) and (G) (* for $p<0.05$, n=3 embryonic brains from different mothers). Scale bars, 10µm. Also see Figure 2.14.

combination with NDE1 shRNA, were nearly all negative for PH3 (Figure 2.13B), with mitotic index reduced to a level comparable to that resulting from NDE1 knockdown (Figure 2.13D). The nuclear envelope in these ventricular surface-arrested cells was also observed to remain intact, as determined by staining for lamin-associated protein 2 (LAP2; Supplementary Fig. 2.14B). DNA remained

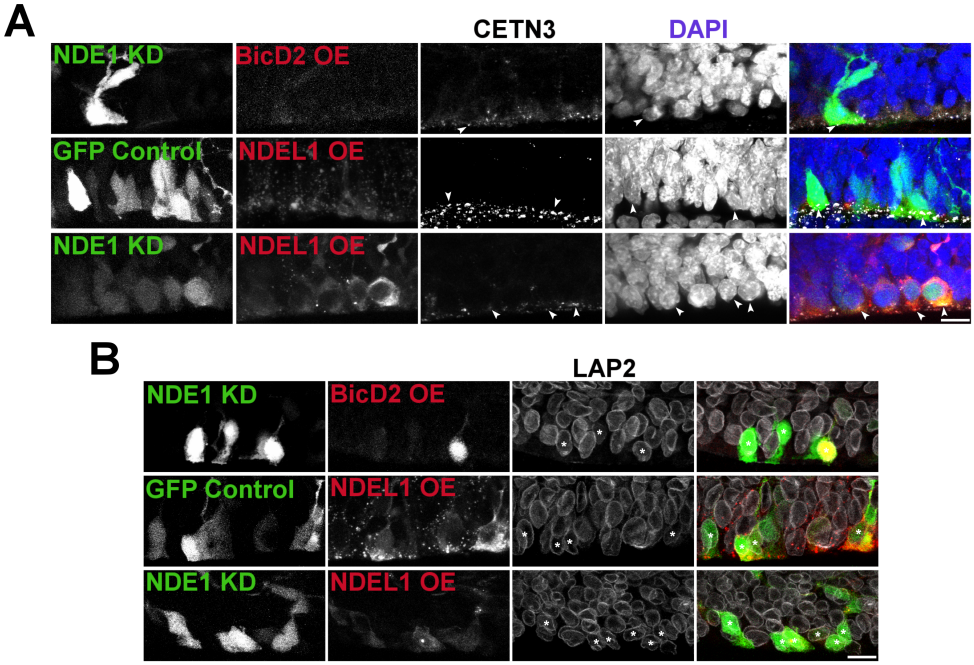

Figure 2.14: RGP cells with nuclei that have accumulated at the ventricular surface appear to be truly premitotic: (A) Staining for centrin3 (CETN3) and DAPI revealed that RGP nuclei that had accumulated at the ventricular surface had uncondensed chromosomes and centrosomes that remained un- separated and localized at the ventricular surface. Arrowheads mark centrosomes and DAPI signal of electroporated RGP cells. (B) Staining for lamin-associated protein 2 (LAP2) across the specified conditions reveals that these RGP nuclei had intact nuclear evidence with no evidence of invagination or breakdown. Asterisks mark the nuclei of electroporated RGP cells. Scale bar, 10µm.

uncondensed, as judged by DAPI staining, and centrosomes remained un-separated at the RGP apical endfoot (Hu et al., 2013; Spear and Erickson, 2012) (Supplementary Fig. 2.14A). Similar results were obtained when RNAi-resistant NDEL1 was used to rescue the NDE1/NDEL1 double knockdown (Figure 2.13E-G).

Thus, NDEL1 overexpression can compensate for NDE1 during G1-to-S progression and apical INM, but excess NDEL1 induces a premitotic arrest in RGP cells even after the nucleus has reached the ventricular surface, preventing them from entering mitosis.

BicD2 Expression Reinforces a Novel G2-to-M Arrest

Our lab previously found that overexpression of BicD2, the limiting protein for dynein recruitment to the nuclear envelope during early G2 (Hu et al., 2013), can rescue RNAi knockdown for genes involved in either the early- or late-G2 dynein recruitment pathways. This resulted in restoration of apical INM as well as subsequent mitosis (Hu et al., 2013). Importantly, BicD2 is only targeted to the nuclear envelope during G2, providing an experimental means to restore nuclear envelope dynein recruitment exclusively during this cell cycle stage (Baffet et al., 2015).

In the current study, overexpression of BicD2 along with NDE1 shRNA fully rescued apical INM, though, in this case, nuclei accumulated at the ventricle for prolonged periods of time without detectable signs of mitotic entry (Figure 2.15A, Supplementary Movie 8). Consistent with these results, the majority of RGP soma in fixed brain sections were located at the ventricular surface (Figure 2.15B-C) with intact nuclear envelope, uncondensed DNA, and un-separated apical centrosomes

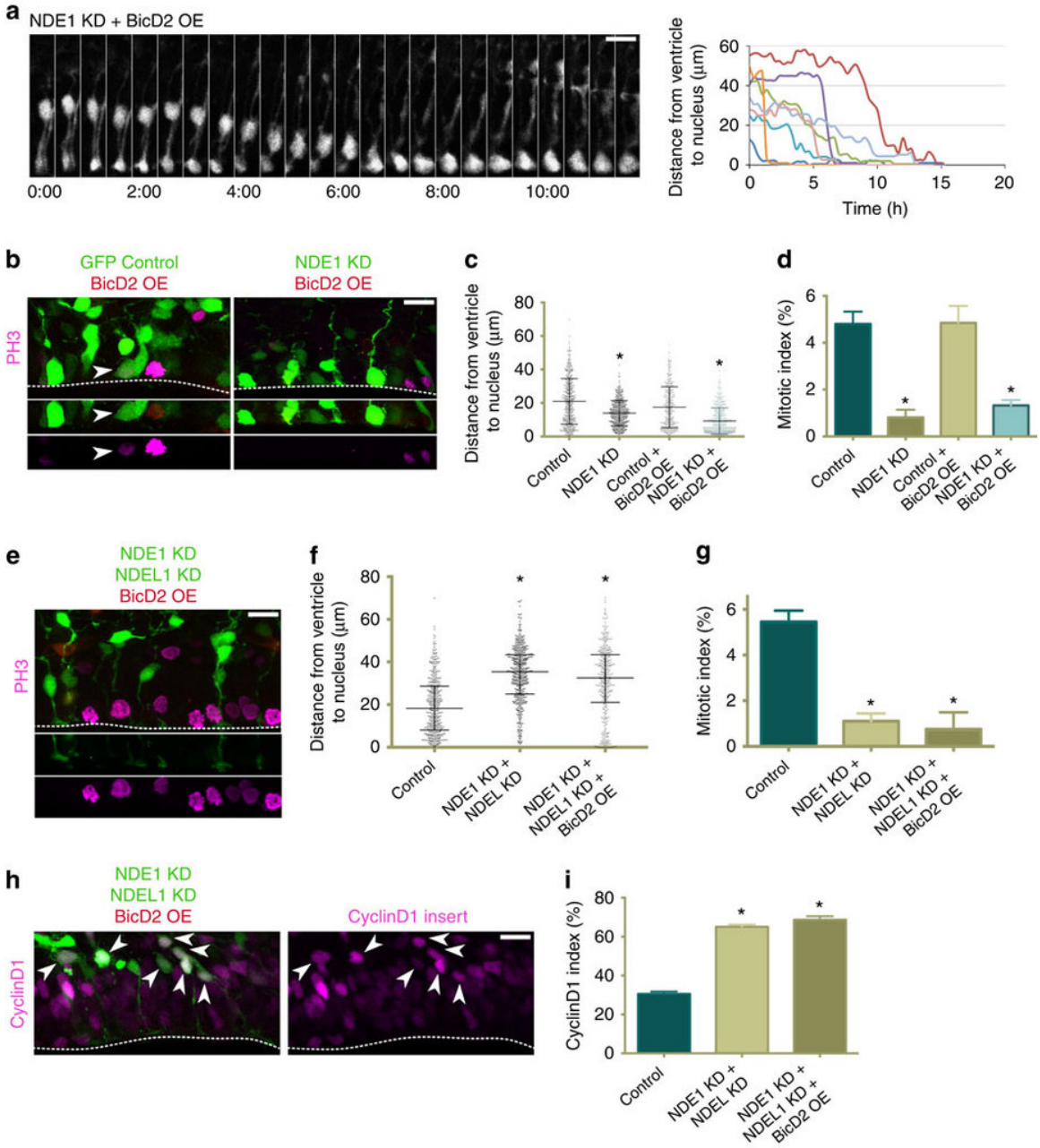

Figure 2.15: BicD2 overexpression rescues apical nuclear migration but not entry into mitosis in radial glia progenitors depleted of NDE1: cDNA for full-length BicD2 was co-electroporated into embryonic rat brains with a GFP control empty vector or along with NDE1 shRNA or NDE1 and NDEL1 shRNAs at E16, and analyzed at E20. **(A)** The overexpression of BicD2 in radial glia progenitors (RGPs) lacking NDE1 restores apical migration, though the soma accumulate at the ventricle for hours without any evidence of mitosis. Montage panels are shown at 30 minute intervals. Full movie can be found in Supplementary Material (see Supplementary Movie 8). **(B)** Representative images of BicD2 overexpression on both a wildtype and NDE1 knockdown background with staining for PH3. Arrowheads mark mitoses in electroporated cells. Dashed line indicates ventricular surface. **(C)** BicD2 overexpression did not alter the somal distribution of control RGP cells but caused the vast majority of NDE1 knockdown RGP soma to accumulate at the ventricular surface. **(D)** Despite the accumulation of RGP soma at the ventricle in NDE1 knockdown with BicD2 overexpression, the mitotic index

remained reduced. **(E)** Representative image of RGP cells with BicD2 overexpression along with double NDE1/NDEL1 knockdown, stained for PH3. Dashed line indicates ventricle. **(F-G)** Overexpression of BicD2 with NDE1/NDEL1 double knockdown fails to rescue the somal distribution pattern (F) or mitotic index (G) of double NDE1/NDEL1 knockdown RGP cells. **(H-I)** The same ratio of RGP nuclei were positive for CyclinD1 whether or not BicD2 was overexpressed along with the double NDE1/NDEL1 knockdown, indicating the prominence of the G1-to-S block in the double knockdown, and the G2 specificity of the BicD2 rescue strategy. Arrowheads mark electroporated RGP nuclei positive for CyclinD1. Dashed line indicates ventricle surface. Data presented as scatterplot in (C) and (F) with bars representing the median ± the interquartile range, and as mean ± SEM in (D), (G), and (I). Kolmogorov-Smirnov test for non-parametric distributions used in (C) (* for $p<0.05$, n=407-591 RGP cells in [C] and n=421-487 RGP cells in [F]). Unpaired t-test used in (D), (G), and (I) (* for $p<0.05$, n=3 embryonic brains from different mothers). Scale bars, 10μm. Also see Figure 2.14.

(Figure 2.14A-B). Altogether these results provide further evidence for the requirement of NDE1 during late-G2 dynein-recruitment to the nuclear envelope, and reveal a new NDE1-specific role after completion of apical INM but before mitotic entry. Notably this NDE1 function cannot be rescued by overexpression of NDEL1 or BicD2.

Intriguingly, when both NDE1 and NDEL1 were knocked down and BicD2 overexpressed, the vast majority of RGP nuclei remain arrested far from the ventricular surface in a CyclinD1 positive state (Figure 2.14E-I), similar to the double NDE1/NDEL1 knockdown condition without BicD2 overexpression. The mitotic index was again severely reduced (Figure 2.14E,G). Since BicD2 overexpression acts solely during G2, these results further confirm that most RGP cells subjected to NDE1/NDEL1 double knockdown were indeed arrested during G1 rather than G2, as suggested earlier by the CyclinD1 and primary cilia results.

NDE1 RNAi Leads to Cortical Lamination Defects and Radial Glia Retention in the Postnatal Neocortex

Though NDE1 and NDEL1 RNAi both block neuronal migration into the cortical plate at E20, it remained unknown whether this was a block in migration or

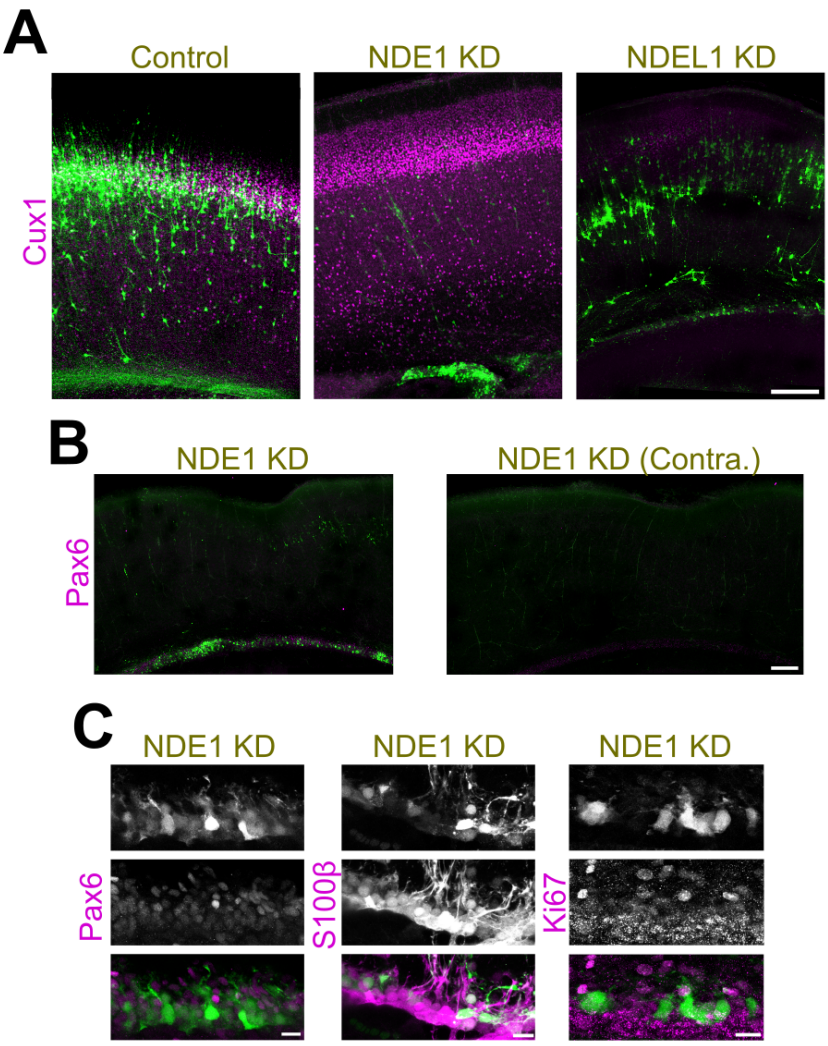

Figure 2.16: NDE1 RNAi blocks neuronal migration and arrests radial glia at the ventricle: (A) Analysis of postnatal day 7 tissue following electroporation at E16 reveals that NDE1 RNAi blocks neuronal migration, while NDEL1 appears to delay neuronal migration. Cux1 used to mark superficial neocortical layers. **(B)** NDE1 RNAi caused a striking accumulation of electroporated radial glia progenitors (RGPs), marked by Pax6, along the ventricle. **(C)** High magnification examination of the arrested RGPs in the postnatal subventricular zone confirm that the electroporated cells are Pax6 positive, are of glial identity and S100ß positive, and some are even positive for the proliferation marker Ki67. Scale bars are 100µm in (A,B), and 10µm in (C).

simply a delay. Co-electroporation of RNAi constructs with a CAG-RFP plasmid for fluorescent labelling revealed that the majority of electroporated cells in the NDE1 RNAi condition remained arrested in the white matter at postnatal day 7 (P7), compared with control cells which nearly all reached the superficial cortical layers II-IV marked by Cux1 staining (Figure 2.16A). Unlike NDE1 RNAi, the majority of NDEL1 RNAi cells migrated out of the white matter and into the neocortex, though many failed to reach layers II-IV (Figure 2.16A). This suggests that while NDE1 RNAi blocked bipolar neuronal migration, NDEL1 RNAi delays it.

Interestingly, there was a large accumulation of NDE1 RNAi electroporated cells lining the ventricle in the SVZ (Figure 2.16B). These cells were never present in control tissue, and stained positive for the RGP maker Pax6, as well as the glial marker S100ß (Figure 2.16B,C). Some of the arrested cells were also positive for the proliferation marker Ki67 (Figure 2.16C). These results suggest that NDE1 RNAi has the potency to arrest RGPs in cell-cycle progression to the point that they are retained at the ventricular surface in a Pax6 positive state, something never seen in control tissue.

The T246 Cdk1 Phosphorylation Site on NDE1 is Critical for G2/M Progression

NDE1 and NDEL1 are the targets of many post-translational modifications, including phosphorylation by cell-cycle dependent kinases such as Cdk1 (Bradshaw et al., 2013). One of the Cdk1 phosphorylation sites on NDE1 – T246 – has been implicated in the G2-to-M transition in cultured cells (Alkuraya et al., 2011). Overexpression of a NDE1 construct in which the T246 residue was replaced with alanine (termed NDE1-T246A) caused an accumulation of HEK293 cells in G2 (Alkuraya et al., 2011), suggesting a role for this residue in mitotic entry. We electroporated NDE1 RNAi and overexpressed RNAi-resistant NDE1-T246A, which rescued apical INM in RGPs but lead to a reduction in the mitotic index, similar to the G2-to-M block seen before (Figure 2.17A-C). Overexpression of NDE1-T246A alone did not appear to have a dominant negative effect, though the mitotic index was slightly reduced from control levels (Figure 2.17B).

Cell culture work on NDE1 phosphorylation from our lab has revealed triply phosphorylated NDE1 (at the T215, T243, and T246 sites) strongly localized to the

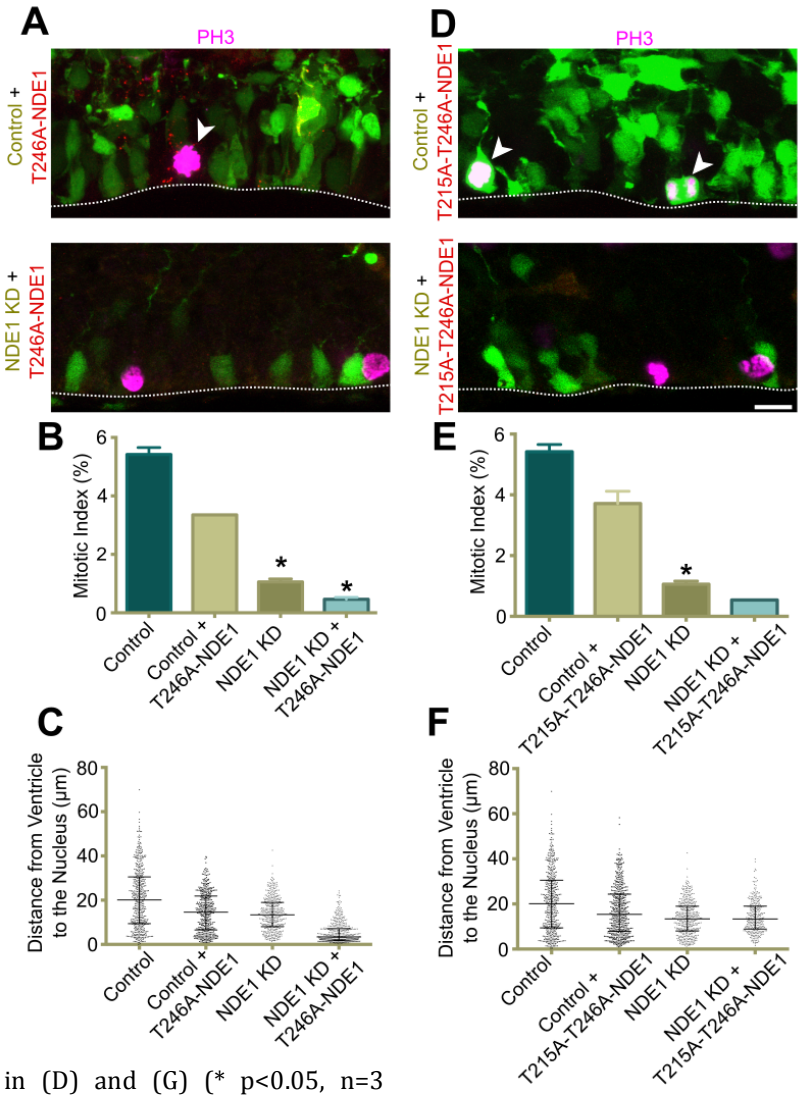

Figure 2.17: The T246 Phosphorylation Site on NDE1 is Involved in the G2-to-M Transition: GFP control plasmid or NDE1 RNAi was electroporated with T246A-NDE1 or T215A-T246A-NDE1 overexpression into E16 embryonic rat brains, and analyzed at E20. **(A-C)** Rescue with the T246A-NDE1 phosphomutant construct recapitulated the G2-to-M arrest seen in Figures 2.14 and 2.15, with a reduction in the mitotic index and an accumulation of radial glia (RGP) nuclei at the ventricle. **(D-F)** Rescue with the T215A-T246A-NDE1 phosphomutant construct does not rescue late-G2 apical INM, and the mitotic index and RGP somal distribution reflect the NDE1 RNAi condition. Data presented as scatterplot in (C) and (F) with bars representing the median ± the interquartile range, and as mean ± SEM in (D) and (E). Unpaired *t*-test used in (D) and (G) (* $p<0.05$, n=3 embryonic brains from different mothers). Scale bars, 10µm.

nuclear envelope during late G2 and pulled down increased amount of CENP-F (Wynne and Vallee, unpublished). NDE1 RNAi followed by rescue with a doubly phosphomutated NDE1 (NDE1-T215A-T246A) did not rescue apical INM, as indicated by apical process length distribution and mitotic index (Figure 2.17D-F). Once again there was a slight reduction of the mitotic index from control tissue where NDE1-T215A-T246A was not overexpressed (Figure 2C, Figure 2.17E). This

data provides preliminary evidence for a role of Cdk1-phosphorylation of NDE1 in RGPs.

Modeling a NDE1 Mutation that Leads to Microcephaly

Intriguingly two separate studies found unrelated families to possess the same mutation in NDE1 that leads to microcephaly (Alkuraya et al., 2011; Bakircioglu et al., 2011). This mutation – a homozygous deletion of two nucleotides at the 684-685 positions – results in a novel C-terminal region on NDE1 after the 229th amino acid, and a premature truncation of the protein. One study found that this resulted in ubiquitination and degradation of all NDE1 (Alkuraya et al., 2011), while another found that NDE1 was still present (Bakircioglu et al., 2011). We recreated the same mutation using a human NDE1 overexpression construct driven by a CAG promoter (termed delAC-NDE1), and found that NDE1 knockdown with overexpression of the delAC-NDE1 construct arrested the majority of RGP nuclei at a distance comparable to NDE1 RNAi alone (Figure 2.18A,B). NDE1 RNAi with delAC-NDE1 overexpression lead to a similar reduction in the mitotic index as seen with NDE1 RNAi alone (Figure 2.18C).

Analysis at P7 revealed that overexpression of delAC-NDE1 following NDE1 knockdown prevented the electroporated cells from reaching the superficial layers, marked by Cux1 staining (Figure 2.18D). The majority of electroporated cells remained clustered in the SVZ along the ventricle, and these cells were strikingly positive for the RGP maker Pax6 (Figure 2.18E). The combination of this data from experiments with the delAC-NDE1 construct reveal that the microcephaly-

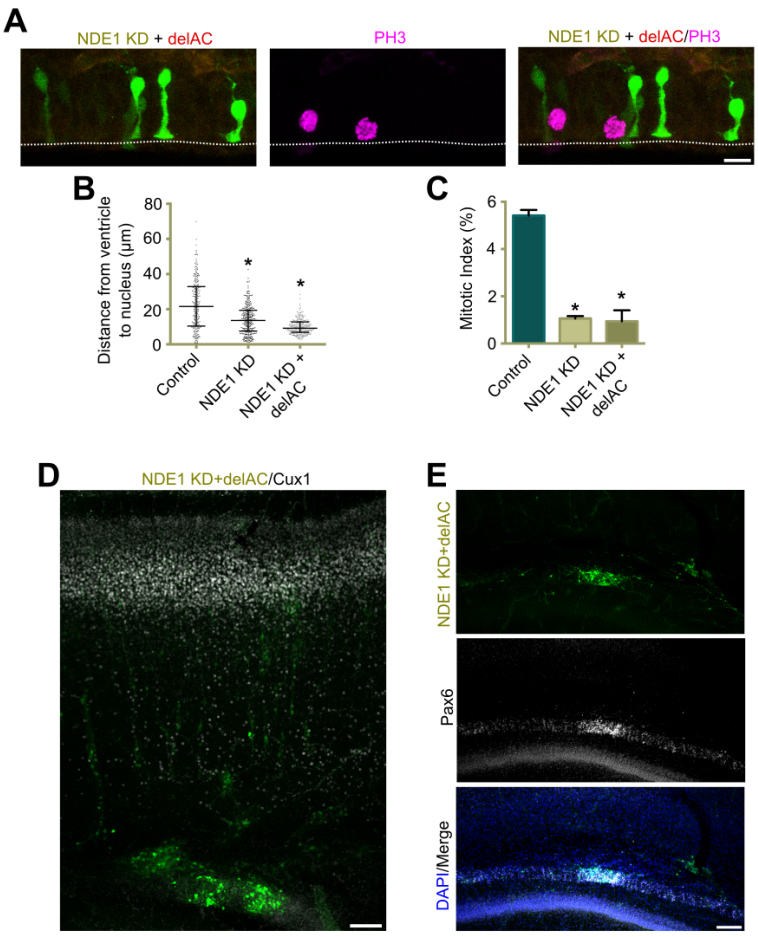

Figure 2.18: A Microcephaly Causing Form of NDE1 Does Not Rescue Apical INM : GFP control plasmid or NDE1 RNAi was electroporated with delAC-NDE1 overexpression into E16 embryonic rat brains, and analyzed at E20. **(A-C)** Rescue with the delAC-NDE1 phosphomutant construct did not rescue apical INM, leading to a reduction in the mitotic index and an accumulation of radial glia (RGP) nuclei within 10-15μm of the ventricle **(D-E)** At P7 NDE1 RNAi expression with delAC-NDE1 overexpression mirrored NDE1 RNAi alone, with many electroporated cells accumulating at the ventricle in a Pax6 positive state. Data presented as scatterplot in (B) with bars representing the median ± the interquartile range, and as mean ± SEM in (C). Kolmogorov-Smirnov test for non-parametric distributions used in (B) (* for $p<0.05$, n=257-285 RGP cells). Unpaired t-test used in (C) (* for $p<0.05$, n=3 embryonic brains from different mothers). Scale bars 10μm in (A) and 100μm (D-E).

associated defects in NDE1 function closely mirror the effects seen with NDE1 RNAi, and reinforce the utility of using RNAi for studying disease processes.

Possible Role for NDE1 in the Pathogenesis of Schizophrenia

A recent study found a cohort of 6 unrelated schizophrenic patients in Japan, all with the same substitution mutation in a single allele of NDE1 (S214F) (Kimura et al., 2014). Since NDE1 mRNA expression levels in the brain sharply drop during the first year of human life, it suggests that this NDE1 mutation may provide a neurodevelopmental predisposition to developing schizophrenia later in life. To test the effect of the schizophrenia-mutation on NDE1 function during neocortical

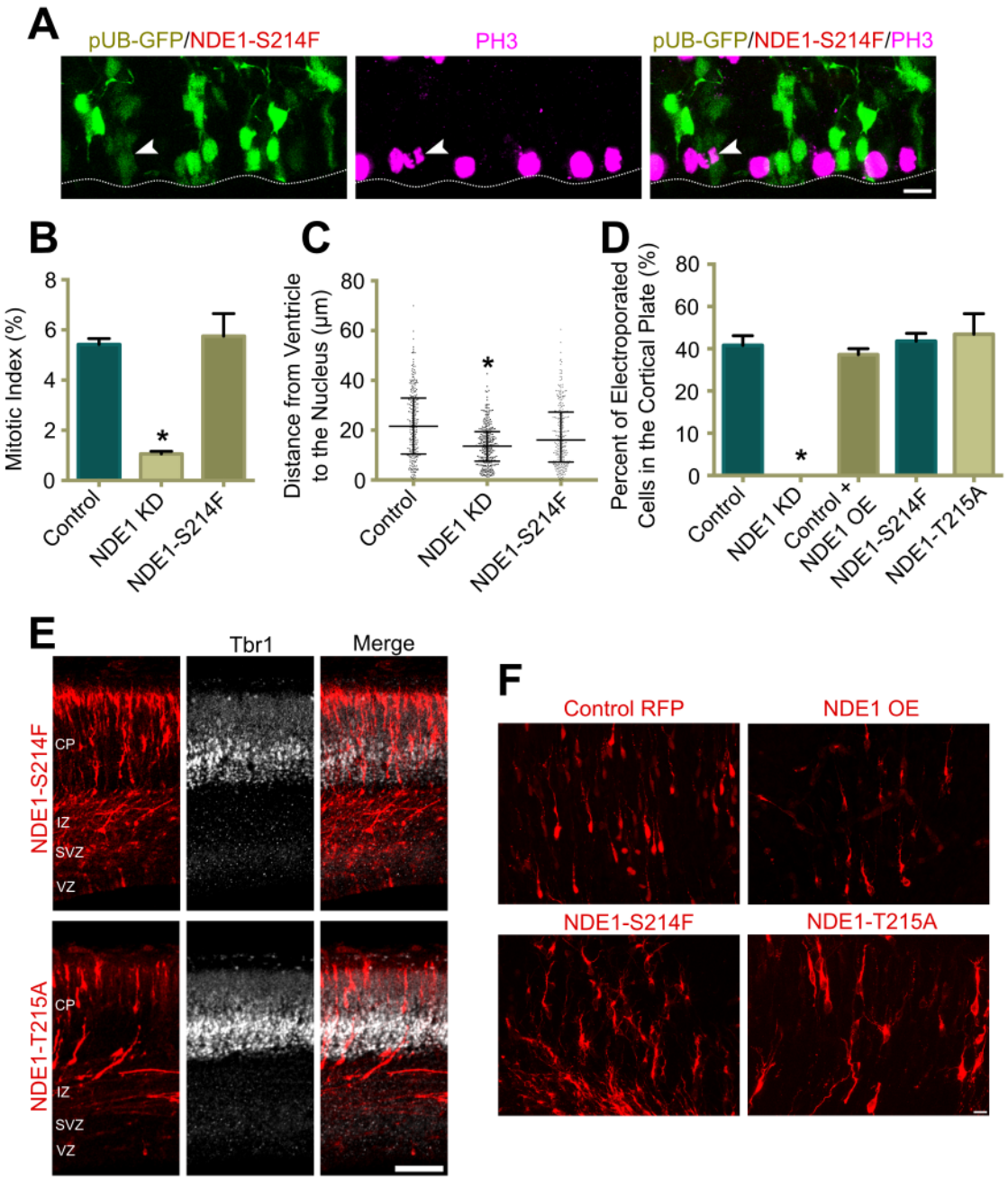

Figure 2.19: The Schizophrenia-Associated Mutation in *NDE1* Impairs Leading Process Formation But Not Radial Glia Proliferation: GFP control plasmid electroporated with S214F-NDE1 or T215A-NDE1 overexpression into E16 embryonic rat brains, and analyzed at E20. **(A-C)** S214F-NDE1 overexpression to mimic the heterozygous schizophrenia-associated *NDE1*-mutations does not impair the mitotic index or somal distribution of radial glia progenitor (RGP) cells. (E-D) S214F-NDE1 or T215A-NDE1 overexpression does not interfere with neuronal migration into the cortical plate when assayed four days after electroporation at E20. (F) The bipolar migrating neurons overexpressing S214F-NDE1 or T215A-NDE1 displayed altered morphology of the leading processes, with many prominent branches instead of a uniformly, tapering process. Arrowheads mark electroporated RGP nuclei positive for CyclinD1. Dashed line indicates ventricle surface. Data presented as scatterplot in (C) and (F) with bars representing the median ± the interquartile range, and as mean ± SEM in (D), (G), and (I). Kolmogorov-Smirnov

test for non-parametric distributions used in (C) (* for $p<0.05$, n=257-285 RGP cells). Unpaired *t*-test used in (B) and (D) (* for $p<0.05$, n=3 embryonic brains from different mothers). Scale bars, 10μm in (A) and (F), and 100μm in (E). Data for Control, NDE1 KD, and Control+NDE1 KD reused from previous datasets in this chapter.

development, we overexpressed the S214F mutant form of NDE1 driven by a CAG promoter (termed S214F-NDE1). Since the schizophrenic patients all have heterozygous mutations in NDE1, overexpression of the S214F mutation was chosen to best recapitulate the human disease-state. Overexpression of S214F in RGPs had no effect on the mitotic distribution of distribution of RGP nuclei in the VZ (Figure 2.19A-C).

Immediately adjacent to the S214 amino acid is the T215 residue, which is thought to be a phosphorylation site for both Cdk1 and Cdk5(Bradshaw et al., 2013). Since it was hypothesized that the S214F mutation may impact the phosphorylation of the T215 residue (Kimura et al., 2014), we also employed a phosphomutant T215A-NDE1 construct in testing the S214F-NDE1 construct. Four days after *in utero* electroporation there was no defect in the migration of cells expressing S214F-NDE1 into the cortical plate (Figure 2.19D-E). Close examination of the migrating bipolar cells, however, revealed that the leading processes were morphologically distinct from the leading processes of control or NDE1 overexpressing cells (Figure 2.19F). The cells overexpressing the T215A-NDE1 or S214F-NDE1 constructs had leading processes with many branches and protrusions, reminiscent of the leading processes seen after Lis1 RNAi (Tsai et al., 2005). Additionally, there were lamination defects seen at P7 following overexpression of S214F-NDE1 or T215A-NDE1, with only a minority of electroporated cells reaching

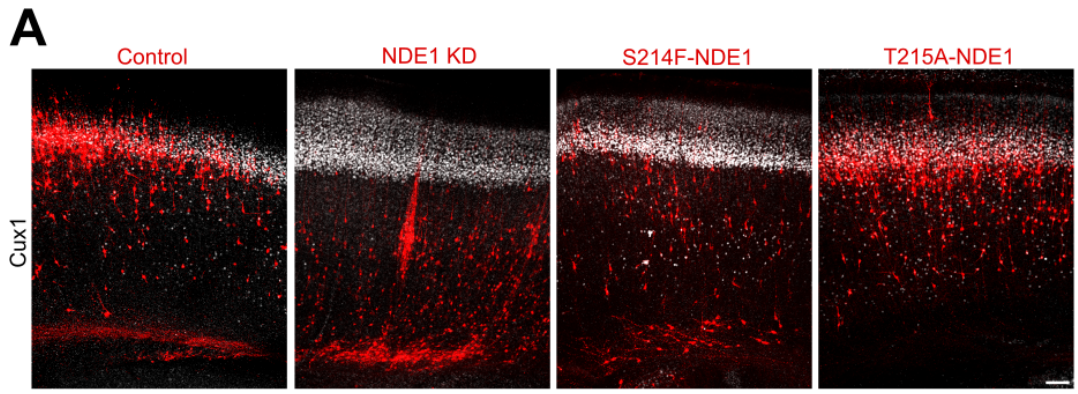

Figure 2.20: The Schizophrenia-Associated Mutation in *NDE1* and the T215A-NDE1 Phosphomutant Impair Migration into the Superficial Layers: (A) GFP control plasmid, NDE1 RNAi, S214F-NDE1, or T215A-NDE1 were electroporated into E16 embryonic rat brains and analyzed at P7. In comparison to NDE1 RNAi, there were very cells arrested in the white matter in S214F-NDE1 or T215A-NDE1 conditions, though there was a decrease in the amount of amount of electroporated cells reaching the superficial cortical layers, marked by Cux1. Scale bar is 100μm.

the superficial layers (Figure 2.20A). This was not nearly as severe of a defect as seen with NDE1 RNAi or NDE1 RNAi with delAC-NDE1 overexpression to recreate the microcephaly conditions, and provides some preliminary insight into the role of cortical lamination in establishing a predisposition for schizophrenia.

DISCUSSION

NDE1 and NDEL1 are each involved in neocortical development, though genetic analysis in rodents and human patients has revealed distinct phenotypic and disease consequence (Alkuraya et al., 2011; Bakircioglu et al., 2011; Feng and Walsh, 2004; Youn et al., 2009). Direct analysis of the functional similarities and differences between the two genes remains very limited, making an understanding of the factors leading to these developmental abnormalities challenging. Although NDE1, in particular, has been implicated in a severe form of human microcephaly (Alkuraya et al., 2011; Bakircioglu et al., 2011; Guven et al., 2012; Paciorkowski et al., 2013), the specific underlying mechanism is uncertain. We find here that NDE1

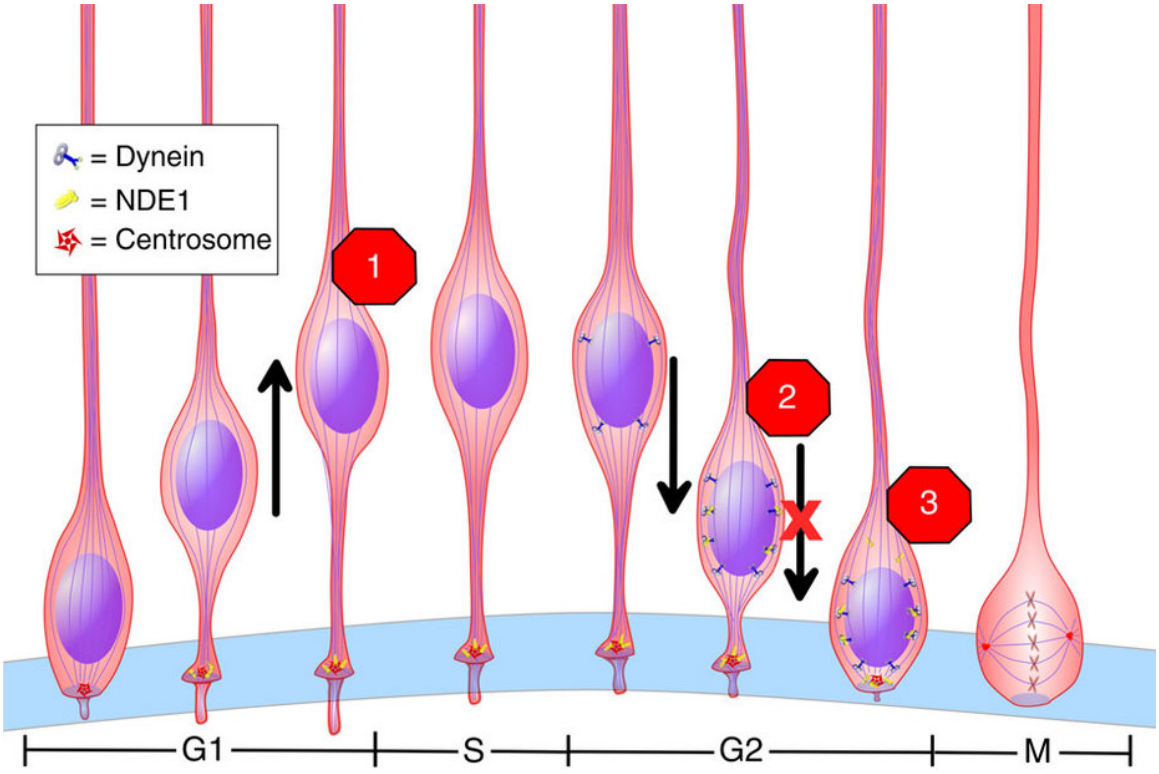

Figure 2.21: Roles of NDE1 and NDEL1 in the Neural Progenitor Cell Cycle. Our data indicate that NDE1 is required for 3 distinct non-mitotic processes in the radial glia progenitor (RGP) cell cycle: G1-to-S progression (1), apical INM during late G2 (2), and G2-to-M transition (3). NDEL1 overexpression rescues (1) and (2), but not (3). Interference with the RGP cell cycle at any or all of these stages is proposed as an important contributor to microcephaly. Scale of image does not reflect actual duration of cell cycle stages.

and NDEL1 can substitute for each other in diverse aspects of neurogenesis and neuronal migration. Our data, however, reveal a strongly predominant role for NDE1 in RGP cell behavior. We identify three distinct non-mitotic stages of RGP cell cycle progression that are susceptible to reduction in NDE1 or both NDE1/NDEL1, each of which should lead to a marked decrease in neurogenesis (Figure 2.21). These observations should help resolve the mechanisms responsible for NDE1-associated microcephaly and other forms of the disease.

We find that NDE1 RNAi causes substantial numbers of RGP nuclei to become arrested during apical INM. This effect blocks the RGP soma from reaching the ventricular surface, preventing these cells from ever entering mitosis (Hu et al.,

2013). The distance from the ventricular surface at which the NDE1 knockdown nuclei arrest is similar to that seen for CENP-F and Nup133 knockdown, the two upstream factors in the late-G2 pathway for recruitment of cytoplasmic dynein to the nuclear envelope (Baffet et al., 2015; Bolhy et al., 2011; Hu et al., 2013). Though definitive G2-immunohistochemical markers are lacking, our live imaging results strongly support G2 arrest, and a failure to enter mitosis at the ventricular surface. Analysis of a *NDE1* null mouse, however, revealed ectopic mitotic figures (Feng and Walsh, 2004), which we do not see in either NDE1, NDEL1, or combined knockdown RGP cells. Conceivably, the residual mitoses in the *NDE1* null mouse could be associated with intermediate progenitor cells located within the SVZ, or result from compensatory upregulation of *NDEL1* in the *NDE1* null mouse.

In examining functional redundancy between NDE1 and NDEL1, we uncovered another premitotic NDE1-specific role during cell cycle progression. According to our data, NDE1 is required to act following completion of apical INM to avoid a block in G2-to-M transition. This arrest occurs prior to histone-H3 phosphorylation, nuclear envelope breakdown, DNA condensation, centrosome separation, and centrosome release from the apical endfoot. Importantly, NDEL1 was unable to compensate for NDE1 knockdown at this stage. In fact, overexpression of NDEL1 induced a similar phenotype, suggesting a dominant-negative effect, perhaps involving formation of heterodimers with NDE1 (Bradshaw et al., 2011). By utilizing BicD2 overexpression we were also able to force NDE1 knockdown RGP cells to complete INM, yet these cells remained unable to enter mitosis. This stands in contrast to BicD2 rescue of CENP-F knockdown in RGP cells,

which were able to complete apical INM and enter mitosis (Hu et al., 2013), and suggests an as yet unidentified, spatially sequestered apical signal responsible for RGP mitotic entry. There has been one prior report of a NDE1 mutation leading to a partial increase in the G2 population of non-neuronal cells (Alkuraya et al., 2011). How these observations may relate to ours is uncertain. Nonetheless, our data point to a NDE1-specific role in the G2-to-M transition, separate from its role in the late-G2 pathway of recruiting dynein to the nuclear envelope, and identify an underlying difference between the two paralogs.

Primary cilia have been implicated in cell cycle progression in a number of cell lines and developing tissue (Hu et al., 2014; Kim and Tsiokas, 2011; Kim et al., 2011; Li et al., 2011). Even though the primary cilia membrane has been shown to be retained for most of the RGP cell cycle (Paridaen et al., 2013), previous reports have provided evidence that resorption of primary cilia needs to be initiated for ciliated cells to transition into S-phase (Kim et al., 2011; Li et al., 2011). NDE1, in particular, has been implicated in this process in ciliated non-neuronal cell lines and during development of the zebrafish head (Kim et al., 2011; Maskey et al., 2015). A similar block in the G1-to-S transition in RGP cells was observed in our experiments, accompanied by the over-elongation of primary cilia. An additionally intriguing aspect of our observations was that this arrest was exacerbated by the double knockdown of NDE1/NDEL1, unlike apical INM inhibition, which was readily apparent when only NDE1 was knocked down. This enhanced G1/S block with double knockdown suggests that each paralog alone can contribute to initiating ciliary resorption in RGPs, and the rescue of this phenotype by inhibiting

ciliogenesis indicates that dysregulation at the primary cilia is causal of the G1/S block in the NDE1/NDEL1 double knockdown in RGP cells.

The precise function of primary cilia in radial glia remains unresolved. Knockout mice for KIF3A or IFT88, proteins integral for cilia formation, have largely normal brain development (Insolera et al., 2014; Tong et al., 2014), and we detected no difference in CyclinD1 labeling or somal distribution in our IFT172 knockdown conditions alone. Nonetheless, lack of primary cilia is very different from dysregulation of the ciliary growth cycle and cilia over-elongation, which may explain why development occurs largely normally without primary cilia, while aberrations in primary cilia length/resorption may block cell proliferation. This view is further supported by a report of a block to RGP cell cycle progression caused by knockdown of TcTex1, which also affects ciliary resorption (Li et al., 2011). Nevertheless, it remains to be resolved whether NDE1 and NDEL1 are playing a role in recruiting specific regulators of the primary cilia, whether they facilitate retrograde intraflagellar transport, or whether they play an entirely separate role in primary cilia regulation/signaling.

Microcephaly arises from impaired proliferation of the progenitor cells, resulting either from defects in S-phase, or more commonly, in mitotic progression (Barkovich et al., 2012). The current study, however, reveals three alternative mechanisms associated with a severe microcephaly-causing gene, *NDE*1, and is the first to link aberrations in apical INM to human disorders of corticogenesis. Relative to rodents, development of the human neocortex relies on an expanded outer subventricular zone containing many additional RGPs (Dehay et al., 2015; Fietz et

al., 2010; Hansen et al., 2010). All of these, however, must derive from apical RGPs in the ventricular zone that must undergo INM to successfully proliferate. Both NDE1 and NDEL1 are known to serve critical functions during mitosis, in particular during spindle alignment (Liang et al., 2007) and chromosome segregation (Stehman et al., 2007; Vergnolle and Taylor, 2007; Yan et al., 2003). Although NDE1 is likely required for these functions in RGPs, our data show that acute NDE1 knockdown arrests RGPs prior to mitotic entry. Our data, therefore, indicate that the inability to reach mitosis is an equally or even more important cause of microcephaly than an arrest within mitosis itself.

Patients with *NDE1* mutations exhibit altered cortical lamination, in addition to reduced brain size (Alkuraya et al., 2011; Bakircioglu et al., 2011; Guven et al., 2012; Paciorkowski et al., 2013), which raises the question of whether defects in proliferation are solely accountable for the laminar deficits seen by MRI. In addition to the three major cell-cycle roles for NDE1 identified in RGP proliferation, NDE1 and NDEL1 were each shown to be crucial for the migration of the postmitotic neuronal precursors into the cortical plate. Thus, these changes in postmitotic migration likely explain the subsidiary cortical laminar dysplasia seen in many of the patients with *NDE1* microcephaly (Alkuraya et al., 2011; Bakircioglu et al., 2011).

Remarkably the RGPs electroporated with NDE1 RNAi remained at the ventricular surface for up to two weeks, persisting in a radial glia-like state even at P7. This persistence of electroporated cells at the ventricle was not seen in control tissue, and suggests that these RGP cells survive but remain arrested for weeks.

There were very few electroporated cells that migrated into the neocortex at P7 following NDE1 knockdown, though NDEL1 knockdown appeared to delay migration rather than block migration. This suggests either a differential ability of the two paralogs to upregulate one another, or essential differences in their function and requirement during bipolar migration.

Cdk1 has been shown to regulate apical INM through phosphorylation of RanBP2 by activating the early G2-dynein recruitment pathway (Baffet et al., 2015),. Additionally NDE1 is a known Cdk1 substrate (Bradshaw et al., 2013). Therefore, Cdk1 phosphorylation of NDE1 could represent a linkage of INM with cell cycle progression. Ongoing work in our lab has found that mutation of three Cdk1 sites on NDE1 (T215, T243, and T246) to phosphomimetic residues enhances its binding to CENP-F *in vitro* and its targeting to the nuclear envelope during late-G2 in HeLa cells (Wynne and Vallee, unpublished). Overexpression of a T215A-T246A phosphomutant form NDE1 (T215A-T246A-NDE1) after NDE1 knockdown fails to rescue apical INM. This same effect is seen after overexpression of a microcephaly-form of NDE1 (delAC-NDE1) with NDE1 RNAi. These results directly implicate apical INM in the pathogenesis of microcephaly, and suggest that Cdk1 may regulate late-G2 dynein recruitment to the nuclear envelope through the NDE1-CENP-F interaction. More work needs to be done to investigate if the delAC-NDE1 construct has dominant-negative effects on cell cycle progression, as well as the phosphomimetic rescues of NDE1 function.

While interference with multiple Cdk phosphorylation sites impedes NDE1-CENP-F binding, there is preliminary evidence that single phosphomutant T246A-

NDE1 expression in HEK293 cells promotes an accumulation in G2 (Alkuraya et al., 2011). Since our work provided evidence that there is a requirement for NDE1 in the G2-to-M transition independent from its role at the nuclear envelope in apical INM, we further tested the involvement of the T246 phosphorylation site in RGP cell function. Intriguingly, NDE1 RNAi with T246A-NDE1 rescue recapitulated the G2-to-M arrest. That the substitution of a single residue on NDE1 could have such a profound impact on RGP function suggests that there may be something unique about the phosphomutant T246A-NDE1, possibly impairing its interaction with select binding partners. Other experiments must be done to investigate whether single mutation of the other two Cdk1 phosphorylation sites of NDE1 – T215 and T243 – will also lead to the G2-to-M arrest, or if this role is unique to the T246 site. Additionally, appropriate experiments involving rescue phosphomimetic forms of NDE1 are warranted.

Though NDE1 has been established in multiple studies as a causative gene for severe forms of human microcephaly (Alkuraya et al., 2011; Bakircioglu et al., 2011; Guven et al., 2012; Paciorkowski et al., 2013), a recent report found the same single substitution mutation in six unrelated schizophrenic patients (Kimura et al., 2014). The mutation was also detected in one healthy control patient, which reinforces the current clinical understanding of schizophrenia as a disease dependent on underlying genetic predisposition compounded by some form of an environmental insult (Sullivan et al., 2012). The current chapter found that this schizophrenia-associated mutation in NDE1 at the S214 site impairs leading process morphology in migrating bipolar neurons and affected early neocortical lamination, but not RGP

proliferation. If this impairment in migration seen at P7 is heterogenous among cortical glutamatergic neruons, then it could impact neocortical connectivity since the neurons do not reach their appropriate layer. Since layer identity for excitatory glutamatergic neurons is established during the multipolar stage (Miyoshi and Fishell, 2012), any defect during bipolar migration may cause neurons destined for superficial layers to be deposited in the deeper layers. Neurons in the different layers have different axonal projection targets and morphologies, which could contribute to altered connectivity in the neocortex. This defect in connectivity fits with the emerging literature that impairments in various biological processes that affect neuronal connectivity could establish a predisposition to developing schizophrenia later in life (Chen et al., 2016; Muraki and Tanigaki, 2015; Sekar et al., 2016).

A final consideration when using rodent models of human brain developmental disease is the extensive difference in neuron density and neocortical size. The neocortex of primates contains the distinct proliferative outer subventricular zone (oSVZ), home to vastly more basal progenitors than the rodent brain, including the specialized outer radial glia (Fietz et al., 2010; Hansen et al., 2010). These cells help to amplify the amount of neurons generated by radial glia, and exhibit a specialized form of migration prior to mitosis termed mitotic somal translocation (Ostrem et al., 2014). Additionally there is a prolonged period of progenitor expansion during human neocortical development, followed by the switch to asymmetric divisions (Lewitus et al., 2013). It is possible that there are expanded roles for NDE1 in human brain development that cannot be modeled

using rodents, and it cannot be ruled out that the baseline differences between human and rodent brain development may contribute to the severity of *NDE1* microcephaly.

All together it appears that the two dynein regulatory proteins NDE1 and NDEL1 have both overlapping and distinct functions during mammalian neocortical development. Though differences in protein expression and posttranslational modification likely contribute to differences as well, our results imply that there is at least one role for NDE1, at the G2-to-M transition, for which NDEL1 cannot functionally compensate. Further work will be required to define the nature of this very interesting function.

EXPERIMENTAL PROCEDURES

In utero electroporation

Plasmids were transfected by intraventricular injection into the cranium of rats at embryonic day 16 (E16) and electroporated. In brief, an E16 gravid rat was anesthetized via intraperitoneal injection of ketamine (75-95 mg/kg) and xylazine (5 mg/kg), and placed on a temporary heat source. Pain management was provided by administration of buprenorphine (0.05mg/kg) and bupivicaine (2mg/kg). Laparotomy was performed and the uterine horns transilluminated with a fiber optic light source to identify the embryonic cerebral ventricles. DNA was mixed with a colored non-toxic dye for easy visualization and 1μL of DNA constructs (1-2μg/μL) was injected into the ventricular space using a high gauge needle made from a glass capillary tube. Post-injection, 5 pulses of electrical current (50V, 5 milliseconds each, with 1 sec intervals) were applied by placing electrodes on the external wall of the uterine horn such that the positive electrode is angled along the lateral aspect of the neocortex adjacent to the lateral ventricle targeted by the injection. The uterus was returned to the abdominal cavity, the incision site closed by suture of the abdominal rectus muscle and closer of the skin via abdominal wound clips. Rats were monitored every day post surgery until the desired developmental time point, and buprenorphine (0.05mg/kg) was provided every 8-12 hours for the first 48 hours of recovery for pain management(Baffet et al., 2016). All animal protocols were approved by the Institutional Animal Use and Care Committee at Columbia University.

Cortical Slice Preparation and Immunostaining

Either 3, 4, or 14 days following the *in utero* electroporation procedures (see Figure legends for precise dates of each experiment), the gravid rat was anesthetized again using ketamine (75-95mg/kg) and xylazine (5mg/kg). Upon proper anesthetic induction, a laparotomy at the site of the previous incision was performed and the uterus exposed. The embryos were excised from the uterus, the brains dissected out and placed overnight in 4% PFA fixative dissolved in PBS at 4°C. When postnatal day 7 (P7) brains were removed the animals were sacrificed by decapitation, and the brains removed. For NDE1/NDEL1 immunostaining, the brain slices were prepared as if for live imaging and the slices were fixed in methanol for at -20˚C for 20min. Following fixation brains were embedded in 4% agarose in PBS and sliced by a vibratome (Zeiss) in 80μm thick coronal sections. Sections were incubated in blocking solution containing PBS and 0.3% Triton X-100 supplemented with 3% normal donkey serum for 1 hr. Primary antibodies were incubated overnight in blocking solution at 4°C, sections were washed 3x in PBS, and secondary antibodies in blocking solution were incubated for 2 hr at room temperature. Sections were mounted on slides using Aqua-Poly/Mount (Polysciences, Inc). For BrdU immunostaining, BrdU (Sigma-Aldrich) was injected intraperitoneally (20mg/mL) into the gravid mother once every 3 hours for cumulative pulses of either 3, 6, 12, or 24 hours duration. For the 30min BrdU pulse, brains were sliced according to the live imaging protocol (described below), immersed in BrdU containing media (20μg/mL) for 30 minutes before fixation with PFA. For BrdU immunohistochemistry, brain slices were first incubated in 2N HCl for 25 min at

37°C. Slices were then washed in 0.1 M sodium borate for 10 min and then PBS, prior to antibody incubation.

Live Imaging

Dissected rat brains were embedded in 4% low melting agarose diluted in artificial cerebrospinal fluid(Baffet et al., 2016) and were sliced into 300μm coronal sections as described above. Slices were placed on 0.4μm, 30mm diameter Millicell-CM inserts (Millipore) in cortical culture medium containing 25% Hanks balanced salt solution, 47% basal MEM, 25% normal horse serum, 1X penicillin/streptomycin/glutamine (GIBCO BRL), and 30% glucose. Slice was transferred to a 50mm glass-bottom dish and imaged on an IX80 laser scanning confocal microscope (Olympus FV100 Spectral Confocal System) at intervals of 10min for up to 24 hours.

RNAi and DNA constructs

shRNA constructs were designed to target internal gene sequences uniquely against NDE1 or NDEL1 and contained in a pRetro-U6G vector (Cellogenetics, MD), which co-expressed GFP and the shRNA target sequences. The target sequence for NDE1 is 5'-GCGTTTGAATCAAGCCATTGA-3'. The target sequence for NDEL1 is 5'-GATGGTGAAGATATACCGGAT-3'. Both target sequences were conserved in mice and rat. Two target sequences for IFT172 were used in combination: 5' GCGGCCATCAACCACTATATT 3' and 5' GCTGCTGATCTCTCATTACTA 3' (Sigma). Empty vectors of pEGFP-C1 and pmCherry-N1 were used as controls (Clontech).

For overexpression of NDE1 and NDEL1, mouse cDNA to either protein was fused to a mCherry fluorescent reporter (mCherry-C1-NDE1 and mCherry-N1-NDEL1) and subcloned into a pCAGEN vector driven by CAG promoter (provided by Connie Cepko (Addgene plasmid #11160)) using XhoI and NotI restriction sites. 5 silent point mutations were made in the cDNA for both NDE1 and NDEL1 so that each was RNAi resistant for their respective shRNAs using KOD Hot Start (Millipore). shRNA sequences directed at the opposite paralog had at least 6 incongruent nucleotides in the target sequence and therefore were specific to either protein. Point mutations were introduced to create the T246A, T215A, and S214F mutations as appropriate, and a double AC duplication was performed to create the delAC-NDE1 construct. pIRES-dsRed-BicD2 was described in Hu et al., 2013. pCAG-Arl13B-mCherry was provided by Dr. Kathryn Anderson.

The siRNA smart pools (GE-Dharmacon) used for NDE1 and NDEL1 RNAi in the human retinal epithelial cell line (hTERT–RPE1–GFP–CSAP, a gift from Dr. Iain Cheeseman) were as follows: siGENOME NDE1 (54820) siRNA – 5'GGACCCAGCUCAAGUUUAA3'; 5'GGAAAGAUCUGGCGAUGAC3'; 5'GGAGGAAGAAGCUAACUAU3'; 5'GGAGGGAAGCCGAGAAUAU3'; and siGENOME NDEL1 (81565) siRNA – 5'GAAGCUAGAGCAUCAAUAU3'; 5'GCUAGGAUAUCAGCACUAA3'; 5'GGACCAAGCAUCACGAAAA3'; 5'GCACAAAGUUCUCUCGAUC3'.

Cell Culture, Western Blotting and ciliogenesis assay

Rat C6 brain glioma cells were cultured in DMEM supplemented with 10% FBS, 1% penicillin/streptomycin and maintained at 37 °C with 5% CO_2. Transfection

with shRNAs against NDE1 and NDEL1 was performed using a Lonza nucleofector kit V and an Amaxa Nucelofector according to manufacturer's instructions. Cells were collected 72 hours later and sorted using FACS to isolate GFP positive cells. Collected cells were lysed on ice in RIPA buffer containing DTT and a protease inhibitor cocktail (Sigma). Purified cell lysates were loaded on a polyacrylamide gel and transferred to a PVDF membrane. The membrane was blocked in PBS+0.5% powdered milk, incubated with primary antibodies to NDE1/NDEL1 (Abnova; 1:1000) and α-tubulin (Sigma; 1:2000) diluted in blocking solution+0.05% Tween for 2 hours, washed and incubated with secondary LI-COR antibodies.

hTERT-immortalized retinal pigment epithelial cell line expressing the centriolar and ciliary axoneme marker GFP–CSAP (hTERT-RPE1–GFP–CSAP; a gift from Dr. Iain Cheeseman) were grown in DMEM/F12 supplemented with 10% FBS, 1% penicillin/streptomycin and maintained at 37 °C with 5% CO2. Transfections with siRNA smart pools were performed using Lipofectamine RNAiMAX (Life Technologies) according to manufacturer's instructions. 48 hours following transfection, cells were washed in PBS re-transfected with the siRNA pools and incubated with serum-free media for an additional 48 h to promote ciliogenesis. Cells were then washed in PBS, fix in 4%PFA for 8min and permeabilized with 0.15% Triton-X-100 in PBS for 2 min. After blocking in donkey serum for 30min, cells were incubated with primary antibodies followed by incubation with fluorophore-conjugated secondary antibodies.

RNA Isolation and qRT-PCR Analysis

C6 cells were transfected with Nde1/Ndel1 shRNA plasmids and rescue constructs using an Amaxa Nucleofactor as described for western blot. 72h following transfection, GFP fluorescent cells were sorted using a FACSAria Cell Sorter (BD). Positive cell lyses, mRNA to cDNA synthesis, and qPCR were performed using the Power SYBR Green Cells-to-Ct Kit (Ambion/ Thermofisher). cDNA were analyzed using quantitative PCR using a ABI 7900 HT qPCR machine. Primers were designed to have TMs of about 60 degrees and to generate amplicons of 70 to 200 base pairs, separated by at least one intron. Three replicas were done for each condition per experiment and experiments were performed in triplicates. Target cDNA levels were analyzed by the comparative cycle (Ct) method and values were normalized against β-actin and GAPDH expression levels. The primers used in this study were: β-actin FW: CCCGCGAGTACAACCTTCT; β-actin RV: CGTCATCCATGGCGAACT; Gapdh FW: CAACTCCCTCAAGATTGTCAGCAA; Gapdh RV:GGCATGGACTGTGGTCATGA; Nde1 FW: GAAAGAGCCAAACGAGCCAC; Nde1 RV:TCAGTCTCTGCACAGATTCTA * (1 mismatch with mouse sequence); Ndel1 FW: GAAGTGGAGGCGTTAAAGGA; Ndel1 RV:CCAGTGAAACTATTGTTGCCC.

Antibodies

Antibodies used in this study were mouse monoclonal against phosphohistone H3 (Abcam, ab14955, 1:500 dilution), phospho-vimentin (Millipore, 05-774, 1:250 dilution), Ki67 (Millipore, MAB4190, 1:250 dilution), centrin3 (Abnova, H00001070-M01, 1:250 dilution), glutamylated tubulin (Addipogen, GT335, 1:250 dilution), rabbit polyclonal against CyclinD1 (Thermo Scientific, RM-9104, 1:250

dilution), CDP/Cux1 (Santa-Cruz, SC-1302, 1:1000 dilution), S100ß (Millipore, 04-1054, 1:250 dilution), Geminin (Santa Cruz, sc-13015, batch J2615, 1:250 dilution), Lamin-associated protein 2 (Santa Cruz, sc-28541, 1:500 dilution), Tbr1 (Abcam, ab31940, 1:500 dilution), Arl13B (Proteintech, 17711-1-AP, 1:250 dilution), and rat monoclonal against BrdU (Abcam, ab6326, 1:250 dilution). Donkey fluorophore-conjugated secondary antibodies (Jackson Labs, 1:500 dilution) were used together with DAPI (4',6-diamidino-2-phenylindole, Thermo Scientific, 62248, 1:1,000 dilution). NDE1 (Abnova, H00054820-M01, 1:1000 dilution) and α-tubulin (Sigma; 1:2000) were used for immunoblotting. To develop in a LICOR system, fluorescent secondary antibodies were acquired from Invitrogen (dilution 1:10,000) and Rockland (dilution 1:10,000) to use for western blotting.

Imaging, Quantification, and Statistical Analysis

All images were collected with an IX80 laser scanning confocal microscope (Olympus FV100 Spectral Confocal System). Brain sections were imaged using a 60x 1.42 N.A. oil objective or a 10x 0.40 N.A. air objective. All drawings were composed using Inkscape open source software. All images were analyzed using ImageJ software (NIH, Bethesda, MD). Distance and primary cilia length measurements were also performed using this software. Live-imaging movies were constructed on ImageJ at 12 fps, with each frame representing a 10 minute progression in real time. Tracings were made by measuring the distance from the ventricular surface to the bottom of the soma – the same as was used for fixed imaging analysis – every 20 minutes, corresponding to every 2 frames in the movies. All statistical analysis was performed using Prism (GraphPad Software, La Jolla, CA, USA). For fixed analysis of

distances of RGP soma from the ventricle (apical process length), distributions were represented as scatterplots with bars plotting the median and interquartile range. This was done to provide a more comprehensive representation of the data, since all conditions failed the D'Agostino & Pearson omnibus normalcy test. Due to the nonparametric nature of these distributions, Kolmogorov-Smirnov tests were used for all comparisons of experimental conditions to the corresponding control condition. The ROUT method was used to identify any outliers, none of which were found across the conditions. Measurements of the distance between RGP nuclei and ventricular surface were made from 3 different embryonic rat brains, each from a different mother. For mitotic index, CyclinD1 ratio, BrdU ratio, Ki67 ratio, and the fraction of electroporated cells reaching the cortical plate, all data are plotted as the mean with standard error of mean. Measurements were all made from at least 3 different embryonic rat brains across at least 2 separate operations per condition. Animals from all successful operations were included in the analysis. For the index measurements, at least 100 RGP cells were counted from at least 3 slices per brain. For results with Gaussian distributions, comparisons were made first using ANOVA tests to determine if there was a significant difference, followed by unpaired *t*-tests in order to compare individual experimental conditions to the appropriate control condition. For all non-Gaussian distributions, a Kruskal-Wallis test was employed first, followed by Kolmogorov-Smirnov tests or Dunn's multiple comparison tests for direct comparison of individual conditions. For all analyses significance was accepted at the level of $p<0.05$.

Data Availability

The authors declare that all relevant data supporting the findings of this study are available on request.

REFERENCES

Alkuraya, F.S., Cai, X., Emery, C., Mochida, G.H., Al-Dosari, M.S., Felie, J.M., Hill, R.S., Barry, B.J., Partlow, J.N., Gascon, G.G., et al. (2011). Human Mutations in NDE1 Cause Extreme Microcephaly with Lissencephaly. The American Journal of Human Genetics *88*, 536–547.

Baffet, A.D., Carabalona, A., Dantas, T.J., Doobin, D.D., Hu, D.J., and Vallee, R.B. (2016). Cellular and subcellular imaging of motor protein-based behavior in embryonic rat brain. Methods Cell Biol. *131*, 349–363.

Baffet, A.D., Hu, D.J., and Vallee, R.B. (2015). Cdk1 Activates Pre-mitotic Nuclear Envelope Dynein Recruitment and Apical Nuclear Migration in Neural Stem Cells. Developmental Cell *33*, 703–716.

Bakircioglu, M., Carvalho, O.P., Khurshid, M., Cox, J.J., Tuysuz, B., Barak, T., Yilmaz, S., Caglayan, O., Dincer, A., Nicholas, A.K., et al. (2011). The Essential Role of Centrosomal NDE1 in Human Cerebral Cortex Neurogenesis. The American Journal of Human Genetics *88*, 523–535.

Bangs, F.K., Schrode, N., Hadjantonakis, A.-K., and Anderson, K.V. (2015). Lineage specificity of primary cilia in the mouse embryo. Nature Cell Biology *17*, 113–122.

Barkovich, A.J., Guerrini, R., Kuzniecky, R.I., Jackson, G.D., and Dobyns, W.B. (2012). A developmental and genetic classification for malformations of cortical development: update 2012. Brain *135*, 1348–1369.

Bolhy, S., Bouhlel, I., Dultz, E., Nayak, T., Zuccolo, M., Gatti, X., Vallee, R., Ellenberg, J., and Doye, V. (2011). A Nup133-dependent NPC-anchored network tethers centrosomes to the nuclear envelope in prophase. The Journal of Cell Biology *192*, 855–871.

Bond, J., Roberts, E., Mochida, G.H., Hampshire, D.J., Scott, S., Askham, J.M., Springell, K., Mahadevan, M., Crow, Y.J., Markham, A.F., et al. (2002). ASPM is a major determinant of cerebral cortical size. Nat Genet *32*, 316–320.

Bradshaw, N.J., Hennah, W., and Soares, D.C. (2013). NDE1 and NDEL1: twin neurodevelopmental proteins with similar 'nature' but different 'nurture'. BioMolecular Concepts *4*, 447–464.

Bradshaw, N.J., Soares, D.C., Carlyle, B.C., Ogawa, F., Davidson-Smith, H., Christie, S., Mackie, S., Thomson, P.A., Porteous, D.J., and Millar, J.K. (2011). PKA phosphorylation of NDE1 is DISC1/PDE4 dependent and modulates its interaction with LIS1 and NDEL1. Journal of Neuroscience *31*, 9043–9054.

Cappello, S., Monzo, P., and Vallee, R.B. (2011). NudC is required for interkinetic nuclear migration and neuronal migration during neocortical development.

Developmental Biology *357*, 326–335.

Carabalona, A., Hu, D.J.-K., and Vallee, R.B. (2016). KIF1A inhibition immortalizes brain stem cells but blocks BDNF-mediated neuronal migration. Nat Neurosci *19*, 253–262.

Chen, T., Wu, Q., Zhang, Y., Lu, T., Yue, W., and Zhang, D. (2016). Tcf4 Controls Neuronal Migration of the Cerebral Cortex through Regulation of Bmp7. Front Mol Neurosci *9*, 94.

Dantas, T.J., Carabalona, A., Jun-Kit Hu, D., and Vallee, R.B. (2016). Emerging Roles for Motor Proteins in Progenitor Cell Behavior and Neuronal Migration during Brain Development. Cytoskeleton (Hoboken).

Dehay, C., Kennedy, H., and Kosik, K.S. (2015). The outer subventricular zone and primate-specific cortical complexification. Neuron *85*, 683–694.

Efimov, V.P., and Morris, N.R. (2000). The LIS1-related NUDF protein of Aspergillus nidulans interacts with the coiled-coil domain of the NUDE/RO11 protein. The Journal of Cell Biology *150*, 681–688.

Ezratty, E.J., Stokes, N., Chai, S., Shah, A.S., Williams, S.E., and Fuchs, E. (2011). A Role for the Primary Cilium in Notch Signaling and Epidermal Differentiation during Skin Development. Cell *145*, 1129–1141.

Feng, Y., Olson, E.C., Stukenberg, P.T., Flanagan, L.A., Kirschner, M.W., and Walsh, C.A. (2000). LIS1 regulates CNS lamination by interacting with mNudE, a central component of the centrosome. Neuron *28*, 665–679.

Feng, Y., and Walsh, C.A. (2004). Mitotic spindle regulation by Nde1 controls cerebral cortical size. Neuron *44*, 279–293.

Fietz, S.A., Kelava, I., Vogt, J., Wilsch-Bräuninger, M., Stenzel, D., Fish, J.L., Corbeil, D., Riehn, A., Distler, W., Nitsch, R., et al. (2010). OSVZ progenitors of human and ferret neocortex are epithelial-like and expand by integrin signaling. Nat Neurosci *13*, 690–699.

Gao, P., Postiglione, M.P., Krieger, T.G., Hernandez, L., Wang, C., Han, Z., Streicher, C., Papusheva, E., Insolera, R., Chugh, K., et al. (2014). Deterministic progenitor behavior and unitary production of neurons in the neocortex. Cell *159*, 775–788.

Guven, A., Gunduz, A., Bozoglu, T.M., Yalcinkaya, C., and Tolun, A. (2012). Novel NDE1 homozygous mutation resulting in microhydranencephaly and not microlyssencephaly. Neurogenetics *13*, 189–194.

Hansen, D.V., Lui, J.H., Parker, P.R.L., and Kriegstein, A.R. (2010). Neurogenic radial glia in the outer subventricular zone of human neocortex. Nature *464*, 554–561.

Hu, D.J.-K., Baffet, A.D., Nayak, T., Akhmanova, A., Doye, V., and Vallee, R.B. (2013). Dynein recruitment to nuclear pores activates apical nuclear migration and mitotic entry in brain progenitor cells. Cell *154*, 1300–1313.

Hu, W.F., Pomp, O., Ben-Omran, T., Kodani, A., Henke, K., Mochida, G.H., Yu, T.W., Woodworth, M.B., Bonnard, C., Raj, G.S., et al. (2014). Katanin p80 Regulates Human Cortical Development by Limiting Centriole and Cilia Number. Neuron *84*, 1240–1257.

Huang, J., Roberts, A.J., Leschziner, A.E., and Reck-Peterson, S.L. (2012). Lis1 acts as a "clutch" between the ATPase and microtubule-binding domains of the dynein motor. Cell *150*, 975–986.

Insolera, R., Bazzi, H., Shao, W., Anderson, K.V., and Shi, S.-H. (2014). Cortical neurogenesis in the absence of centrioles. Nat Neurosci *17*, 1528–1535.

Jackson, P.K. (2011). Do cilia put brakes on the cell cycle? Nat Neuro *13*, 340–342.

Kim, S., and Tsiokas, L. (2011). Cilia and cell cycle re-entry: more than a coincidence. Cell Cycle *10*, 2683–2690.

Kim, S., Zaghloul, N.A., Bubenshchikova, E., Oh, E.C., Rankin, S., Katsanis, N., Obara, T., and Tsiokas, L. (2011). Nde1-mediated inhibition of ciliogenesis affects cell cycle re-entry. Nature Cell Biology *13*, 351–360.

Kimura, H., Tsuboi, D., Wang, C., Kushima, I., Koide, T., Ikeda, M., Iwayama, Y., Toyota, T., Yamamoto, N., Kunimoto, S., et al. (2014). Identification of Rare, Single-Nucleotide Mutations in NDE1 and Their Contributions to Schizophrenia Susceptibility. Schizophr Bull *41*, 744–753.

Kriegstein, A., and Alvarez-Buylla, A. (2009). The Glial Nature of Embryonic and Adult Neural Stem Cells. Annual Review of Neuroscience *32*, 149–184.

Lewitus, E., Kelava, I., and Huttner, W.B. (2013). Conical expansion of the outer subventricular zone and the role of neocortical folding in evolution and development. Front Hum Neurosci *7*, 424.

Li, A., Saito, M., Chuang, J.-Z., Tseng, Y.-Y., Dedesma, C., Tomizawa, K., Kaitsuka, T., and Sung, C.-H. (2011). Ciliary transition zone activation of phosphorylated Tctex-1 controls ciliary resorption, S-phase entry and fate of neural progenitors. Nat Neuro *13*, 402–411.

Liang, Y., Yu, W., Li, Y., Yu, L., Zhang, Q., Wang, F., Yang, Z., Du, J., Huang, Q., Yao, X., et al. (2007). Nudel modulates kinetochore association and function of cytoplasmic dynein in M phase. Molecular Biology of the Cell *18*, 2656–2666.

Lipka, J., Kujipers, M., Jaworski, J., and Hoogenraad, C.C. (2013). Mutations in

cytoplasmic dynein and its regulators cause malformations of cortical development and neurodegenerative diseases. Biochemical Society Transactions *41*, 1605–1612.

Maskey, D., Marlin, M.C., Kim, S., Kim, S., Ong, E.-C., Li, G., and Tsiokas, L. (2015). Cell cycle-dependent ubiquitylation and destruction of NDE1 by CDK5-FBW7 regulates ciliary length. The EMBO Journal *34*, 2424–2440.

McKenney, R.J., Vershinin, M., Kunwar, A., Vallee, R.B., and Gross, S.P. (2010). LIS1 and NudE induce a persistent dynein force-producing state. Cell *141*, 304–314.

Miyoshi, G., and Fishell, G. (2012). Dynamic FoxG1 expression coordinates the integration of multipolar pyramidal neuron precursors into the cortical plate. Neuron *74*, 1045–1058.

Muraki, K., and Tanigaki, K. (2015). Neuronal migration abnormalities and its possible implications for schizophrenia. Front Neurosci *9*.

Nicholas, A.K., Khurshid, M., Désir, J., Carvalho, O.P., Cox, J.J., Thornton, G., Kausar, R., Ansar, M., Ahmad, W., Verloes, A., et al. (2010). WDR62 is associated with the spindle pole and is mutated in human microcephaly. Nat Genet *42*, 1010–1014.

Niethammer, M., Smith, D.S., Ayala, R., Peng, J., Ko, J., Lee, M.S., Morabito, M., and Tsai, L.H. (2000). NUDEL is a novel Cdk5 substrate that associates with LIS1 and cytoplasmic dynein. Neuron *28*, 697–711.

Noctor, S.C., Martínez-Cerdeño, V., Ivic, L., and Kriegstein, A.R. (2004). Cortical neurons arise in symmetric and asymmetric division zones and migrate through specific phases. Nat Neurosci *7*, 136–144.

Ostrem, B.E.L., Lui, J.H., Gertz, C.C., and Kriegstein, A.R. (2014). Control of outer radial glial stem cell mitosis in the human brain. CellReports *8*, 656–664.

Paciorkowski, A.R., Keppler-Noreuil, K., Robinson, L., Sullivan, C., Sajan, S., Christian, S.L., Bukshpun, P., Gabriel, S.B., Gleeson, J.G., Sherr, E.H., et al. (2013). Deletion 16p13.11 uncovers NDE1 mutations on the non-deleted homolog and extends the spectrum of severe microcephaly to include fetal brain disruption. Am. J. Med. Genet. A *161A*, 1523–1530.

Paridaen, J.T., and Huttner, W.B. (2014). Neurogenesis during development of the vertebrate central nervous system. EMBO Reports *15*, 351–364.

Paridaen, J.T.M.L., Wilsch-Bräuninger, M., and Huttner, W.B. (2013). Asymmetric inheritance of centrosome-associated primary cilium membrane directs ciliogenesis after cell division. Cell *155*, 333–344.

Sasaki, S., Shionoya, A., Ishida, M., Gambello, M.J., Yingling, J., wynshaw-Boris, A., and Hirotsune, S. (2000). A LIS1/NUDEL/cytoplasmic dynein heavy chain complex in the

developing and adult nervous system. Neuron *28*, 681–696.

Sauer, F.C. (1935). Mitosis in the neural tube. Journal of Comparative Neurology *62*, 377–405.

Sekar, A., Bialas, A.R., de Rivera, H., Davis, A., Hammond, T.R., Kamitaki, N., Tooley, K., Presumey, J., Baum, M., Van Doren, V., et al. (2016). Schizophrenia risk from complex variation of complement component 4. Nature *530*, 177–183.

Shmueli, A., Segal, M., Sapir, T., Tsutsumi, R., Noritake, J., Bar, A., Sapoznik, S., Fukata, Y., Orr, I., Fukata, M., et al. (2009). Ndel1 palmitoylation: a new mean to regulate cytoplasmic dynein activity. The EMBO Journal *29*, 107–119.

Spear, P.C., and Erickson, C.A. (2012). Apical movement during interkinetic nuclear migration is a two-step process. Developmental Biology *370*, 33–41.

Splinter, D., Tanenbaum, M.E., Lindqvist, A., Jaarsma, D., Flotho, A., Yu, K.L., Grigoriev, I., Engelsma, D., Haasdijk, E.D., Keijzer, N., et al. (2010). Bicaudal D2, dynein, and kinesin-1 associate with nuclear pore complexes and regulate centrosome and nuclear positioning during mitotic entry. PLoS Biol *8*, e1000350.

Stehman, S.A., Chen, Y., McKenney, R.J., and Vallee, R.B. (2007). NudE and NudEL are required for mitotic progression and are involved in dynein recruitment to kinetochores. The Journal of Cell Biology *178*, 583–594.

Sullivan, P.F., Daly, M.J., and O'Donovan, M. (2012). Genetic architectures of psychiatric disorders: the emerging picture and its implications. Nat. Rev. Genet. *13*, 537–551.

Thornton, G.K., and Woods, C.G. (2009). Primary microcephaly: do all roads lead to Rome? Trends Genet. *25*, 501–510.

Tong, C.K., Han, Y.-G., Shah, J.K., Obernier, K., Guinto, C.D., and Alvarez-Buylla, A. (2014). Primary cilia are required in a unique subpopulation of neural progenitors. Proc. Natl. Acad. Sci. U.S.a. *111*, 12438–12443.

Tsai, J.W., Chen, Y., Kriegstein, A.R., and Vallee, R.B. (2005). LIS1 RNA interference blocks neural stem cell division, morphogenesis, and motility at multiple stages. The Journal of Cell Biology *170*, 935–945.

Tsai, J.-W., Bremner, K.H., and Vallee, R.B. (2007). Dual subcellular roles for LIS1 and dynein in radial neuronal migration in live brain tissue. Nat Neurosci *10*, 970–979.

Tsai, J.-W., Lian, W.-N., Kemal, S., Kriegstein, A.R., and Vallee, R.B. (2010). Kinesin 3 and cytoplasmic dynein mediate interkinetic nuclear migration in neural stem cells. Nat Neurosci *13*, 1463–1471.

Vergnolle, M.A.S., and Taylor, S.S. (2007). Cenp-F links kinetochores to Ndel1/Nde1/Lis1/dynein microtubule motor complexes. Current Biology *17*, 1173–1179.

Yan, X., Li, F., Liang, Y., Shen, Y., Zhao, X., Huang, Q., and Zhu, X. (2003). Human Nudel and NudE as regulators of cytoplasmic dynein in poleward protein transport along the mitotic spindle. Molecular and Cellular Biology *23*, 1239–1250.

Youn, Y.H., Pramparo, T., Hirotsune, S., and Wynshaw-Boris, A. (2009). Distinct dose-dependent cortical neuronal migration and neurite extension defects in Lis1 and Ndel1 mutant mice. Journal of Neuroscience *29*, 15520–15530.

ACKNOWLEDGEMENTS

We thank Drs. Alexandre Baffet and Daniel Hu for critical reading of the manuscript, the members of the Vallee lab, Drs. Hynek Wichterle, Franck Polleux, Ellen Ezratty, Luis Oliveira, and Gregg Gundersen for technical expertise and feedback, and Drs. Kathryn Anderson and Iain Cheeseman for providing reagents. This project was supported by NIH HD40182 to R.B.V., NINDS F30NS095577 to D.J.D., and an AHA/ASA 15POST25080068 postdoctoral fellowship to T.J.D.

COMPETING INTERESTS STATMENT

The authors declare no competing financial interests.

AUTHOR CONTRIBUTIONS

Conceptualization, R.B.V., D.J.D, S.K., and T.J.D.; Methodology, D.J.D., S.K., with T.J.D. for primary cilia related experiments and qRTPCRs; Data Acquisition D.J.D. with T.J. D. for primary cilia related experiments, and A.C. for schizophrenia-associated mutation experiments; Writing – Original Draft, D.J.D. and S.K.; Writing – Review & Editing, D.J.D., T.J.D., S.K., and R.B.V.

Chapter 3

The Pathogenic Potential of Various Isolates of Zika Virus

Elements of this chapter will be submitted for publication with the authors Amy Rosenfeld*, David Doobin*, Audrey Warren, Richard Vallee, and Vincent Racaniello.

ABSTRACT:

Within the past several years, Zika virus (ZIKV) has transitioned from an emerging disease into a global pandemic. Fetal infection with ZIKV has been associated with multiple adverse outcomes, including the development of microcephaly and cortical malformations as part of the congenital Zika virus syndrome (CZVS). It is unknown whether a change occurred in ZIKV itself to allow it to infect and damage fetal tissue, and if ZIKV preferentially infects the fetus at certain gestation ages. Using organotypic mouse embryonic brain slice cultures, we show that nearly all isolates of ZIKV efficiently infect and replicate in the embryonic brain, though strains from the Asian/American lineages induce greater levels of apoptosis in the brain slices. A single isolate from a Nigerian patient in 1954 does not infect or replicate in brain slices, though introduction of the viral RNA from this strain into neuronal progenitors permitted for the single cycle replication event. All other ZIKV isolates efficiently replicated in early and mid-gestation embryonic tissue, though only one recent isolate replicated in the late-gestation embryonic tissue. This isolate preferentially infected neurons in the cortical plate. These data indicate some heterogeneity among the ZIKV isolates in their neurovirulence and pathogenic potential, and provide evidence for the mechanism of ZCS.

INTRODUCTION:

Embryonic development of the central nervous system is an exquisitely coordinated process reliant upon multiple distinct phases of cellular proliferation and maturation (Paridaen and Huttner, 2014). In the neocortex, which constitutes the outer region of the brain, proper proliferation of the neural stem cells – radial glia progenitors (RGPs) – and the subsequent migration of their postmitotic progeny is required during embryonic development (Kriegstein and Alvarez-Buylla, 2009; Noctor et al., 2004). Interference with neurogenesis or neuronal migration leads to malformations of cortical development, such as microcephaly (a disease characterized by reduced brain size) or lissencephaly (a disease characterized by a lack of neocortical gyration) (Guerrini and Dobyns, 2014). Aberrations in neocortical development can occur due to genetic disorders, vascular insufficiency *in utero*, or mother-to-child vertical transmission of an infectious agent (Hagen et al., 2014). Pathogens implicated in microcephaly include *Toxoplasma gondii*, cytomegalovirus, Herpes Simplex Virus (Neu et al., 2015). Recently, the arbovirus Zika Virus (ZIKV) was identified as a pathogen responsible for primary microcephaly (Driggers et al., 2016; Mlakar et al., 2016; Steele, 2016). Lissencephaly and other cortical malformations have been associated with ZIKV infection, in addition to microcephaly (Soares de Oliveira-Szejnfeld et al., 2016; Štrafela et al., 2016). Together these malformations of cortical development comprise the congenital Zika virus syndrome (CZVS), along with stunted growth from intrauterine growth restrictions and opthamological/otolaryngological disorders, including deafness and blindness (World Health Organization, 2016).

ZIKV is a single-stranded (+) RNA virus within the *Flaviviridae* family, which includes other neuropathic viruses such as West Nile virus, Japanese encephalitis virus, and tick-borne encephalitis virus (Pierson and Diamond, 2012). Initially isolated from a febrile monkey in the Zika forest in Uganda in 1947 (DICK et al., 1952), the first human case of ZIKV was identified in Nigeria in 1954 (MACNAMARA, 1954). Much of the population within Africa (MACNAMARA, 1954; SMITHBURN, 1952), India (SMITHBURN et al., 1954), and southeast Asia (SMITHBURN, 1954) was subsequently found to be seropositive for ZIKV antibodies, suggesting that the virus had been circulating throughout these regions for many years (Lessler et al., 2016). It was not until 2007 that there was a substantial outbreak of ZIKV on Yap Island in the Federal States of Micronesia. The symptoms of patients infected during this outbreak included rash, arthralgia, and conjunctivitis (Duffy et al., 2009). During this time 73% of the population of Yap Island was believed to have been infected (Duffy et al., 2009). The next major outbreak was in 2013 on French Polynesia, where approximately 66% of the population was infected with ZIKV (Cao-Lormeau et al., 2014). Notably, retrospective studies found that there was a rise in Guillian-Barré syndrome accompanying the ZIKV outbreak, which is a temporary, ascending paralysis (Cao-Lormeau et al., 2016). This was the first identified neurological sequela of ZIKV infection. Intriguingly, another retrospective study also identified a surge in microcephaly cases among newborns in French Polynesia during this outbreak (Cauchemez et al., 2016).

In late 2014 the first cases of ZIKV infection were identified in northern Brazil (Campos et al., 2015), though the virus is thought to have arrived in Brazil in

November or December, 2013 (Lessler et al., 2016). Subsequently ZIKV spread throughout the region leading to outbreaks of Guillain-Barré and microcephaly (Faria et al., 2016; Lessler et al., 2016). Recent reports also suggest that ZIKV may have been spreading in Haiti at roughly the same time, complicating the narrative about ZIKV spread in the Americas (Lednicky et al., 2016). Nonetheless, ZIKV has continued to disseminate through 40 countries within western hemisphere, all with local transmission by the *Aedes aegypti* mosquito (Chan et al., 2016), and CZVS continues to impact newborns at an alarming rate.

Unlike fetuses exposed to ZIKV, most adults with ZIKV infection are asymptomatic, though symptoms can include fever, rash, conjunctivitis, and arthralgia, all of which are self-limiting (Lessler et al., 2016). During the outbreak on YAP island 19% of people with serological evidence of recent ZIKV infection reported symptoms, suggesting that the majority of cases in adults are asymptomatic (Duffy et al., 2009). For patients who develop symptoms, onset is generally within 6 to 11 days post-exposure, and 99% of patients have no virus detectable in the blood by 24 days post-exposure (Lessler et al., 2016), mirroring reports of ZIKV exposure in rhesus macaque models (Dudley et al., 2016). Interestingly, pregnant patients can remain viremic for up to 10 weeks post-exposure (Driggers et al., 2016), a finding recapitulated in rhesus macaque studies (Dudley et al., 2016), though when these pregnancies came to term the viremia cleared within a week (Driggers et al., 2016). This suggests that the fetus, once infected, can act as a reservoir for ongoing ZIKV production. Antibodies to ZIKV develop around 9 days post-exposure (Lessler et al., 2016), and the current thinking

is that ZIKV-antibodies are similar to antibodies to other flaviviruses and last for life (Murphy and Whitehead, 2011).

Perhaps the most alarming feature of the ZIKV epidemic is the impact on pregnancies and the surge in microcephaly cases among newborns in epidemic regions. A prospective study from Rio de Janeiro suggests that there is a 29% chance of CZVS – including fetal growth restriction, CNS complications, and/or fetal demise – in symptomatic mothers seropositive for ZIKV infection (Brasil et al., 2016). Notably only 1 in 4 fetuses with abnormalities in ZIKV-seropositive mothers met the criteria for microcephaly (Brasil et al., 2016), emphasizing the need to understand CZVS beyond microcephaly. As mentioned, neuroradiological and neuropathological examination of affected infants and fetuses have found malformations of cortical development beyond microcephaly (Soares de Oliveira-Szejnfeld et al., 2016; Štrafela et al., 2016).

There have been many attempts to generate mouse models of ZIKV infection in an attempt to better understand the neuropathology. Early work determined that mice with compromised innate immune systems were particularly susceptible to ZIKV infection (Aliota et al., 2016; Lazear et al., 2016), with many adult mice dying after subcutaneous ZIKV exposure. Subcutaneous injection of ZIKV in pregnant adult mice that were both immunocompetent (Cugola et al., 2016) and lacking interferon signaling response (Miner et al., 2016a), caused intrauterine fetal growth restriction, with preliminary evidence for increased apoptosis. Other studies where ZIKV was injected into the lateral ventricle of embryonic brains revealed subsequent ZIKV infection of the neocortex, expression of cleaved-caspase 3, and

impairments in RGP proliferation (Li et al., 2016b; Shao et al., 2016). Other reports of ZIKV infection in the developing mouse brain argue that there is no increase in apoptosis (Brault et al., 2016; Retallack et al., 2016) and CZVS is more likely the result of impairments in RGP proliferation. Vaginal exposure to ZIKV leads to viral replication in the vaginal tract of both wild-type and immunocompetent mice, and solely vaginal exposure permits for ZIKV transmission to fetuses in pregnant mice, resulting in CZVS-like symptoms in embryos (Yockey et al., 2016).

Mouse models have also begun to investigate other sequelae of ZIKV infection. The virus can invade and remain in other immune-privileged sites, such as the eye (Miner et al., 2016b) and testes (Govero et al., 2016), though this has only been found to occur in immunocompromised mice lacking interferon signaling. Notably, virus has been found in the semen of human patients up to 60 days post-infection (Venturi et al., 2016), suggesting an ability of the virus to persist in immune-privileged locations. Although the mice with persistent ZIKV in the testes suffered damage to the tissue beyond the blood-testes barrier, they were able to mate with non-infected females, none of whom became infected (Govero et al., 2016).

These studies provide the basis for understanding the pathogenesis of ZIKV, though the varying genetic backgrounds of mice, developmental time windows analyzed, and isolates of ZIKV used all contribute to great uncertainties in what is known about ZIKV infection and the ability of the virus to cause microcephaly. Using organotypic brain slices from wild-type mice, kept in culture for up to 8 days, we have investigated the ability of different isolates of ZIKV to infect and replicate.

Additionally, we can examine the variability of the virus isolates across different embryonic stages. We have found that nearly all isolates of ZIKV replicate in mid- and early-gestation embryonic brain tissue (embryonic days 15 and 13, respectively), and lead to great increases in cell death across areas of infection. Cells positive for immunostaining of ZIKV envelope protein (ZKV-E) are overwhelmingly negative for apoptotic markers, suggesting that areas of cell death surround infected cells and may act as a protective mechanism to block further viral spread. Notably, an isolate from a Nigerian patient in 1968 does not infect or replicate in embryonic mouse brain tissue, despite replicating in non-neuronal tissue. This block can be overcome by deproteinating this isolate and introducing the viral RNA into the RGPs, which then allows for a one-time replication event. There are four putative amino acid substitutions in the envelope protein unique to this Nigerian isolate, which may be residues that determine neurovirulence of ZIKV. Almost none of the ZIKV isolates replicate in the late-gestation tissue (embryonic day 19), except for one recent isolate from Honduras that predominantly infects the neurons in the cerebral cortex. This may explain why CZVS is associated more often with ZIKV infection during the first or second trimesters, though recent cases of third trimester infections resulting in fetal complications may be due to mutations occurring in the virus as it spreads across the hemisphere.

RESULTS:

ZIKV Infects and Replicates in Brain Slices, Leading to Cell Death and Impaired Neuronal Migration

To investigate the pathogenic potential of various isolates of ZIKV, a well-validated organotypic brain slice culture method (Baffet et al., 2015; Betizeau et al., 2013; Lukaszewicz et al., 2005) was combined with ZIKV infection. Swiss Webster mice were sacrificed at embryonic day 15 (E15), embryonic brains removed, embedded in 4% agarose, and sliced at 300µm thickness (Figure 3.1A). The slices were infected for an hour, washed thoroughly with PBS, and cultured for up to 8 days (Figure 3.1B for the isolates used). During this time half of the media was

A

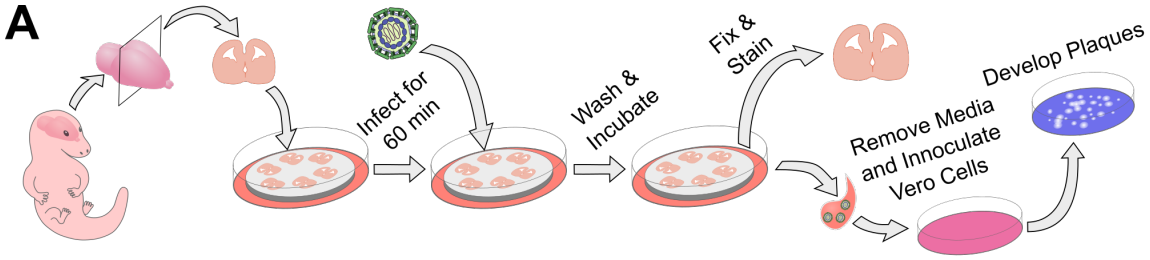

B

Isolate Name	Location	Year Isolated	Source	BEI Ref.
30656	Nigeria	1968	Human	NR-50066
MR766	Uganda	1947	Rhesus	NR-50065
DHK (DAR AR 41524)	Senegal	1984	Mosquito	NR-50338
Malay	Malaysia	1966	Mosquito	NR-50245
Brazil	Brazil	2015	Human	--
FLR	Colombia	2015	Human	NR-50183
PRV	Puerto Rico	2015	Human	NR-50240
Hond	Honduras	2016	Human placenta	NR-50355

Figure 3.1: Protocol Schematic and Zika Isolates Used: **(A)** Embryos were removed from pregnant Swiss Webster mice, the brains of which were dissected out, sliced at 300µm thickness, and slices placed on a filter with culture media. Slices were bathed in media containing the Zika (ZIKV) isolate of interest for 60 minutes, which was then removed and slices were washed three times with PBS. They were kept in culture for up to 8 days post infection, and each day half of the media was removed and replaced so that plaque-forming assay on a monolayer of Vero cells could be performed. After the culture period ended, brain slices were fixed and immunohistochemistry performed. **(B)** A table of the ZIKV isolates used, with abbreviations, their country of origin, year of isolation, source from which they were isolated, and BEI reference number.

removed each day and inoculated over a monolayer of Vero cells to establish a plaque-forming assay, and at the end of the culture period the slices were fixed and immunohistochemistry performed.

ZIKV envelope protein signal (ZKV-E) could be seen as soon as 3 days post-infection (DPI) (Figure 3.2A). The strongest fluorescent signal was near the ventricular surface, suggesting a predilection of the virus for neural stem cells, which others have reported in culture (Qian et al., 2016; Tang et al., 2016). There is clear ZKV-E signal in RGP cells in a perinuclear pattern (Figure 3.2B), though consistent preservation of the ventricular zone was difficult to achieve in the organotypic slices, and hence proliferative capacity of RGPs was not analyzed. Despite the fact that the slices are bathed a solution containing the virus for an hour, ZKV-E immunohistochemical signal indicates the infection is not uniform throughout the slices (Figure 3.2A). ZKV-E signal is distributed in focal areas and in radial columns throughout the developing neocortex, and is also present in the midbrain and diencephalon (Figure 3.2A).

After 8 DPI there is clear ZIKV infection across the neocortex in all isolates tested, with the exception of the Nigerian 30656 isolate, and this is reflected in the ability of these isolates to replicate and generate infectious progeny (Figure 3.3A-B). The 30656 isolate replicated, albeit poorly, in U87 cells, a human primary glioblastoma cell line (Figure 3.4A). Staining for cleaved caspase-3 (CC3) indicates a large increase in apoptosis across slices infected with various ZIKV isolates, compared to mock treated slices or those infected with polio (which does not infect wild-type murine tissue) or the 30656 isolate (Figure 3.3A,C). The CC3 signal does

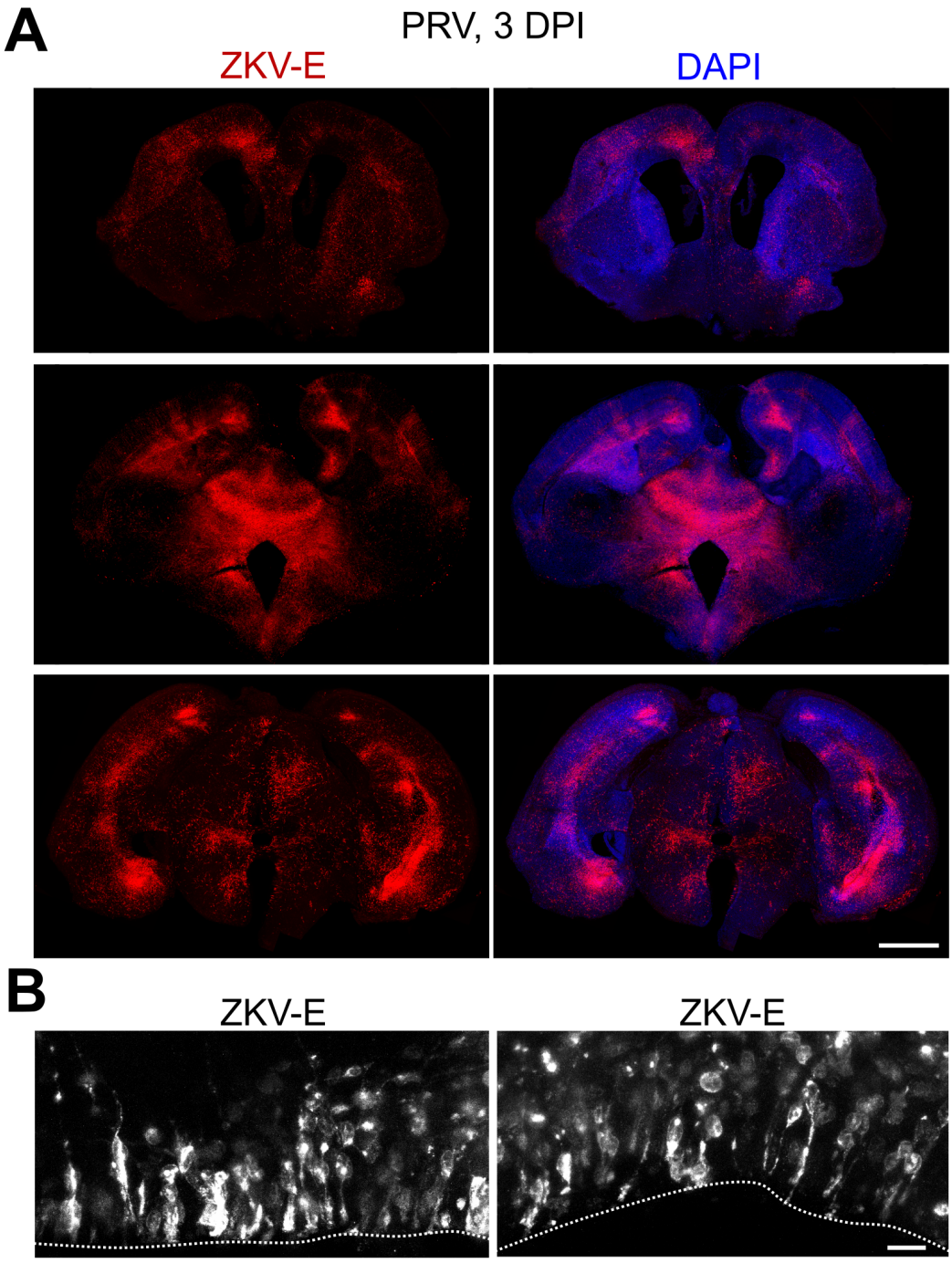

Figure 3.2: Zika Virus Infects Brain Slices in Focal Regions Including Radial Glia Progenitors: **(A)** Representative rostral, medial, and caudal embryonic day 15 slices from 3 days post infection (DPI) with the PRV isolate, stained for Zika virus envelope protein (ZKV-E). There is diffuse ZKV-E signal throughout the brain slice, though it occurs in focal areas and in radial columns. In the caudal slice staining around the proliferative regions is noticeably strong. ZKV-E signal is also found throughout the neocortex but also throughout other areas of the telencephalon and diencephalon. Scale bar is 500µm. **(B)** Radial glia progenitors (RGPs) lining the lateral ventricle demonstrated strong ZKV-E signal 3 DPI. Staining was perinuclear consistent with other reports of Zika in RGPs (Brault et al., 2016; Li et al., 2016a). Dotted line marks ventricular surface. Scale bar is 10µm.

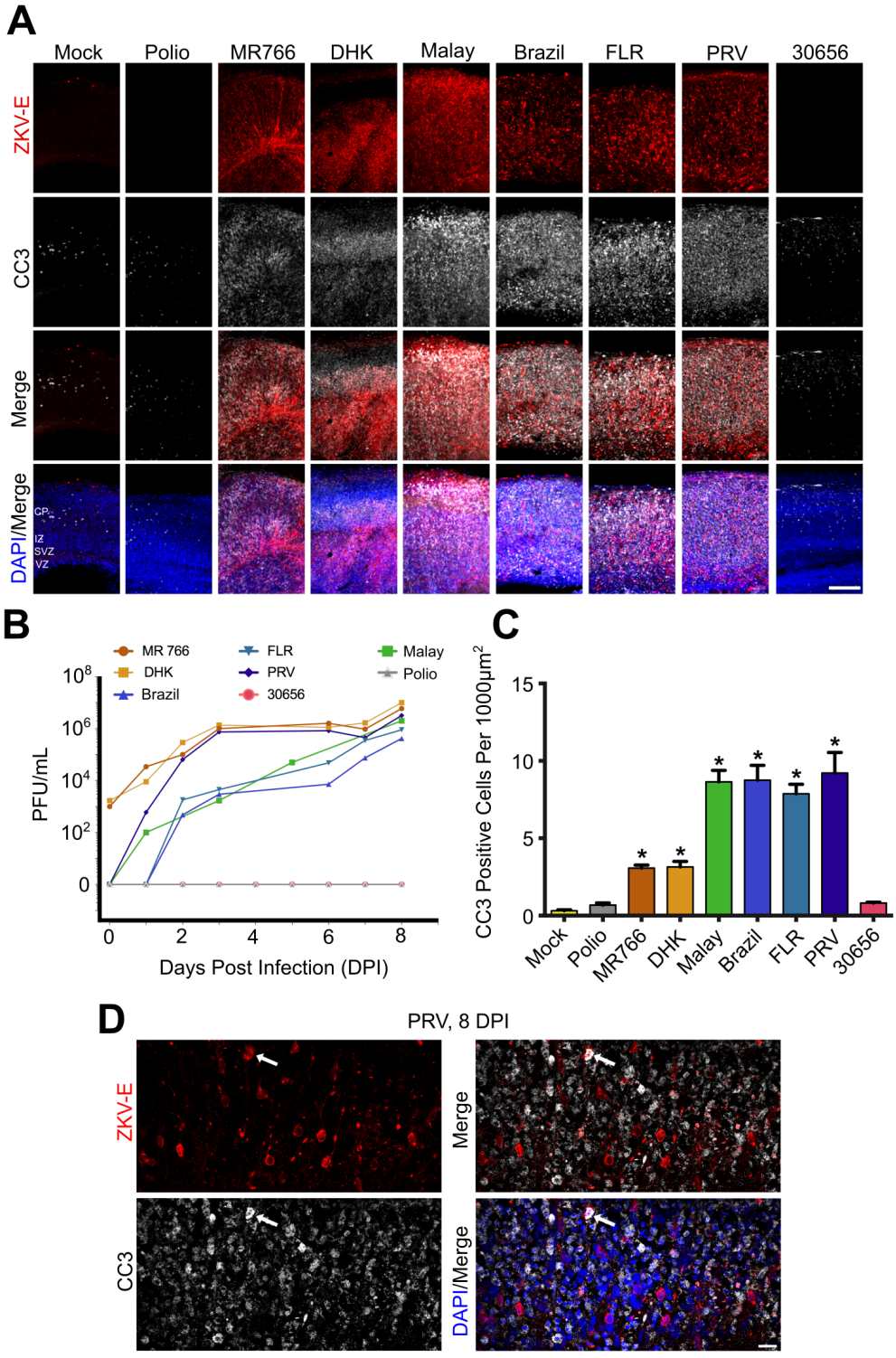

Figure 3.3: **Zika Virus Replicates and Induces Increased Levels of Apoptosis in Brain Slices**: **(A)** All isolates of Zika virus (ZIKV) tested infected brain slices and lead to increases in cleaved caspase-3 (CC3), a marker of apoptosis, except for the Nigerian 30656 isolate. There was no regional specificity to the apoptosis induced in brain slices. Zika virus envelope (ZKV-

E) antibody was used to evaluate infection, and the increase in CC3 positive cells overlapped with regions of ZKV-E staining. **(B)** Additionally all isolates replicated productively by plaque-forming assay, with the exception of the 30656 isolate and Polio Virus, which does not infect mouse brain tissue. The isolates from the Asian/American lineages (Malay, Brazil, FLR, PRV) showed the greatest exponential increase in replication. The African lineages had some productive plaque formation at day zero, suggesting that these virus were more difficult to wash off of the slices, unlike the Asian/American lineages which washed off entirely. All plaque-forming assay curves are depicted as a representative line for each condition, though each experiment was performed in at least 3 replicates **(C)** There are significantly greater levels of apoptosis in the brain slices infected with ZIKV, and a notable increase between isolates from the African and Asian/American lineages. Once again, the 30656 isolate did not lead to increased apoptosis. **(D)** Higher magnification of the cortical plate of brain slices infected with the PRV isolate reveal that the majority of ZKV-E positive cells are indeed negative for CC3 (91.13% 0.132 standard deviation), though there are many CC3 positive cells surrounding the ZIKV infected cells. The only cell in frame that is CC3-positive and ZKV-E-positive is marked with a white arrow. Data presented as scatterplot in (C) and mean ± S.E.M. in (D). Unpaired t-test used in (D) (* for $p<0.05$, n=3 embryonic brains across different replicate experiments). Scale bar is 100μm in (A) and 10μm in (B).

not appear to be localized to any specific zone of the developing neocortex (Figure 3.3A). U87 cells infected with various isolates began to show caspase 3 cleavage between days 3 and 4 by Western blot, with Asian/American lineage strains showing cleavage of caspase 3 earlier (data not shown). The delay in cleavage of caspase 3 beyond the third day post infection was also seen with ZIKV infection of other cultured cell lines (Offerdahl et al., 2016). Intriguingly, isolates from the Asian/American lineages induced significantly more cell death in brain slices than isolates from the African lineage (Figure 3.3A,C). This mirrors one report that an isolate from Cambodia induced greater activation of p53 than the MR766 isolate, as measured by RNA sequencing (Zhang et al., 2016). Examination of the cortical plate of the infected slices revealed that the majority of ZKV-E positive cells are negative for CC3 (91.13% ± 0.132 standard deviation, Figure 3.3E). These cells are often surrounded by CC3 positive cells, suggesting that cells visibly infected with ZIKV are triggering the death of neighboring cells.

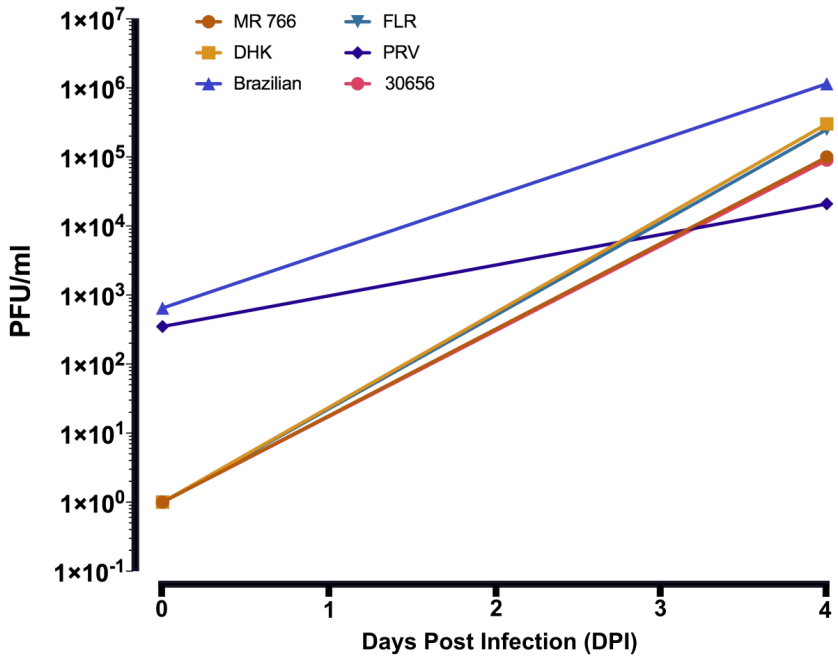

Figure 3.4: All Zika Virus Isolates Replicate in Cultured Cells: Plaque-Forming Assay curves for various Zika virus (ZIKV) isolates in U87 cells over 4 days post infection. All isolates tested replicated in U87 cells.

Given the propensity of ZIKV to target RGPs and spread throughout the radial column, and the frequency of other cortical malformations such as lissencephaly occurring as part of the CZVS, we sought to investigate whether neuronal migration and lamination was impacted. Using *ex utero* electroporation of E15 brains with a control GFP plasmid, neuronal migration of RGP progeny was examined across DHK, FLR, and Brazil isolates (Figure 3.5A). ZIKV from African and Asian lineages both impaired the migration of neurons through the cortical plate 4 DPI (Figure 3.5A-B), with many fewer neurons making it to the outer region of the cortical plate. Vimentin staining, to label RGP basal processes upon which neurons migrate, revealed altered basal process morphology following infection (Figure 3.5C). This was similar to one previous report in human brain tissue (Onorati et al., 2016). However, because of the large areas of cell death and because of any effect that ZIKV

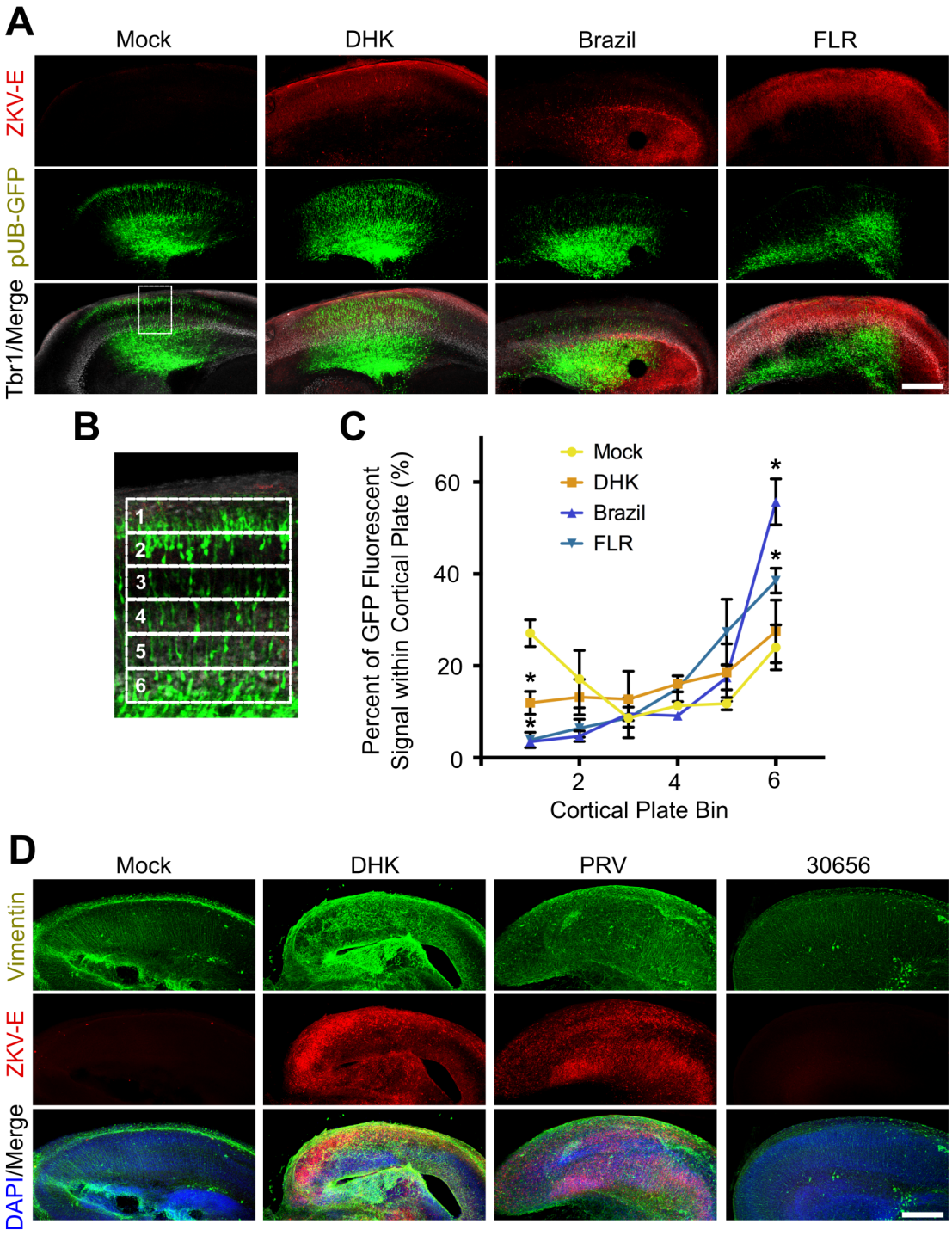

Figure 3.5: Neuronal Migration is Impaired in the Presence of Zika Virus Infection: (A) A GFP control plasmid (pUB-GFP) was electroporated into embryonic day 15 mouse brains using an *ex utero* electroporation procedure, and then slices were infected and cultured as before. Four days post infection (DPI) there was a noticeable impairment in the migration of bipolar neurons through the cortical plate (defined as the region that is Tbr1 positive) in ZIKV infected regions. **(B-C)** The cortical plate was binned into six regions of equal size, and the percentage of GFP

fluorescent intensity in each bin over the whole six bins was calculated. Unlike in Mock treated slices, where there was an accumulation of neurons in the most superficial bin indicating that they had reached their terminal location, DHK, Brazil, and FLR treated slices had significantly less neurons in bin 1. Additionally, there was a large accumulation of electroporated neurons in bin 6 in the Brazil and FLR conditions. **(D)** Vimentin staining was used to mark the radial glia progenitor (RGP) basal processes, which are the tracks upon which bipolar neurons migrate. In slices treated with African (DHK) or Asian/American (PRV) lineage isolates there was disarray of the RGP basal processes, which may contribute to impaired migration through the cortical plate. Data represented as mean ± SEM for each condition in each bin in (C). Unpaired t-test used in (C) (* for $p<0.05$, n=3 embryonic brains across different replicate experiments). Scale bar is 250μm in (A) and (C).

may have intrinsically on migrating neurons, causality for the impaired neuronal migration cannot be established.

Forcing Neurovirulence of the Nigerian 30656 Isolate

Though the 30656 isolate is not able to replicate or infect neuronal tissue, it is able to replicate in non-neuronal cell lines, suggesting that some stage of the viral lifecycle is impaired in neuronal cells. The ZIKV virion is typical of Flaviviruses, with a membrane derived from host endoplasmic reticulum (ER) and studded with viral-derived envelope protein (Kostyuchenko et al., 2016). ZIKV is proposed to undergo a replication cycle similar to other flaviviruses by using the envelope protein to bind host cell receptors, which for ZIKV are proposed to be TIM/TAM tyrosine kinase receptors (Hamel et al., 2015). Clathrin-mediated endocytosis of the virus particle then occurs, and pH-dependent fusion of the virion membrane allows the single-stranded (+) RNA (ssRNA) to enter the host cell cytoplasm (Pierson and Diamond, 2012). Here the ssRNA is directly read by ribosomes, and there is synthesis of new viral proteins that use membrane from the host cell ER to form new viral particles (Pierson and Diamond, 2012). These immature virions are trafficked from the ER through the Golgi and eventually undergo exocytosis to leave the host cell, and

during this export process the virion matures in part through furin cleavage of premembrane proteins (Pierson and Diamond, 2012).

In utero and *ex utero* electroporation have long been used to study brain development through selectively introduction of cDNA plasmids into RGP cells lining the ventricles (Baffet et al., 2015; Bai et al., 2003; Imayoshi et al., 2013; Noctor et al., 2004). Since ZIKV is an ssRNA virus, electroporation of the nonenveloped genetic information into RGPs should allow us to experimentally bypass the steps of virion receptor binding, endocytosis, and virion/endosome membrane fusion. To do this viral isolates were deproteinated, the ssRNA was injected into the lateral ventricles of E15 embryonic brains, and *ex utero* electroporation was performed (Figure 3.6A). The organotypic brain slice protocol was then followed as in previous experiments, with plaque assay and immunohistochemical staining of slices being the experimental endpoints (Figure 3.6A). Human rhinovirus 16 (HRV16), which does not infect murine or neuronal tissue, as well as ZIKV ssRNA treated with RNAase were used as negative controls.

Four days after electroporation there was robust replication of the PRV isolate and the 30656 isolate (Figure 3.6D), though the 30656 isolate replication plateaued after 3 days, which suggests that the virions generated after ssRNA electroporation could not go on to re-infect the brain slice. This technique also allowed for viral spread to be more closely monitored, since the injection and placement of the electrode paddles determines where infection will originate. The electroporations targeted only one hemisphere of neocortex, with some residual labeling of the midbrain due to the injected solution spreading into the third

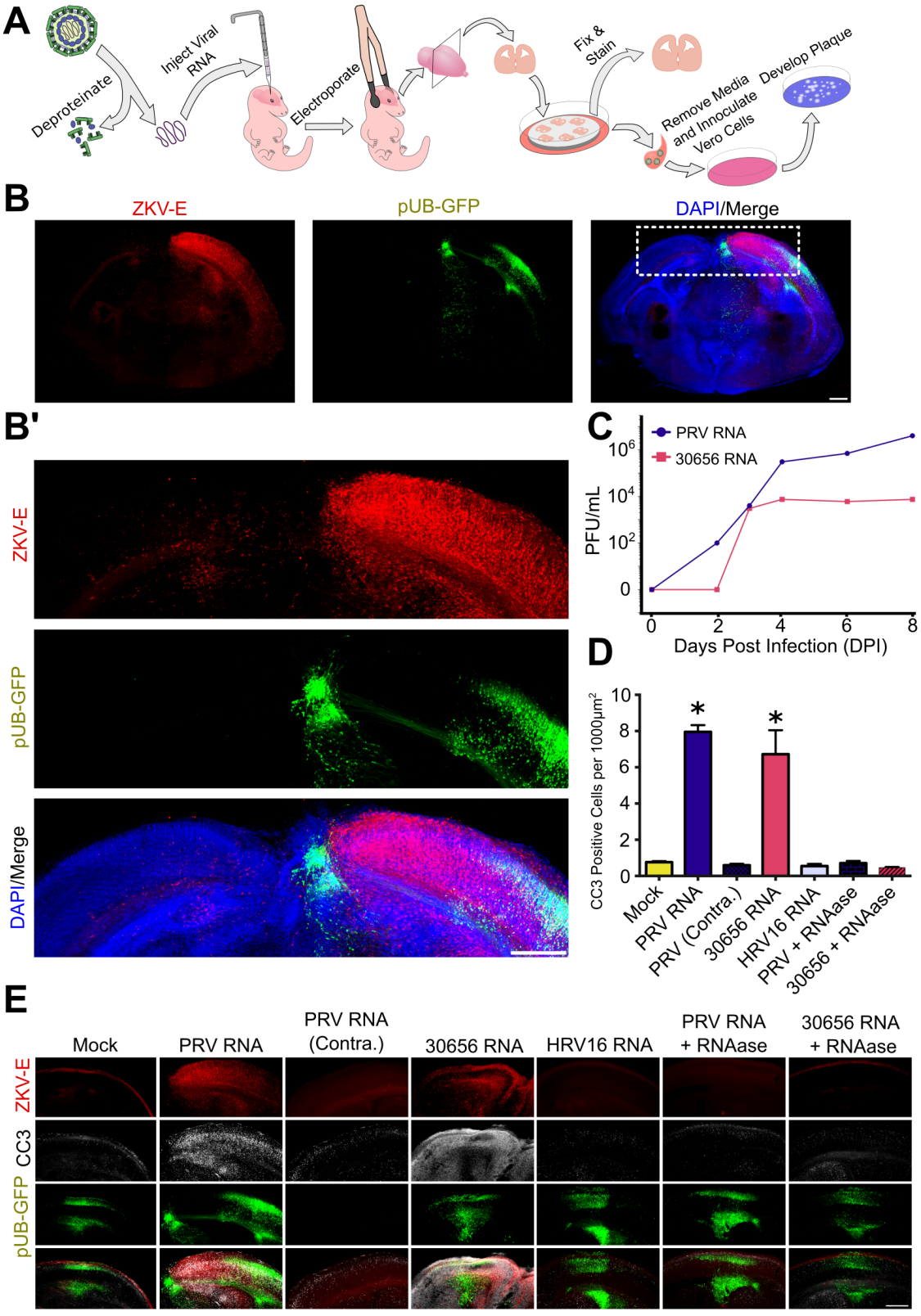

Figure 3.6: *Ex Utero* Electroporation of the Zika Virus Genome Into Mouse Brain Supports Replication of the 30656 Isolate: (A) Schematic of the protocol whereby Zika (ZIKV) virus iso-

lates were deproteinated and the single-stranded positive RNA (ssRNA) was injected into the lateral ventricle of embryos *ex utero*, electroporated, and brain slices then generated in accordance with the previous protocol (Figure 3.1A). **(B)** Example of whole-brain staining from electroporation of PRV ssRNA. Zika-virus envelope (ZKV-E) protein signal was very strong in the dorsomedial region of the electroporated hemisphere, which was marked by co-electroporation of a GFP plasmid (pUB-GFP). **(B')** Notably the ZKV-E signal also extended to the contralateral hemisphere, where there was no pUB-GFP signal present. **(C)** Plaque-forming units from electroporation of PRV or 30656 ssRNA demonstrates that both strains could replicate efficiently, though the 30656 strain plateaued after 4 days post-electroporation. There was no viral replication when each ssRNA was treated with RNAase, or with ssRNA for a human rhinovirus (HRV16) that does not replicate in mouse neuronal tissue. **(D-E)** Electroporation of the PRV or 30656 ssRNA led to significant increases in apoptosis, measured by cleaved-caspase 3 (CC3) staining. There was no corresponding increase of CC3 in the contralateral hemisphere (excluding the dorsomedial region where there were some ZKV-E positive cells) of PRV ssRNA electroporated slices, or in slices electroporated with HRV16 or RNAase treated ssRNA. Data presented as mean ± SEM in (D). Unpaired t-test used in (D) (* for $p<0.05$, n=3 embryonic brains across different replicate experiments). Scale bar is 250μm in (B), (B'), and (C).

ventricle, as seen by labeling with the pUB-GFP fluorescent plasmid that was co-injected with ssRNA (Figure 3.6B-C). ZKV-E signal did not completely overlap with the pUB-GFP fluorescence, indicating some spread of the virus especially in the dorsomedial direction (Figure 3.6B-C). Interestingly, in the original ZIKV infection protocol the most dorsal and ventral aspects of the neocortex often had the strongest ZKV-E signal (Figure 3.2A), though it is unclear why the virus may have a predilection for these neuroanatomical regions. Surprisingly, the ZKV-E signal was not confined unilaterally, and it spread to the contralateral hemisphere, though the staining was mostly limited to the dorsomedial region and not nearly as robust as in the electroporated hemisphere (Figure 3.6C).

Examination of the brain slices 8 days after electroporation revealed increases in apoptosis within the ZKV-E positive regions, but not throughout the brain slices, consistent with local infection triggering cell death (Figure 3.6E-F). Interestingly, the electroporation of 30656 ssRNA triggered a level of apoptosis close to the PRV ssRNA (Figure 3.6E-F). None of the slices electroporated with

HRV16 or PRV/30656 ssRNA treated with RNAase had ZKV-E signal (Figure 3.6E-F) or caused any plaque formation (Figure 3.6D).

Only One Recently Found Isolate of ZIKV is Able to Replicate in Late-Gestation Neuronal Tissue

Epidemiological studies have indicated that the greatest risk of fetal complications from ZIKV infection are during the first and second trimester (Brasil et al., 2016; Pacheco et al., 2016), though recent reports have indicated that complications in pregnancy may occur as late as in the 36th week of gestation (Soares de Souza et al., 2016), and secondary microcephaly may occur after birth in previously non-microcephalic children (Moura da Silva et al., 2016; van der Linden et al., 2016). No studies have yet been able to systematically investigate the potential of ZIKV to infect embryonic neuronal tissue across various gestation periods, but using organotypic slice culture we can easily test the infectious potential of ZIKV isolates across embryonic ages. Slices generated from E13 embryos robustly supported viral replication across all isolates with the exception of the 30656 isolate (Figure 3.7A-B). As soon as 3 DPI there were clear focal areas of ZKV-E staining in the E13 slices (Figure 3.7A), all consistent with a predilection of ZIKV to infect and replicate in early- and mid-gestation embryonic tissue.

Late-gestation embryonic tissue was examined by culturing brain slices derived from E19 embryos. No ZIKV isolates were able to replicate after 8 DPI, except for a recent isolate from Honduras (Figure 3.8B). In accordance with this, no ZKV-E signal was seen in E19 slices 8 DPI except for the Honduran isolate conditions, which displayed strong immunohistochemical signal in the neocortex of

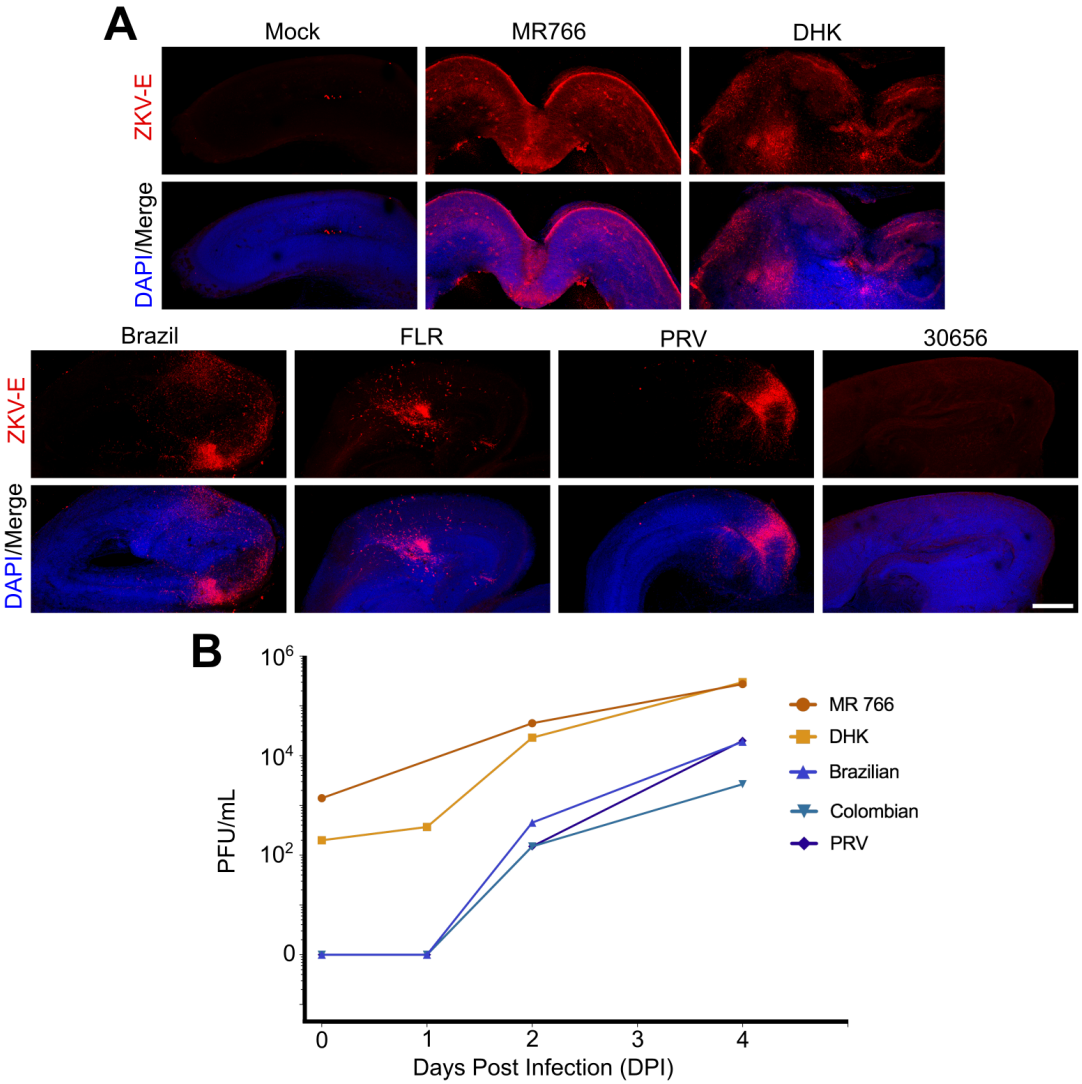

Figure 3.7: Zika Virus Infects and Robustly Replicates in Early Gestation Neuronal Tissue: (A) Embryonic day 13 (E13) brain slices were infected with Zika virus isolates, fixed 3 days post infection (DPI), and stained for Zika virus envelope protein (ZKV-E). There were focal areas of infection across the African and Asian/American lineage conditions, with the exception of the 30656 isolate. Scale bar is 250μm. **(B)** Plaque forming unit curve for various isolates in E13 brain tissue.

E19 slices (Figure 3.8A). There was a corresponding increase in apoptosis in the E19 slices infected with the Honduran isolate in comparison with slices in the mock condition or exposed to the PRV isolate (Figure 3.9A-B). In the upper cortical plate nearly all infected cells stained positive for Cux1, a marker of neurons in superficial cortical layers (Figure 3.9C). No cells that stained positive for ZKV-E were positive

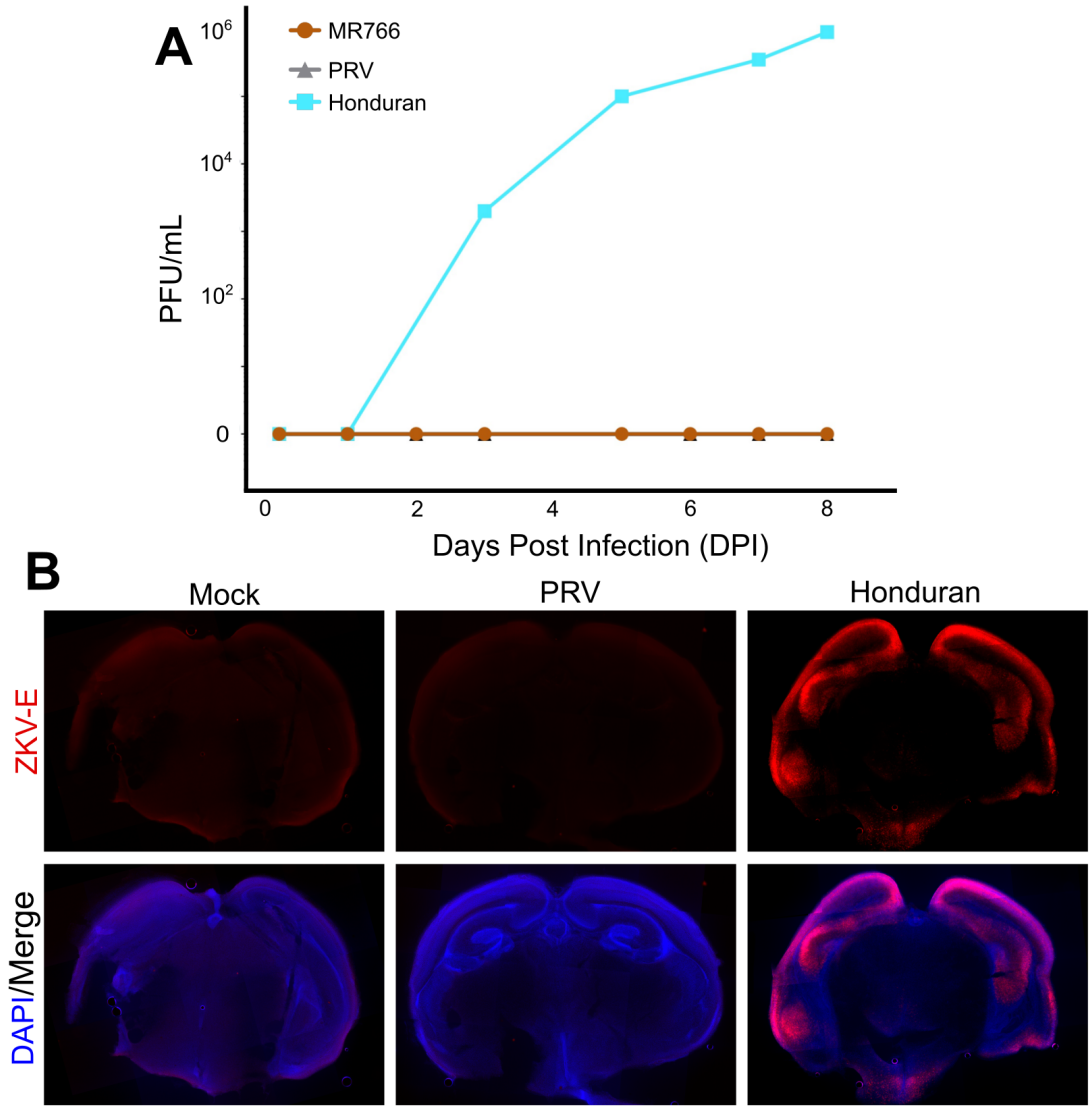

Figure 3.8: Only the Honduran Isolate Infects and Replicates in Late Gestation Neuronal Tissue: (A) None of the Zika virus isolates tested replicated in embryonic day (E19) brain slices except for the Honduran isolate, which was the most recently isolated condition tested. **(B)** Brain slices 8 days post infection (DPI) stained for Zika virus envelope protein (ZKV-E) after mock infection or infection with PRV or Honduran. ZKV-E signal in the Honduran condition was almost entirely restricted to the neocortical region. Scale bar is 500μm in (B).

for GFAP, a marker of astrocytes (Figure 3.9D). The Honduran isolate was also able to infect and replicate in E15 brain slices, leading to resulting increases in apoptosis (Figure 3.10A-C). These results suggest that the Honduran isolate of ZKV-E has the

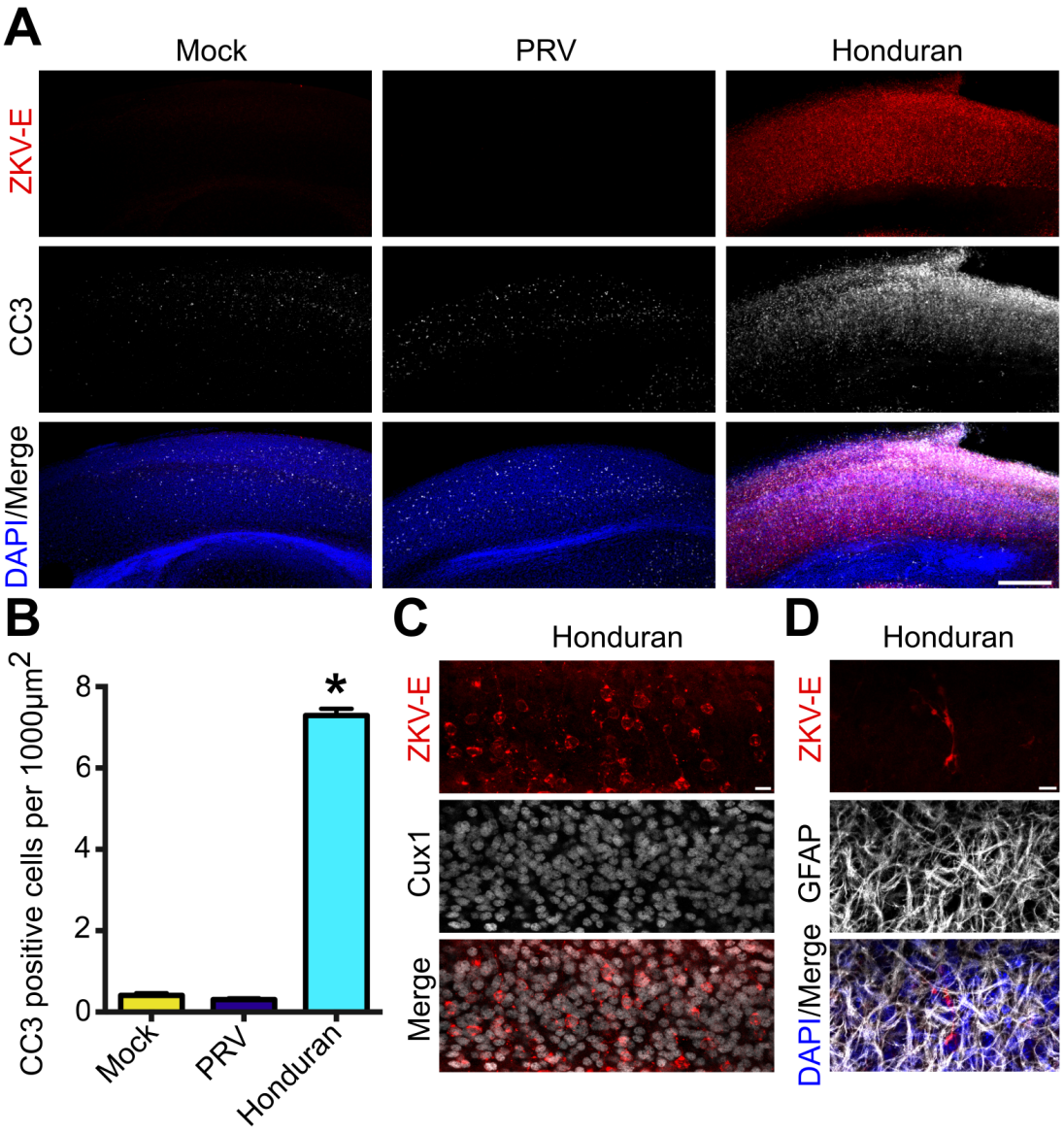

Figure 3.9: The Honduran Isolate Leads to Increased Apoptosis and Preferentially Infects Neurons in Late Gestation Neuronal Tissue: (A) Representative images from embryonic day 19 (E19) brain slices infected with mock, PRV, or Honduran Zika virus isolates, and stained for Zika virus envelope protein (ZKV-E) and cleaved-caspase 3 (CC3). **(B)** There was a demonstrative increase in CC3 staining in areas of ZKV-E staining after infection with the Honduran isolate. **(C)** Nearly all ZKV-E positive cells in the superficial layers of the neocortex stained positive for Cux1, a marker of layer II/III/IV neurons. **(D)** No ZKV-E positive cells also stained positive for the astrocyte and glia progenitor marker GFAP. Data presented as mean ± SEM in (B). Unpaired t-test used in (B) (* for $p<0.05$, n=3 embryonic brains across different replicate experiments). Scale bar is 250μm in (A) and 10μm in (C) and (D).

potential to infect and replicate in late-gestation embryonic brain tissue, but also may be able to infect and replicate in neurons.

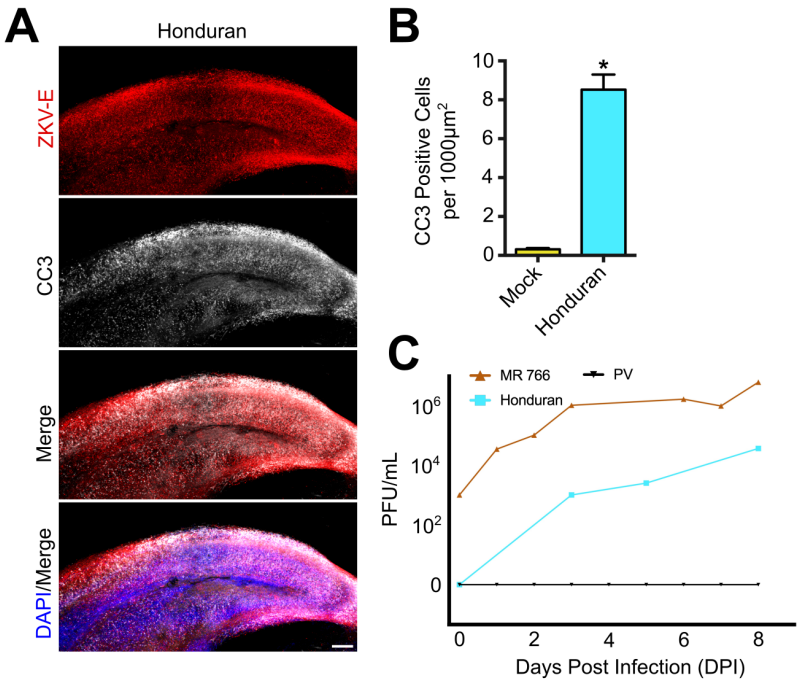

Figure 3.10: The Honduran Isolate Infects, Replicates, and Leads to Apoptosis in Mid-Gestation Neuronal Tissue: (A) Representative staining of Zika virus envelope protein (ZKV-E) in an E15 brain slice 8 days post infection (DPI) with the Honduran isolate. There does not appear to be a restriction of the ZKV-E signal to the cortical plate, though the signal is strongest in the developing neocortex. **(B)** There is an increase in apoptosis in E15 brain slices infected with the Honduran isolate. Mock data set reproduced from Figure 3.3. **(C)** The Honduran isolate replicates efficiently in E15 neuronal tissue. Mock data set reproduced from Figure 3.3. Data presented as mean ± SEM in (B). Unpaired t-test used in (B) (* for $p<0.05$, n=3 embryonic brains across different replicate experiments). Scale bar is 100μm in (A).

DISCUSSION:

The past decade has seen the rapid spread of ZIKV through much of the Western Hemisphere, with every country except Canada now recording cases of local ZIKV transmission. This epidemic has been accompanied by the emergence of a wave of microcephaly, part of the broader CZVS (Lessler et al., 2016). A causal link between ZIKV and microcephaly has been established (World Health Organization, 2016), but the full extent of CZVS is just beginning to emerge as an increasing number of children are born with malformations of cortical development beyond microcephaly (Soares de Oliveira-Szejnfeld et al., 2016; Štrafela et al., 2016). Various studies have suggested different mechanisms by which ZIKV may cause CZVS (Brault et al., 2016; Li et al., 2016b; Miner et al., 2016a; Retallack et al., 2016), but it

has been difficult to reconcile and compare across the reports with different findings. Here we have used organotypic brain slices from immunocompetent embryonic mice to systematically investigate the ability of different isolates of ZIKV to infect, replicate, and damage the developing brain. All isolates of ZIKV tested replicated in E13 and E15 brain tissue and led to extensive cell death, with the exception of the Nigerian 30656 isolate that was obtained in 1968. This isolate was able to replicate in neuronal tissue when its ssRNA was electroporated into RGPs, suggesting a defect in virion entry into the host cell. Notably no isolates were able to replicate in late gestation tissue, except for the most recent isolate tested from Honduras. This Honduran isolate preferentially infected neurons in the neocortex, and retained the capacity to infect and replicate in E15 brain tissue as well. These results expand our understanding of the pathogenesis of malformations of cortical development caused by various circulating isolates of ZIKV, and the importance infection timing during pregnancy.

Many of the animal models used to study ZIKV infection rely on immunocompromised mice in which interferon signaling is impaired (Govero et al., 2016; Lazear and Diamond, 2016; Miner et al., 2016a; 2016b). Blocking the innate immune system, but not the adaptive immune system, facilitates ZIKV infection of adult mice (Lazear and Diamond, 2016), though injection of the virus into the lateral ventricle of immunocompetent ICR strain mice permitted viral infection (Li et al., 2016b). Here Swiss Webster mice were used, which are fully immunocompetent (Colton et al., 2010), and there was productive ZIKV replication across a variety of isolates. This is the first study to monitor ZIKV replication in embryonic brain tissue

by plaque-forming assay, which measures infectious virus production and not just viral RNA levels or viral protein (such as ZKV-E) levels. These results suggest that once most isolates of ZIKV reach the early- and mid-gestation embryonic brain, they will be able to replicate efficiently and productively.

One of the most striking effects of ZIKV infection seen in our slice culture technique is the widespread cell death across ZIKV isolate infection. All ZIKV isolates that infected brain tissue lead to increased apoptosis, though isolates of the Asian/American lineages – including isolates from Malaysia, Brazil, Columbia, Puerto Rico, and Honduras – appeared to cause an even greater increase in apoptosis than isolates from the African lineage. There is one other report that an isolate from Cambodia caused increased p53 activation compared to the MR766 strain, as measured by RNA sequencing of infected cell culture (Zhang et al., 2016). This increase in apoptosis among the isolates of the Asian lineage may explain the increase in microcephaly and CZVS seen during the recent outbreak, though there are many other possible causes for this. Our study was not able to examine how the virus may reach the embryonic brain after the mother is infected, which is another critical component of how isolates may have mutated to cause increased disease burden (Lessler et al., 2016). Other potential explanations include a faster and more virulent spread of ZIKV due to mutations effecting its lifecycle in the mosquito, unique human genetics among the populations effected by the epidemics, or synergistic interactions of preexisting immunity to other flaviviruses in predisposing patients to severe complications from ZIKV infection (Lessler et al., 2016).

In addition to the increase in apoptosis there was the peculiar finding that the majority of cells positive for ZKV-E were not positive for CC3. This culling of apparently non-ZIKV infected cells suggests that either the ZKV-E signal in these dying cells is too low to be visualized by immunohistochemistry, or that the infected cells are releasing some cytokine to induce apoptosis in neighboring cells. We looked at cleaved-caspase 8 (CC8) activation, which is cleaved in response to TNF signaling as it triggers the extrinsic apoptosis pathway, though there was no immunohistochemical signal in brain slices, and western blot of U87 cell lysate showed no cleavage of caspase 8 (data not shown). These data do not rule out that the CC3 activation in cells surrounding ZKV-E positive cells are dying in response to a cytokine signal, but complicate the picture beyond the traditional extrinsic apoptosis pathway.

While the organotypic brain slices used here allowed us to confirm that ZIKV readily infects RGP cells, the difficulty in preserving the ventricular surface and the cytoarchitecture of the ventricular zone over long periods in culture prevents us from assessing the impact of ZIKV on RGP proliferation. Other reports of intraventricular injection or infection of brain organoids with ZIKV have all suggested that there is a decrease in the mitotic index of RGPs (Li et al., 2016b; Qian et al., 2016; Wu et al., 2016). It remains unknown whether this mitotic index decrease is due to impairments in RGP cell cycle progression that would lower the mitotic index (Doobin et al., 2016), or if the increased apoptosis we see throughout the slices is also reducing the number of RGPs in the ventricular zone, subsequently lowering the mitotic index. Either with improvements in our slice culture technique,

or the initiation of *in vivo* studies involving lateral ventricle injections of ZIKV, we will be able to investigate the impact of various isolates on RGP proliferative capacity.

The cortical malformations associated with CZVS extend beyond microcephaly to include lissencephaly, pachygyria (too few gyrations), subcortical calcifications, and ventriculomegaly (an expansion of the ventricular space) (Soares de Oliveira-Szejnfeld et al., 2016; Štrafela et al., 2016). Subcortical calcifications are long-term, nonspecific pathological changes to tissue resulting from damage, and these pathological changes and the microcephaly are likely explained by the large increase in apoptosis following ZIKV infection. Through electroporation of an empty GFP vector prior to slice culture, we also found that neuronal migration was impaired by ZIKV infection. RGP basal processes serve as ladders upon which neurons migrate to their final locations in the cortical plate, and vimentin staining of RGP basal processes following ZIKV infection indicated gross disruption. A similar aberrant vimentin staining was seen in human brain tissue following ZIKV infection (Onorati et al., 2016). Since RGP basal processes are required for neuronal migration, these impairments to their structure may contribute to the neuronal migration defects, potentially leading to cortical lamination defects (Barkovich et al., 2012), though these impairments in neuronal migration could also be due to increased apoptosis throughout the brain, or ZIKV infection intrinsic to the migrating neurons.

An unexpected finding was that not all ZIKV isolates were neurovirulent. One of the older isolates examined, from a human patient in Nigeria in 1968, did not

replicate or infect neuronal tissue or cells. It was capable of replicating in non-neuronal cells and U87 cells in culture, and intriguingly, the electroporation of the genetic material from deproteinated virus permitted for its infection and one-phase replication. This suggests that there is something intrinsically different about the 30656 isolate that prevents either: 1) it's binding to the putative host cell receptor, 2) the ability of the host cell to endocytose it, or 3) the fusion of the endosome membrane with the virion membrane (Figure 3.11). Analysis of the isolate genomes reveals four amino acid substitutions in the viral envelope protein unique to the 30656 isolate. Two of these amino acid substitutions – a serine in place of an alanine at position 214, and a glutamic acid in place of a glycine at 219 – are very close to each other and change the hydrophobic nature of that part of the protein. The generation of infectious clones from the 30656 isolate (the ZIKV genome is approximately 10.7kb) will allow us to investigate if these residues indeed do confer neurovirulence to ZIKV.

Another finding from the *ex utero* electroporation of the positive ssRNA experiments was that the spread of the virus in our experimental model was rather limited. After 8 days in culture, the virus would often spread beyond the region of electroporation, particularly into the dorsomedial aspect of the neocortex. The virus even spread a bit into the contralateral hemisphere, as displayed by the PRV ssRNA electroporation. Interestingly across experiments the entire slice was never positive for ZKV-E, and this mirrors the initial focal areas of infection seen 3 DPI in the first protocol we employed (Figure 3.1A). Despite bathing the slices in solution containing ZIKV and placing the slices on a rocker, the infection always began from

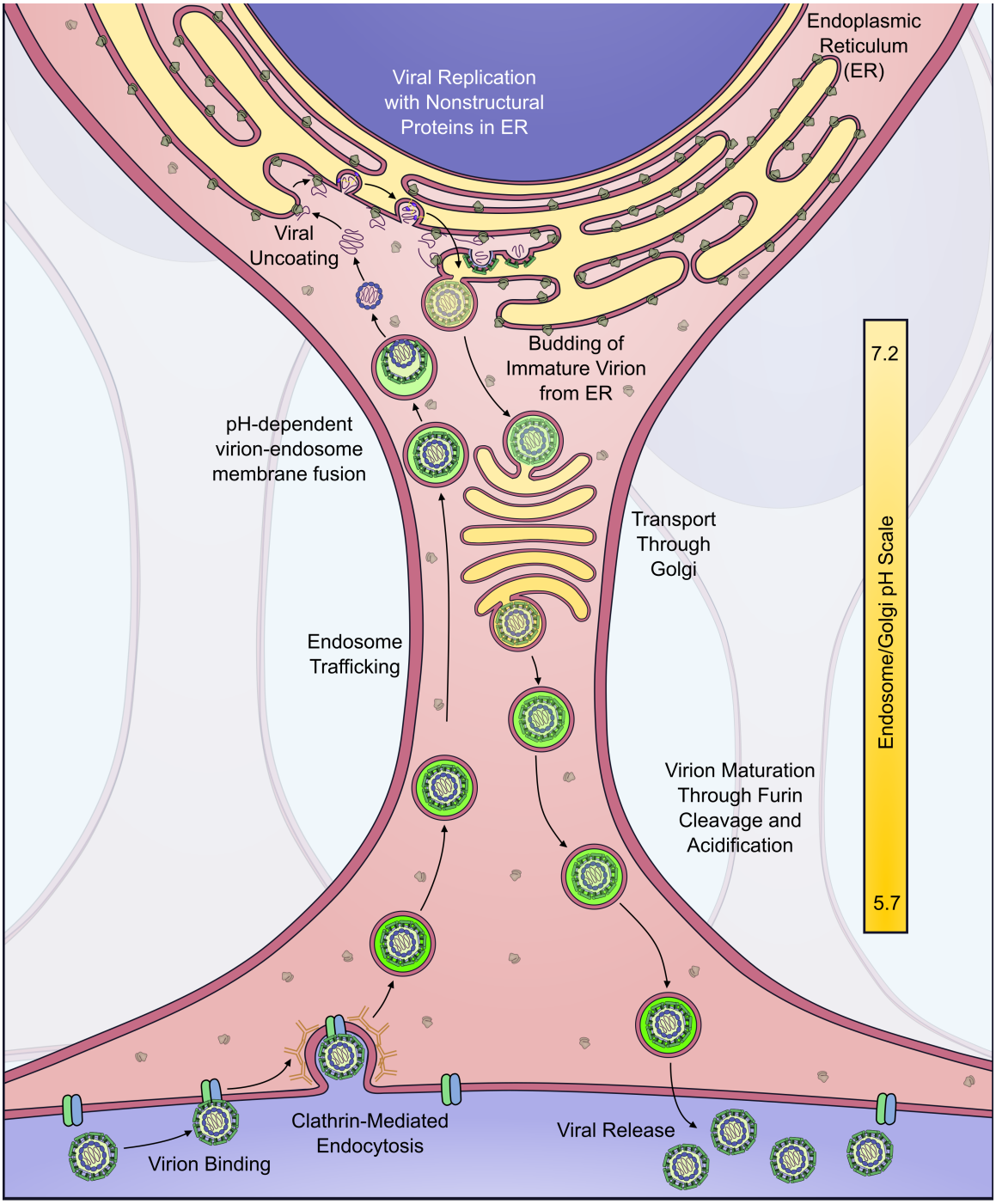

Figure 3.11: Proposed Model of Zika Virus Lifecycle in Radial Glia: A model of the proposed Zika virus (ZIKV) replication cycle in radial glia progenitors (RGPs), largely based on what is known of the replication cycle for other flaviviruses. Neuronal infection of the Nigerian 30656 isolate does not produce infectious particles unless the RNA genome is directly introduced into the cell. This observation suggests that early steps of infection, including attachment, entry and uncoating may be isolate specific. For a more thorough explanation of the steps in the Flavivirus replication cycle please see Pierson and Diamond, 2012.

focal areas, indicating that ZIKV infection of neuronal tissue is not guaranteed, even if the virus is directly exposed to the cells.

Finally, using organotypic slices from different embryonic days allowed us to examine the propensity of the virus to infect and replicate in neural tissue from different gestation periods. While all ZIKV isolates other than the 30656 isolate infected and replicated in E13 and E15 tissue (corresponding to late-first trimester and early-second trimester neocortical development in humans), only the most recently isolated ZIKV sample – an isolate from Honduras from 2016 – infected and replicated in E19 tissue. The ZKV-E signal from the Honduran isolate was largely restricted to the neocortex, which suggested that the isolate had a propensity to infect neurons. Though there are still RGPs present in E19 slices, after 8 days in culture the RGPs have only been producing astrocytes for a few days, and are just beginning to produce oligodendrocytes (Kriegstein and Alvarez-Buylla, 2009). Therefore the majority of the cells in the developing neocortex are expected to be young neurons, and this was confirmed by the overlap of Cux1 with ZKV-E in this region. Unlike the 30656 isolate, there are no overt, unique mutations in the coding region of the RNA of the Hondoran isolate, though there is considerable variation in the 5' and 3' UTR. These regions often vary among ZIKV isolates, and increasing evidence has shown that untranslated regions can play prominent roles in determining neurovirulence (Butrapet et al., 2000; Evans et al., 1985; Gromowski et al., 2015).

All together it becomes evident that various isolates of ZIKV behave differently. Nearly all isolates infected and replicated in early- and mid-gestation

embryonic tissue, though only one replicated in late-gestation tissue. The Asian/American lineage isolates led to greater levels of apoptosis, particularly of the cells neighboring infected cells, than the African lineage isolates. Furthermore, the analysis of the 30656 isolate provides a hint as to how ZIKV may have adapted to posses neurovirulence and lead to microcephaly and CZVS.

EXPERIMENTAL PROCEDURES

Brail Slice Preparation and Culture: Timed pregnant Swiss Webster mice were purchased from Taconic Labs at ages E13, E15, E17 and E19; E1 was defined as the day of confirmation of sperm-positive vaginal plug. Mice were sacrificed and embryos were harvested. Fetal brains were dissected into ice-cold artificial cerebrospinal fluid (ACSF) consisting of 125mM NaCl, 5mM KCl, 1.25mM NaH_2PO_4, 1mM $MgSO_4$, 2mM $CaCl_2$, 25mM $NaHCO_3$, and 20mM glucose, pH7.4, 310 $mOsm1^{-1}$. Brains were embedded in 4% low melting point agarose dissolved in ACSF and sliced into 300mm coronal sections using a vibratome (Zeiss). Slices were then transferred to Millicell-CM filter-paper inserts (Millipore; 0.4mm, 30mm diameter), which were placed a 6-well culture plate above 1mL of cortical culture medium (CCM) containing 25% Hanks balanced salt solution, 47% basal MEM, 25% normal horse serum, 1X penicillin-streptomycin-glutamine, and 30% glucose. Cultures were maintained in a humidified incubator at 37 °C with constant 5% CO_2 supply.

Zika Virus Stocks: Zika viruses (ZIKV) used include: MR766 (Ugandan origin), DAK (Senegal), IbH30656 (Nigerian), FLR (Colombia), PRVABC59 (Puerto Rico) and R103451 (Honduras), and P-6740 (Malaysia) were obtained from BEI Resources. Brazilian isolate (ZIKV-Paraiba/2015) was kindly provided by Lucia Gama (Johns Hopkins, Baltimore Maryland). All viruses were propagated in Vero cells. Viral titers were determined by plaque assay.

Virus infections: Organotypic brain slice cultures were infected with were infected with 10^5 pfu of ZV isolates: MR766 African, DHK Senegal, Nigerian IbH 30656, Brazilian, FLR, PRVABC59, P 6-740 Malaysia, and R103451 Honduras, poliovirus

(P1/Mahoney) or encephalomyocarditis virus (EMCV). Virus inoculum was added to the top of the filter, bathing the slices as the dish was placed on a rocker, and the viruswas allowed to adsorb to the slices for 1h at 37 °C. The inoculum was removed, and the slices were washed 2X in 1X PBS. Infected slices were cultured in CCM for up to 8 days. 500ml of culture medium was removed and replenished at the described points post infection for plaque-assay purposes.

Immunohistochemistry: Either 3, 4, or 8 days post infection, the medium was removed from Zika virus infected or uninfected organotypic brain slices cultures and the cultures were placed for 2hrs in 4% paraformaldehyde (PFA) fixative dissolved in 1X PBS at room temperature. Following fixation, slices were washed 3x5min in 1X PBS, and were incubated in blocking solution of PBS, 0.3% Triton X-100 and 3% donkey serum. Slices were incubated overnight at 4 °C in blocking solution containing appropriate primary antibodies. Sections were washed 3x5min in 1X PBS, and incubated with fluorophore-conjugated secondary antibodies in blocking solution. Sections were washed 3x5min in 1X PBS, and mounted on slides using Aqua-Poly/Mount (Polysciences, Inc).

***Ex-utero* electroporation:** Plasmids and isolated viral encoding RNA were transfected by intraventricular injection into the left lateral ventricle of dissected embryonic brains at the appropriate embryonic age. DNA or RNA was mixed with colored non-toxic dye and 1μg of nucleic acid was injected into the ventricular space using a high gauge needle made from glass capillary tube. Post injection, five pulses of electrical current (50V, 5ms each, with 1s intervals) were applied by directly placing electrodes on the outer surface of the embryonic head, with the positively

charged paddle placed at the dorsolateral aspect of the head on the ipsilateral side of injection. Brain slices were generated following transfection and cultures were maintained up to 8 days post electroporation. Viral titers were determined by plaque assay. An ubiquitin-promoter GFP was used as an empty vector (obtained on Addgene from the laboratory of Connie Cepko) to assay neuronal migration, or in combination with viral-RNA to label the electroporation.

Isolation of viral RNA: Supernatants from virus-infected cells were centrifuged in an SW41 rotor (Beckman) for 2h at 40,000 rpm. The pellet was resuspended in DMEM and viral RNA was isolated using TRIzol reagent (Invitrogen) according to the manufacturer's protocol. Isolated viral RNA was treated with RNAase for 1hr at 37˚C for control conditions.

Cell culture: Vero cells were grown in Dulbecco's modified Eagle medium (Invitrogen, Carlsbad, CA), 10% fetal calf serum (HyClone, Logan, UT), and 1% penicillin-streptomycin (Invitrogen). U-87 MG (human glioblastoma, ATCC) cells were grown in Dulbecco's modified Eagle medium (Invitrogen, Carlsbad, CA), 10% fetal calf serum (HyClone, Logan, UT), and 1% penicillin-streptomycin (Invitrogen).

Plaque assay: Vero cells were seeded on 60mm plates for approximately 70% confluence at the time of plaquing. Next, 100l portions of serial 10-fold virus dilutions were incubated with cells for 1 h at 37 °C. Two overlays were added to the infected cells. The first overlay consisted of 2 ml of 1 DMEM, 0.8% Noble agar, 0.1% bovine serum albumin, 40 mM $MgCl_2$, and 10% bovine calf serum. After solidification, a second liquid overlay was added that was composed of 1 DMEM, 0.1% bovine serum albumin, 40 mM $MgCl_2$, 0.2% glucose, 2 mM pyruvate, 4 mM

glutamine, and 4 mM oxaloacetic acid. The cells were incubated at 37 °C for 6-8 days and developed by using 10% trichloroacetic acid and crystal violet.

Antibodies: Antibodies used in this study were mouse monoclonal against E glycoprotein (Millipore, MAB 10216, 1:250 dilution), rabbit polyclonal against CDP/Cux1 (Santa-Cruz, SC-1302, 1:1000 dilution), cleaved caspase 3 (Cell Signaling, 9661, 1:500 dilution), cleaved caspase 8 (Cell Signaling, 8592, 1:100 dilution), cleaved caspase 9 (Cell Signaling, 9509, 1:500 dilution), Pax6 (Covance, PRB-278P, 1:500 dilution), Tbr1 (Abcam, ab31940, 1:500 dilution), and chicken polyclonal against vimentin (Millipore, AB5733, 1:1000 dilution). Donkey fluorophore-conjugated secondary antibodies (Jackson Labs, 1:500 dilution) were used together with DAPI (4',6-diamidino-2-phenylindole, Thermo Scientific, 62248, 1:1,000 dilution).

Imaging, Quantification, and Statistical Analysis: All images were collected with an IX80 laser scanning confocal microscope (Olympus FV100 Spectral Confocal System). Brain sections were imaged using a 60x 1.42 N.A. oil objective or a 10x 0.40 N.A. air objective. All drawings were composed using Inkscape open source software. All images were analyzed using ImageJ software (NIH, Bethesda, MD). Apoptotic index and neuronal migration analysis was performed using this software. Apoptotic index was quantified by defining and measuring a region of viral infection in a single z-plane and counting the number of cleaved-caspase positive cells in that region. Neuronal migration was quantified by converting the GFP signal on an entire slice into grayscale, isolating an evenly electroporated region of the cortical plate (defined based on Tbr1 positivity) that overlapped with viral signal,

dividing that region into six bins of equal area, and measuring the fluorescent intensity of GFP signal across each bin. For apoptotic index and neuronal migration assays, at least 3 slices were quantified from 3 separate replicates of the same experiment. All statistical analysis was performed using Prism (GraphPad Software, La Jolla, CA, USA). Unpaired t-tests were used for comparison of apoptotic indices and neuronal migration bin fluorescent intensity. For all analyses significance was accepted at the level of $p<0.05$. The ROUT method was used to identify any outliers, none of which were found across the conditions. For plaque-forming assay quantifications, each experiment was replicated at least 3 times, and the representative plot for plaque-formation was depicted for each condition.

REFERENCES:

Aliota, M.T., Caine, E.A., Walker, E.C., Larkin, K.E., Camacho, E., and Osorio, J.E. (2016). Characterization of Lethal Zika Virus Infection in AG129 Mice. PLoS Negl Trop Dis *10*, e0004682.

Baffet, A.D., Hu, D.J., and Vallee, R.B. (2015). Cdk1 Activates Pre-mitotic Nuclear Envelope Dynein Recruitment and Apical Nuclear Migration in Neural Stem Cells. Developmental Cell *33*, 703–716.

Bai, J., Ramos, R.L., Ackman, J.B., Thomas, A.M., Lee, R.V., and LoTurco, J.J. (2003). RNAi reveals doublecortin is required for radial migration in rat neocortex. Nat Neurosci *6*, 1277–1283.

Barkovich, A.J., Guerrini, R., Kuzniecky, R.I., Jackson, G.D., and Dobyns, W.B. (2012). A developmental and genetic classification for malformations of cortical development: update 2012. Brain *135*, 1348–1369.

Betizeau, M., Cortay, V., Patti, D., Pfister, S., Gautier, E., Bellemin-Ménard, A., Afanassieff, M., Huissoud, C., Douglas, R.J., Kennedy, H., et al. (2013). Precursor diversity and complexity of lineage relationships in the outer subventricular zone of the primate. Neuron *80*, 442–457.

Brasil, P., Pereira, J.P., Raja Gabaglia, C., Damasceno, L., Wakimoto, M., Ribeiro Nogueira, R.M., Carvalho de Sequeira, P., Machado Siqueira, A., Abreu de Carvalho, L.M., Cotrim da Cunha, D., et al. (2016). Zika Virus Infection in Pregnant Women in Rio de Janeiro - Preliminary Report. N. Engl. J. Med.

Brault, J.-B., Khou, C., Basset, J., Coquand, L., Fraisier, V., Frenkiel, M.-P., Goud, B., Manuguerra, J.-C., Pardigon, N., and Baffet, A.D. (2016). Comparative Analysis Between Flaviviruses Reveals Specific Neural Stem Cell Tropism for Zika Virus in the Mouse Developing Neocortex. Ebiom 1–23.

Butrapet, S., Huang, C.Y., Pierro, D.J., Bhamarapravati, N., Gubler, D.J., and Kinney, R.M. (2000). Attenuation markers of a candidate dengue type 2 vaccine virus, strain 16681 (PDK-53), are defined by mutations in the 5' noncoding region and nonstructural proteins 1 and 3. J. Virol. *74*, 3011–3019.

Campos, G.S., Bandeira, A.C., and Sardi, S.I. (2015). Zika Virus Outbreak, Bahia, Brazil. Emerging Infect. Dis. *21*, 1885–1886.

Cao-Lormeau, V.-M., Blake, A., Mons, S., Lastère, S., Roche, C., Vanhomwegen, J., Dub, T., Baudouin, L., Teissier, A., Larre, P., et al. (2016). Guillain-Barré Syndrome outbreak associated with Zika virus infection in French Polynesia: a case-control study. Lancet *387*, 1531–1539.

Cao-Lormeau, V.-M., Roche, C., Teissier, A., Robin, E., Berry, A.-L., Mallet, H.-P., Sall,

A.A., and Musso, D. (2014). Zika virus, French polynesia, South pacific, 2013. Emerging Infect. Dis. *20*, 1085–1086.

Cauchemez, S., Besnard, M., Bompard, P., Dub, T., Guillemette-Artur, P., Eyrolle-Guignot, D., Salje, H., Van Kerkhove, M.D., Abadie, V., Garel, C., et al. (2016). Association between Zika virus and microcephaly in French Polynesia, 2013-15: a retrospective study. Lancet *387*, 2125–2132.

Chan, J.F.W., Choi, G.K.Y., Yip, C.C.Y., Cheng, V.C.C., and Yuen, K.-Y. (2016). Zika fever and congenital Zika syndrome: An unexpected emerging arboviral disease. J. Infect. *72*, 507–524.

Colton, L., Zeidner, N., Lynch, T., and Kosoy, M.Y. (2010). Human isolates of Bartonella tamiae induce pathology in experimentally inoculated immunocompetent mice. BMC Infect. Dis. *10*, 229.

Cugola, F.R., Fernandes, I.R., Russo, F.B., Freitas, B.C., Dias, J.L.M., Guimarães, K.P., Benazzato, C., Almeida, N., Pignatari, G.C., Romero, S., et al. (2016). The Brazilian Zika virus strain causes birth defects in experimental models. Nature 1–15.

DICK, G.W.A., KITCHEN, S.F., and HADDOW, A.J. (1952). Zika virus. I. Isolations and serological specificity. Trans. R. Soc. Trop. Med. Hyg. *46*, 509–520.

Doobin, D.J., Kemal, S., Dantas, T.J., and Vallee, R.B. (2016). Severe NDE1-mediated microcephaly results from neural progenitor cell cycle arrests at multiple specific stages. Nature Communications *7*, 12551.

Driggers, R.W., Ho, C.-Y., Korhonen, E.M., Kuivanen, S., Jääskeläinen, A.J., Smura, T., Rosenberg, A., Hill, D.A., DeBiasi, R.L., Vezina, G., et al. (2016). Zika Virus Infection with Prolonged Maternal Viremia and Fetal Brain Abnormalities. N. Engl. J. Med.

Dudley, D.M., Aliota, M.T., Mohr, E.L., Weiler, A.M., Lehrer-Brey, G., Weisgrau, K.L., Mohns, M.S., Breitbach, M.E., Rasheed, M.N., Newman, C.M., et al. (2016). A rhesus macaque model of Asian-lineage Zika virus infection. Nature Communications *7*, 12204.

Duffy, M.R., Chen, T.-H., Hancock, W.T., Powers, A.M., Kool, J.L., Lanciotti, R.S., Pretrick, M., Marfel, M., Holzbauer, S., Dubray, C., et al. (2009). Zika virus outbreak on Yap Island, Federated States of Micronesia. N. Engl. J. Med. *360*, 2536–2543.

Evans, D.M., Dunn, G., Minor, P.D., Schild, G.C., Cann, A.J., Stanway, G., Almond, J.W., Currey, K., and Maizel, J.V. (1985). Increased neurovirulence associated with a single nucleotide change in a noncoding region of the Sabin type 3 poliovaccine genome. Nature *314*, 548–550.

Faria, N.R., Azevedo, R.D.S.D.S., Kraemer, M.U.G., Souza, R., Cunha, M.S., Hill, S.C., Thézé, J., Bonsall, M.B., Bowden, T.A., Rissanen, I., et al. (2016). Zika virus in the

Americas: Early epidemiological and genetic findings. Science *352*, 345–349.

Govero, J., Esakky, P., Scheaffer, S.M., Fernandez, E., Drury, A., Platt, D.J., Gorman, M.J., Richner, J.M., Caine, E.A., Salazar, V., et al. (2016). Zika virus infection damages the testes in mice. Nature.

Gromowski, G.D., Firestone, C.-Y., and Whitehead, S.S. (2015). Genetic Determinants of Japanese Encephalitis Virus Vaccine Strain SA14-14-2 That Govern Attenuation of Virulence in Mice. J. Virol. *89*, 6328–6337.

Guerrini, R., and Dobyns, W.B. (2014). Malformations of cortical development: clinical features and genetic causes. Lancet Neurol *13*, 710–726.

Hagen, von der, M., Pivarcsi, M., Liebe, J., Bernuth, von, H., Didonato, N., Hennermann, J.B., Bührer, C., Wieczorek, D., and Kaindl, A.M. (2014). Diagnostic approach to microcephaly in childhood: a two-center study and review of the literature. Dev Med Child Neurol *56*, 732–741.

Hamel, R., Dejarnac, O., Wichit, S., Ekchariyawat, P., Neyret, A., Luplertlop, N., Perera-Lecoin, M., Surasombatpattana, P., Talignani, L., Thomas, F., et al. (2015). Biology of Zika Virus Infection in Human Skin Cells. J. Virol. *89*, 8880–8896.

Imayoshi, I., Isomura, A., Harima, Y., Kawaguchi, K., Kori, H., Miyachi, H., Fujiwara, T., Ishidate, F., and Kageyama, R. (2013). Oscillatory control of factors determining multipotency and fate in mouse neural progenitors. Science *342*, 1203–1208.

Kostyuchenko, V.A., Lim, E.X.Y., Zhang, S., Fibriansah, G., Ng, T.-S., Ooi, J.S.G., Shi, J., and Lok, S.-M. (2016). Structure of the thermally stable Zika virus. Nature.

Kriegstein, A., and Alvarez-Buylla, A. (2009). The Glial Nature of Embryonic and Adult Neural Stem Cells. Annual Review of Neuroscience *32*, 149–184.

Lazear, H.M., and Diamond, M.S. (2016). Zika Virus: New Clinical Syndromes and its Emergence in the Western Hemisphere. J. Virol.

Lazear, H.M., Govero, J., Smith, A.M., Platt, D.J., Fernandez, E., Miner, J.J., and Diamond, M.S. (2016). A Mouse Model of Zika Virus Pathogenesis. Cell Host Microbe.

Lednicky, J., De Rochars, V.M.B., Badry, El, M., Loeb, J., Telisma, T., Chavannes, S., Anilis, G., Cella, E., Ciccozzi, M., Rashid, M., et al. (2016). Zika Virus Outbreak in Haiti in 2014: Molecular and Clinical Data. PLoS Negl Trop Dis *10*, e0004687.

Lessler, J., Chaisson, L.H., Kucirka, L.M., Bi, Q., Grantz, K., Salje, H., Carcelen, A.C., Ott, C.T., Sheffield, J.S., Ferguson, N.M., et al. (2016). Assessing the global threat from Zika virus. Science *353*, aaf8160.

Li, C., Xu, D., Ye, Q., Hong, S., Jiang, Y., Liu, X., Zhang, N., Shi, L., Qin, C.-F., and Xu, Z.

(2016a). Zika Virus Disrupts Neural Progenitor Development and Leads to Microcephaly in Mice. Cell Stem Cell.

Li, H., Saucedo-Cuevas, L., Regla-Nava, J.A., Chai, G., Sheets, N., Tang, W., Terskikh, A.V., Shresta, S., and Gleeson, J.G. (2016b). Zika Virus Infects Neural Progenitors in the Adult Mouse Brain and Alters Proliferation. Stem Cell 1–16.

Lukaszewicz, A., Savatier, P., Cortay, V., Giroud, P., Huissoud, C., Berland, M., Kennedy, H., and Dehay, C. (2005). G1 phase regulation, area-specific cell cycle control, and cytoarchitectonics in the primate cortex. Neuron *47*, 353–364.

MACNAMARA, F.N. (1954). Zika virus: a report on three cases of human infection during an epidemic of jaundice in Nigeria. Trans. R. Soc. Trop. Med. Hyg. *48*, 139–145.

Miner, J.J., Bin Cao, Govero, J., Smith, A.M., Fernandez, E., Cabrera, O.H., Garber, C., Noll, M., Klein, R.S., Noguchi, K.K., et al. (2016a). Zika Virus Infection during Pregnancy in Mice Causes Placental Damage and Fetal Demise. Cell 1–14.

Miner, J.J., Sene, A., Richner, J.M., Smith, A.M., Santeford, A., Ban, N., Weger-Lucarelli, J., Manzella, F., Rückert, C., Govero, J., et al. (2016b). Zika Virus Infection in Mice Causes Panuveitis with Shedding of Virus in Tears. CellReports *16*, 3208–3218.

Mlakar, J., Korva, M., Tul, N., Popovic, M., Poljšak-Prijatelj, M., Mraz, J., Kolenc, M., Resman Rus, K., Vesnaver Vipotnik, T., Fabjan Vodušek, V., et al. (2016). Zika Virus Associated with Microcephaly. N. Engl. J. Med. *374*, 951–958.

Moura da Silva, A.A., Ganz, J.S.S., Sousa, P.D.S., Doriqui, M.J.R., Ribeiro, M.R.C., Branco, M.D.R.F.C., Queiroz, R.C. de S., Pacheco, M. de J.T., Vieira da Costa, F.R., Silva, F. de S., et al. (2016). Early Growth and Neurologic Outcomes of Infants with Probable Congenital Zika Virus Syndrome. Emerging Infect. Dis. *22*, 1953–1956.

Murphy, B.R., and Whitehead, S.S. (2011). Immune response to dengue virus and prospects for a vaccine. Annu. Rev. Immunol. *29*, 587–619.

Neu, N., Duchon, J., and Zachariah, P. (2015). TORCH infections. Clin Perinatol *42*, 77–103–viii.

Noctor, S.C., Martínez-Cerdeño, V., Ivic, L., and Kriegstein, A.R. (2004). Cortical neurons arise in symmetric and asymmetric division zones and migrate through specific phases. Nat Neurosci *7*, 136–144.

Offerdahl, D.K., Dorward, D.W., Hansen, B.T., and Bloom, M.E. (2016). Cytoarchitecture of Zika virus infection in human neuroblastoma and Aedes albopictus cell lines. Virology *501*, 54–62.

Onorati, M., Li, Z., Liu, F., Sousa, A.M.M., Nakagawa, N., Li, M., Dell'Anno, M.T., Gulden,

F.O., Pochareddy, S., Tebbenkamp, A.T.N., et al. (2016). Zika Virus Disrupts Phospho-TBK1 Localization and Mitosis in Human Neuroepithelial Stem Cells and Radial Glia. CellReports *16*, 2576–2592.

Pacheco, O., Beltrán, M., Nelson, C.A., Valencia, D., Tolosa, N., Farr, S.L., Padilla, A.V., Tong, V.T., Cuevas, E.L., Espinosa-Bode, A., et al. (2016). Zika Virus Disease in Colombia - Preliminary Report. N. Engl. J. Med.

Paridaen, J.T., and Huttner, W.B. (2014). Neurogenesis during development of the vertebrate central nervous system. EMBO Reports *15*, 351–364.

Pierson, T.C., and Diamond, M.S. (2012). Degrees of maturity: the complex structure and biology of flaviviruses. Curr Opin Virol *2*, 168–175.

Qian, X., Nguyen, H.N., Song, M.M., Hadiono, C., Ogden, S.C., Hammack, C., Yao, B., Hamersky, G.R., Jacob, F., Zhong, C., et al. (2016). Brain-Region-Specific Organoids Using Mini- bioreactors for Modeling ZIKV Exposure. Cell 1–18.

Retallack, H., Di Lullo, E., Arias, C., Knopp, K.A., Sandoval-Espinosa, C., Laurie, M.T., Zhou, Y., Gormley, M., Mancia Leon, W.R., Krencik, R., et al. (2016). Zika Virus in the Human Placenta and Developing Brain: Cell Tropism and Drug Inhibition (Cold Spring Harbor Labs Journals).

Shao, Q., Herrlinger, S., Yang, S.-L., Lai, F., Moore, J.M., Brindley, M.A., and Chen, J.-F. (2016). Zika virus infection disrupts neurovascular development and results in postnatal microcephaly with brain damage. Development.

SMITHBURN, K.C. (1952). Studies on certain viruses isolated in the tropics of Africa and South America; immunological reactions as determined by cross-neutralization tests. J. Immunol. *68*, 441–460.

SMITHBURN, K.C. (1954). Neutralizing antibodies against arthropod-borne viruses in the sera of long-time residents of Malaya and Borneo. Am J Hyg *59*, 157–163.

SMITHBURN, K.C., KERR, J.A., and GATNE, P.B. (1954). Neutralizing antibodies against certain viruses in the sera of residents of India. J. Immunol. *72*, 248–257.

Soares de Oliveira-Szejnfeld, P., Levine, D., Melo, A.S. de O., Amorim, M.M.R., Batista, A.G.M., Chimelli, L., Tanuri, A., Aguiar, R.S., Malinger, G., Ximenes, R., et al. (2016). Congenital Brain Abnormalities and Zika Virus: What the Radiologist Can Expect to See Prenatally and Postnatally. Radiology 161584.

Soares de Souza, A., Moraes Dias, C., Braga, F.D.C.B., Terzian, A.C.B., Estofolete, C.F., Oliani, A.H., Oliveira, G.H., Brandão de Mattos, C.C., de Mattos, L.C., Nogueira, M.L., et al. (2016). Fetal Infection by Zika Virus in the Third Trimester: Report of 2 Cases. Clin. Infect. Dis. ciw613.

Steele, R.W. (2016). Zika Virus: An Explosive Pandemic and a New TORCH Agent. Clin Pediatr (Phila) *55*, 698–700.

Štrafela, P., Vizjak, A., Mraz, J., Mlakar, J., Pižem, J., Tul, N., Županc, T.A., and Popovic, M. (2016). Zika Virus-Associated Micrencephaly: A Thorough Description of Neuropathologic Findings in the Fetal Central Nervous System. Arch. Pathol. Lab. Med.

Tang, H., Hammack, C., Ogden, S.C., Wen, Z., Qian, X., Li, Y., Yao, B., Shin, J., Zhang, F., Lee, E.M., et al. (2016). Zika Virus Infects Human Cortical Neural Progenitors and Attenuates Their Growth. Cell Stem Cell.

van der Linden, V., Pessoa, A., Dobyns, W., Barkovich, A.J., van der Linden Júnior, H., Filho, E.L.R., Ribeiro, E.M., de Carvalho Leal, M., de Araújo Coimbra, P.P., de Fátima Viana Vasco Aragão, M., et al. (2016). Description of 13 Infants Born During October 2015–January 2016 With Congenital Zika Virus Infection Without Microcephaly at Birth — Brazil. MMWR. Morbidity and Mortality Weekly Report *65*.

Venturi, G., Zammarchi, L., Fortuna, C., Remoli, M.E., Benedetti, E., Fiorentini, C., Trotta, M., Rizzo, C., Mantella, A., Rezza, G., et al. (2016). An autochthonous case of Zika due to possible sexual transmission, Florence, Italy, 2014. Euro Surveill. *21*.

World Health Organization (2016). Surveillance for Zika virus infection, microcephaly and Guillain-Barré syndrome. WHO Surveillance Report 1–9.

Wu, K.-Y., Zuo, G.-L., Li, X.-F., Ye, Q., Deng, Y.-Q., Huang, X.-Y., Cao, W.-C., Qin, C.-F., and Luo, Z.-G. (2016). Vertical transmission of Zika virus targeting the radial glial cells affects cortex development of offspring mice. Cell Res. *26*, 645–654.

Yockey, L.J., Varela, L., Rakib, T., Khoury-Hanold, W., Fink, S.L., Stutz, B., Szigeti-Buck, K., Van den Pol, A., Lindenbach, B.D., Horvath, T.L., et al. (2016). Vaginal Exposure to Zika Virus during Pregnancy Leads to Fetal Brain Infection. Cell *166*, 1247–1256.e4.

Zhang, F., Hammack, C., Ogden, S., Cheng, Y., Lee, E., Wen, Z., Qian, X., Nguyen, H.N., Li, Y., Yao, B., et al. (2016). Molecular signatures associated with ZIKV exposure in human cortical neural progenitors.

ACKNOWLEDGEMENTS

We thank the members of the Vallee lab, Drs. Alex Baffett, Hynek Wichterle, Franck Polleux, Gregg Gundersen, Elisa Canepa, Stav Kameny, and Leslie Vosshall for technical expertise and feedback, and Drs. Connie Cepko and Lucia Gama for providing reagents. This project was supported by NIH HD40182 to R.B.V., NINDS F30NS095577 to D.J.D.

COMPETING INTERESTS STATMENT

The authors declare no competing financial interests.

AUTHOR CONTRIBUTIONS

Conceptualization, A.R., D.J.D., V.R., and R.B.V.; Methodology, D.J.D. for all neurobiology, A.R. for all virology with A.W. for plaque assay and viral stock assistance; Data Acquisition D.J.D. for all neurobiology and A.R. for all virology; Writing – Original Draft, D.J.D., with the help of A.R. on methods; Editing, D.J.D.

Chapter 4

How Investigations of Genetic Forms of Microcephaly Can Inform Research on the Zika Virus

ABSTRACT:

Malformations of cortical development (MCDs) of both genetic and infectious etiologies represent a significant health burden on society. Chapters 2 and 3 provide an example of how careful dissection of a genetic form of an MCD – *NDE1* microlissencephaly – can enhance our understanding of elemental cell biology while providing a working model system to understand an emerging infectious disease outbreak. This chapter discusses how the 3 roles for Nde1 discussed at length in Chapter 2 have broader implications for cellular processes such as ciliary regulation, and apical INM in correct brain development and cell cycle progression. Additionally the preliminary evidence for phosphorylation of Nde1 and its implications for diseases such as schizophrenia are discussed. We further elaborate on how our investigations of *NDE1* microcephaly can be employed to better understand Zika (ZIKV) microcephaly, and what the organotypic brain slices have illuminated about ZIKV-induced pathology. The implications of our work on ZIKV mutations and viral evolution are discussed, as well as the relevancy for our work to the current effort to develop a universal ZIKV-vaccine.

NDE1 MICROCEPHALY

Role of the Primary Cilia in the G1-to-S Transition of Radial Glia:

The primary cilia is an organelle adjacent to the centrosome that extends into extracellular space and plays a crucial role in signaling (Pedersen and Rosenbaum, 2008). The primary cilia participates primarily in sonic hedgehog (Shh) signaling through the Smoothened and Gli pathways (Huangfu et al., 2003), though it is also capable of Notch signaling (Ezratty et al., 2011). During cell cycle progression the

primary cilia emerges off of the basal body of the centrosome, growing during G1, and initiating resorption at the G1-to-S border so that it is resorbed throughout S and G2 phases, being completely resorbed by the onset of mitosis (Han and Alvarez-Buylla, 2010; Paridaen et al., 2013). Intraflagellar transport (IFT) proteins are required for anterograde and retrograde transport along the microtubules in the primary cilia to facilitate signaling. The genes encoding these IFT proteins, such as *Ift88*, were some of the first ciliary genes to be associated with neuronal development abnormalities when mutated (Han and Alvarez-Buylla, 2010). Crucially, all of the neurodevelopment abnormalities occurred with mutations resulting in hypomorphic forms of these proteins. This is critical because it was later found that complete knockout of these proteins, such as *Ift88* or *Kif3a* knockout, blocked the primary cilia from ever forming and brain development was mostly fine (Insolera et al., 2014; Tong et al., 2014). Knockout of other, more auxiliary primary cilia proteins, such as *Arl13b*, do not block primary cilia formation, and therefore caused brain developmental abnormalities. However, these defects were most likely associated with events such as neural tube closure or gross delamination of radial glia progenitors (RGPs), and not cell-cycle dependent changes (Higginbotham et al., 2013). If the primary cilium was dispensable for largely normal brain development, it called into question the necessity of the organelle.

At this point it becomes critical to distinguish between absence and dysfunction. The multiple human ciliopathies where patients present with intellectual disability and neurodevelopmental delays, including Joubert syndrome and Bardet-Biedl syndrome, reinforce the biological relevance of primary cilia

function (Guo et al., 2015). While the lack of primary cilia may not impede cell cycle progression of RGPs, as seen with RNAi to *Ift172* in Chapter 2, dysregulation of the primary cilia, as seen by ciliary lengthening with RNAi to *Nde1/Ndel1*, does block RGPs in G1. This is consistent with interference of either Nde1 or Ndel1 leading to blocks in G1-to-S transition in other systems (Izawa et al., 2015; Kim et al., 2011; Maskey et al., 2015). Though there are many other primary cilia genes that lead to ciliopathies with neuronal pathology when mutated in humans (Guo et al., 2015), only interference with TcTex recapitulated the G1 accumulation of RGPs seen with *Nde1/Ndel1* RNAi (Li et al., 2011). A partial explanation is that interference with other primary cilia genes, such as *Bub1B*, *Kif7*, and *Ift80*, lowered the mitotic index of RGPs, but a further mechanism was never examined, and the genes could very well act through a G1-to-S phase mechanism (Guo et al., 2015).

The exact role for Nde1 or Ndel1 at the primary cilia remains unresolved, though evidence points to a potential role in transportation of retrograde ciliary motor components to the primary cilia. There was a strong immunohistochemical signal for Nde1/Ndel1 at the base of the RGP cilia, around the pericentriolar matrix, but Nde1/Ndel1 signal never overlapped with the Arl13b signal in the actual primary cilia. The Nde1/Ndel1 antibody, as well as GST-Nde1 and GST-Ndel1, were each able to pull down the heavy chain of cytoplasmic Dynein-2 (DYNC2H1), which is the sole retrograde motor in IFT (data not shown). The light intermediate chain (Lic3) and intermediate chain (Wdr34) specific to Dynein-2 were also pulled down in this experiment, which suggests that Nde1 or Ndel1 interact with the Dynein-2 complex, possibly to transport the elements of this complex from the Golgi to the

primary cilia. Since Nde1 and Ndel1 were never found within the primary cilia, it is unlikely that they are required for the active Dynein-2 complex. However, RNAi to *Lic3* caused the same G1 accumulation of RGPs as *Nde1/Ndel1* RNAi (data not shown), suggesting that they may be acting through the mechanism at the primary cilia. A single previous studied examined *Dync2h1* mutations in mice resulting in a missense mutation or premature truncations, both of which caused dorsoventral patterning defects in the telencephalon (May et al., 2005). Most embryos died by E12 of pericardial edema and heart failure, which prevented more extensive analysis of the role of Dynein-2 during neocortical development. Thus there is increased precedent for revisiting the role of Dynein-2 and retrograde IFT in RGPs during neocortical development, which is ongoing in lab.

Solidifying the Late-G2 Pathway of Dynein Recruitment During INM

Our lab has done extensive work to demonstrate that cytoplasmic dynein-1 is required at the nuclear envelope of RGP cells to complete apical interkinetic nuclear migration during G2 (Baffet et al., 2015; Hu et al., 2013; Tsai et al., 2005; 2010). Work done in cell culture and in the brain has indicated that there are two sequential pathways by which dynein is brought to the nuclear envelope (reviewed extensively in Chapter1.2) (Baffet et al., 2015; Bolhy et al., 2011; Hu et al., 2013). One aspect that had remained uncertain was whether either of the paralog proteins Nde1 or Ndel1 played a dominant role in the late-G2 pathway of dynein recruitment. Chapter 2 now elucidates that it is primarily Nde1 that is required for binding CENP-F and recruiting dynein, though Ndel1 overexpression can compensate for a lack of Nde1 at the nuclear envelope.

There are still components of the dynein recruitment pathway whose involvement in apical INM requires further specification. While Lis1 appears to be involved in both the early and late pathway in HeLa cells (Baffet et al., 2015), the effects of *Lis1* knockdown have not been investigated since the last decade and are worth revisiting in the context of new knowledge (Tsai et al., 2005; 2010; 2007). Similarly, in the last few years dynactin has emerged as a critical adapter protein for the dynein complex (McKenney et al., 2014; Urnavicius et al., 2015), but very little is known about its role in RGP cells. Work done in HeLa cells indicates that dynactin is always present at the nuclear envelope when BicD2 is present but CENP-F remains nuclear (Baffet et al., 2015). This strongly suggests that it is involved in the early-G2 pathway, though it's role in the late-G2 pathway has yet to be investigated. Additionally, the contributions of Lic1 and Lic2 to apical INM have not been examined in RGPs, providing a further means of dissecting the dynein pathway, as do phosphorylation studies of CENP-F, Nde1, and Lic1/Lic2.

Though INM-behavior is seen in the development of a variety of tissues across species (see Chapter 1.2 for full review), these other forms of INM employ mainly actomyosin motors (Meyer et al., 2011; Norden et al., 2009; Strzyz et al., 2015). There is only one report that myosin IIb is important in RGPs, where it is reported to be involved in basal INM while dynein is still required for apical INM (Schenk et al., 2009). This report never examined movement of the RGP nuclei, however, and our lab has found no contribution from myosin IIb during basal INM, which is instead dependent upon the kinesin Kif1A (Carabalona et al., 2016; Tsai et al., 2010). Nonetheless, Schenk et al. (2009) examined E14 mouse tissue, which is

much earlier than our lab has ever investigated INM. All of the other tissues in which INM occurs, and where it is actomyosin dependent, are a fraction of the thickness of the neocortex during late neurogenesis (E18-E20 in the rat) (Norden et al., 2009; Strzyz et al., 2015). As cells elongate they often require greater stabilization from the microtubule cytoskeleton, and therefore these cells may switch to microtubule-dependent motors as they elongate. It is plausible that neuroepithelial cells may use primarily actomyosin motors for INM during early neocortical development, when the neocortex is much thinner and only one cell layer thick. As the neocortex continues to develop, however, and expands in thickness, it could be that RGPs transition to a microtubule-dependent motor system.

This is now easily testable using the model systems described in Chapters 2 and 3. We can now make embryonic organotypic brain slices from gestation days as early as E13, at which point the neocortex is a small fraction of the thickness as at E19. By either employing *ex utero* electroporation of a GFP empty vector to label RGPs (which should express within 12 hours of electroporation), or Syto11 dye to quickly label all nuclei (Pilaz and Silver, 2014), RGP cells will be fluorescently labelled for live imaging. The slices could be cultured in blebbistatin, which has been successfully employed in organotypic brain slices to inhibit myosin II (Tsai et al., 2010), and then analyzed by fixed and live imaging to determine if there is an accumulation of RGP nuclei at any point during INM. This could be done across a variety of embryonic time points and across mouse and rat embryos. Furthermore, Ciliobrevin D, an inhibitor of cytoplasmic dynein, could be further optimized (currently our lab can only get it to work in low-serum conditions) and hopefully

used to block dynein in these slices. These experiments would finally allow us to conclusively say whether INM during corticogenesis is exclusively microtubule-motor dependent, or whether there is dependence on different motor proteins based on the morphology and developmental stage of the progenitor cells.

Clarifying the Role of Nde1 at the G2-to-M Transition

One of the largest unresolved questions left after the experiments from Chapter 2 is the role of Nde1 at the G2-to-M transition. The field has long thought that if apical INM is completed, and the nucleus moves close enough to the centrosome, then the RGP cell will enter mitosis. There was one occasion where *Nup133* RNAi was rescued by *BicD2* overexpression, and RGP cells completed apical INM but failed to enter mitosis, though this was interpreted as being due to defects in nuclear pore composition following *Nup133* RNAi (Hu et al., 2013). Here, multiple different experimental models all point to the same conclusion – that there is some unique role for Nde1 in mitotic entry, independent of its role at the nuclear envelope during apical INM. This last point is subtle, but since *CENP-F* knockdown could be fully rescued by BicD2 overexpression (Hu et al., 2013), and Nde1 is downstream of CENP-F in the late-G2 pathway, the inability of *Nde1* knockdown/*BicD2* overexpression to rescue the mitotic index suggests that there is a role for Nde1 beyond the nuclear envelope.

What this role could be remains elusive, but there are clues pointing towards a few potential cellular processes. In Chapter 2 we provided evidence that the centrosomes in the RGP cells arrested at the G2-to-M transition remain anchored at the apical endfoot. In *Drosophila* there has been growing appreciation for a

centrosome-orientation checkpoint (COC), which is a checkpoint in asymmetrically dividing stem cells at the G2-to-M transition (Cheng et al., 2008; Inaba et al., 2015; Venkei and Yamashita, 2015). If the centrosome is not properly oriented at the end of G2, then the asymmetrically dividing stem cells in the *Drosophila* embryo will delay entry into mitosis. Since Nde1 is a known centrosome scaffolding protein, and there is a strong Nde1/Ndel1 immunohistochemical signal at the centrosome, combined with the fact that RGP cells are almost exclusively undergoing asymmetric division by E20, it seems plausible that this could be a mammalian equivalent of the COC. However, the centrosomes in the RGP cells arrested at the G2-to-M transition are not separated and remain close together at the apical endfoot, which would be a departure from the misaligned centrosomes seen in COC checkpoint failures in *Drosophila* (Cheng et al., 2008; Inaba et al., 2015). Closer analysis of the centrosome, especially by methods such as transmission electron microscopy, could be useful in improving our understanding of centrosome positioning in the RGPs arrested at the G2-to-M transition, and whether thinking along the lines of the COC is applicable.

Another potential experiment involves examining the centrosome behavior in *Nde1* RNAi cells by live imaging. In developing neural tissue in both the rat brain and chick spinal cord it has been shown that the centrosome will detach from the apical endfoot near the end of INM nucleokinesis, and move up towards the descending nucleus as it enters mitosis slightly before reaching the ventricular surface (Hu et al., 2013; Spear and Erickson, 2012). In *CENP-F* and *Nup133* RNAi, there was a reduction of "centrosome-hopping" events compared to control RGP cells, suggesting that there was a reduction of forces from the nuclear envelope on

the microtubule network to pull the centrosome towards the nucleus (Hu et al., 2013). While examining "centrosome hopping" in *Nde1* knockdown alone may not reveal much, as the amount of dynein at the nuclear envelop is expected to be reduced, examining this phenomenon in the *Nde1* knockdown/*BicD2* overexpression RGP cells could provide important evidence regarding centrosome motility. Specifically, it is thought that there are short microtubules that emanate from the centrosome and help to anchor it to the apical endfoot (*personal communication with members of the Song-Hai Shi laboratory*), and these may need to be severed for centrosome release and mitotic entry. Labelling these RGP cells with Arl13B revealed no detectable primary cilia remnants (data not shown), which is important since some reports have suggested that the primary cilia plays a more vestigial role in anchoring the centrosome in the apical endfoot (Insolera et al., 2014). Similarly, Monastrol treatment of brain slices could be used to block centrosome separation to see if it recapitulates the G2-to-M block, though evidence from cell culture suggests that this would mainly arrest cells in metaphase (Chin and Herbst, 2006).

Finally, we have an important finding that a single-site phosphomutant of Nde1 recapitulates the G2-to-M arrest. Specifically, there is something about the T246A site that is required for the G2-to-M transition. Preliminary evidence from experiments with Nde1-T215A indicates that it does not block cells at the G2-to-M transition (data not shown), though experiments have not been done with Nde1-T243A alone. Regardless, there appears to be a functional difference between Nde1 and Nde1-T246A. Biotinylation studies have been employed often recently to

identify transient interactions among proteins and have a high sensitivity (Firat-Karalar and Stearns, 2015). A comparison of the mass spectrometry results from biotinylation studies of Nde1 versus Nde1-T246A expression in RGP cells may reveal protein interactions specific to either form of Nde1, which could provide insight into the subcellular role for Nde1 at the G2-to-M transition.

The Association of *NDE1* Mutations with Schizophrenia

Very rarely are different mutations in a single protein associated with diseases as varied as microcephaly and schizophrenia, though *NDE1* mutations present such an example. While the association between Nde1 and microcephaly has been made evident through the previous chapters and multiple studies (Alkuraya et al., 2011; Bakircioglu et al., 2011; Doobin et al., 2016; Feng and Walsh, 2004; Guven et al., 2012; Paciorkowski et al., 2013), we only begin to touch on a putative role for Nde1 in the pathogenesis of schizophrenia. Notably overexpression of the S214F schizophrenia-associated form of Nde1 did not impair RGP proliferation, but altered the leading process of migrating bipolar neurons and affected neocortical lamination assayed one week after birth. These changes suggest that the S214F mutation in NDE1 may alter neocortical lamination, but we need to look at later postnatal time points to conclude if lamination is still disrupted. Since excitatory glutamatergic neurons establish their layer identity in the multipolar stage (Miyoshi and Fishell, 2012), blocks in bipolar neuronal migration could cause neurons with superficial layer identity to be deposited in layers 5/6. Because the neurons in different layers have different morphologies and projection targets

(Marín and Müller, 2014), a heterogeneous deposition of neurons in the incorrect layers could impact connectivity in the brain.

Though very little is known about its pathogenesis, schizophrenia can be thought of as a disease of impaired connectivity, whether involving general gray matter deficits (Cannon et al., 2002), dendritic spine density (Garey et al., 1998; Glantz and Lewis, 2000), synaptic pruning (Sekar et al., 2016), inhibitory neocortical circuitry (Lewis et al., 2012), or neuronal migration (Muraki and Tanigaki, 2015). The variety of neurobiological processes implicated in schizophrenia reiterate an important concept regarding the disease: schizophrenia is best thought of as a syndrome of multiple diseases with a common symptom profile and disease course (Fischer and Carpenter, 2009). Just as congestive heart failure is a syndrome of impaired filling and ejection of blood from the heart that may result from a myriad of diseases including infectious, metabolic, genetic, and physiologic etiologies (DAWBER et al., 1951; Long and Fox, 2016), schizophrenia is likely a syndrome of positive and negative symptoms that may result from a variety of biological processes. A unifying theme resulting from these biological processes is the impaired connectivity of neurons, which likely leads to system level disturbances, which could produce the positive and negative symptoms (such as delusions/hallucinations and dulled affect/cognitive slowing, respectively) seen with schizophrenia. The development of schizophrenia is thought to require a genetic or developmental predisposition coupled with an environmental trigger, which can vary from psychosocial insults to infectious agents to chronic marijuana use (Kuepper et al., 2011; McGrath et al., 2010). The study of the S214F mutation in

NDE1 has the promise of helping us better understand the developmental predispositions that may underlie schizophrenia.

ZIKA VIRUS

Potential Reasons for Increased Zika Virus Pathology and Spread

Zika virus (ZIKV) has emerged as a global epidemic in the last few years as it has begun to rapidly spread across the Western Hemisphere (Lessler et al., 2016). As the virus has explosively spread through the Americas, the association of ZIKV with Guillain-Barré syndrome and microcephaly has become the greatest concern (Lessler et al., 2016). There are four plausible hypotheses for why ZIKV is causing new clinical syndromes with more severe pathology: 1) changes in the genetics of the virus to facilitate its pathogenecity in humans or 2) in mosquitos, 3) different unique genetics among the host population in the Americas, or 4) complex interplay involving pre-existing immunity to other flaviviruses, such as dengue (DENV), that predisposes an individual to more severe ZIKV infection. The last possibility actually is responsible for much of the lethality of DENV virus – when a patient is infected with DENV of a slightly different serotype than their first DENV exposure, the antibodies that the patient already has to DENV may bind the virion, but they do so incompletely (Pierson and Graham, 2016). The Fc regions of the antibodies that are now glued to the still active virions then bind to Fcγ-receptors on monocytes, and enhance the viral spread and innate immune response to the virus in a process termed antibody-dependent enhancement (ADE) (Murphy and Whitehead, 2011; Pierson and Graham, 2016). This can trigger the release of cytokines and increase inflammation, and ADE has been shown to occur for ZIKV infection with antibodies

against DENV (Dejnirattisai et al., 2016). It is also important to consider the question of different host population genetics, and whether the introduction of ZIKV into the Americas was a random exposure to an immunologically naïve populace (Lessler et al., 2016). Continuous ZIKV exposure in Asia over the 20th Century may have led to small outbreaks of disease and pregnancy complications, but superimposed on the spread of other viruses, and combined with the often lifelong immunity of flaviviruses (Murphy and Whitehead, 2011), it may have gone medically unnoticed. The achilles heel of this theory, though, is that it does not explain why ZIKV so quietly existed in Asia and Africa for so long, and then acquired epidemic potential in small isolations such as Yap island and French Polynesia (Cao-Lormeau et al., 2014; Duffy et al., 2009), followed by explosive virulence in the Americas.

A more plausible option is that ZIKV mutated to allow for its increased spread and virulence. Since ZIKV is an RNA virus, and RNA viruses make many errors when replicating, the risk of mutations is quite high and could explain changes in ZIKV behavior (Musso and Gubler, 2016). Other arboviruses (in which the genus of *Flaviviruses* are included), such as chikungunya (Tsetsarkin et al., 2007) and West Nile Virus (WNV) (Brault et al., 2007), have experienced mutations associated with epidemic spread. These mutations could affect the viral lifecycle in mosquitos or human hosts. While the virus primarily is transmitted by the *Aedes aegypti* mosquito, with demonstrated potential for transmission by the *Aedes albopictus* mosquito (Lessler et al., 2016), it is more difficult to study mutations that

could impact the mosquito life cycle of ZIKV compared to mutations that could effect human pathology.

Chapter 3 demonstrated how an organotypic brain slice method, similar to the one used in Chapter 2, can be quickly employed to study the pathogenesis of ZIKV. This allowed us to both monitor viral replication by plaque forming assay, as well as assess the pathological changes that occurred to the brain slices during development. Most importantly, we could rather rapidly test many different isolates across a variety of embryonic time points. In our slice culture model all isolates of ZIKV caused increased apoptosis, with isolates of the Asian/American lineages causing substantially more cell death. This would suggest that there is a genetic difference in the virus that arose between the African and Asian lineages that enhances its pathogenic potential (its ability to cause disease). One recent report found at least 72 changes in the ZIKV genome between the Asian and African lineages (Pettersson et al., 2016), which provides many potential avenues regarding pathogenic changes between virus isolates.

A clue as to which of these changes in the viral genome may enhance its pathogenic potential is provided by how the apoptosis was occurring in the brain slices. Only 8.87% of the cells in the cortical plate positive for the ZIKV envelope protein (ZKV-E) were positive for cleaved caspase 3 (CC3), though many of the ZKV-E positive cells were surrounded by CC3 positive cells. There are a few possible explanations for this: that the ZKV-E signal in the CC3-positive cells was too weak to be visualized, that they were infected but initiated a cell-intrinsic apoptotic pathway to suppress viral production, or that the infected cells are releasing some cytokine to

induce apoptosis in surrounding cells. In flaviviruses it is common for viral proteins to suppress apoptotic pathways in order to facilitate viral replication (Pierson and Diamond, 2012), so the second option is unlikely. We examined whether these CC3 positive cells were undergoing the extrinsic apoptosis pathway, where tumor necrosis factor (TNF) stimulates the cleavage of caspase 8 (CC8), which eventually cleaves caspase 3 through a series of downstream effectors (Troy and Jean, 2015; Unsain and Barker, 2015). There was no CC8 staining in the brain, however, and cell lysate from ZIKV infected Vero cells suggested that CC8 was not cleaved. While this suggests that TNF signaling is not involved in inducing apoptosis in ZIKV infection, it does not eliminate the idea that infected cells may trigger the death of neighboring cells in an effort to contain the ZIKV infection. The logical extension is that microcephaly and other malformations of cortical development that comprise the congenital Zika virus syndrome (CZVS) may occur as side effects of the fetus trying to contain the ZIKV infection, much as the same way that the symptoms of the common cold are the body's way of containing and eliminating the pathogen.

The Nigerian 30656 Isolate and the Zika Virus Lifecycle

An important clue regarding the pathogenic potential of ZIKV came from the Nigerian 30656 isolate that we tested. This isolate never efficiently replicated in the embryonic mouse brain slices and never visibly infected the brain slices. It was able to replicate in Vero cells, which are derived from the renal epithelium, and U87 cells, a human glioblastoma cell line, suggesting that it has a defect with mouse neuronal tissue. Critically we devised a way to deproteinate the ZIKV to isolate the positive single-strand RNA (ssRNA), which we were able to inject and electroporate into the

RGPs of the developing brain. This allowed us to determine if the 30656 isolate contained all of the necessary genetic information to replicate in neuronal tissue. Surprisingly, the isolate was able to replicate, but about 4 days after electroporation the amount of viral replication plateaued, which is suggests that the virus generated from the 30656 ssRNA is not able to re-infect the brain tissue. This plateau was not seen with electroporation of PRV ssRNA, though there was a strong spatial restriction of the PRV ssRNA infection that was mostly found in the electroporated hemisphere. With the 30656 ssRNA there was no ZKV-E signal on the contralateral side of the electroporation, but intriguingly there was the same dorsomedial spread of the ZKV-E signal beyond the pUB-GFP electroporated region. Why this occurs is unknown, and either suggests that the 30656 isolate retains some limited capacity to spread in neuronal tissue once infection begins, or that ssRNA does not spatially respond to the same electrical field as dsDNA.

These experiments provide important insight into the ZIKV lifecycle in neuronal tissue. ZIKV, like other flaviviruses, is thought to bind a tyrosine-kinase surface receptor, which triggers clathrin mediated endocytosis, and then in the acidic endosome the virion membrane fuses with the endosome membrane to allow for the release of the ssRNA into the host cell (Pierson and Diamond, 2012). Since we are able to introduce the ssRNA for the 30656 and get corresponding viral replication, it must be one of these first three steps during which the 30656 isolate is failing. The envelope (E) protein of ZIKV is thought to be responsible for binding the host cell and permitting viral entry (Sapparapu et al., 2016). There are 4 amino acid substitutions that are unique to the 30656 isolate E protein and not seen in any

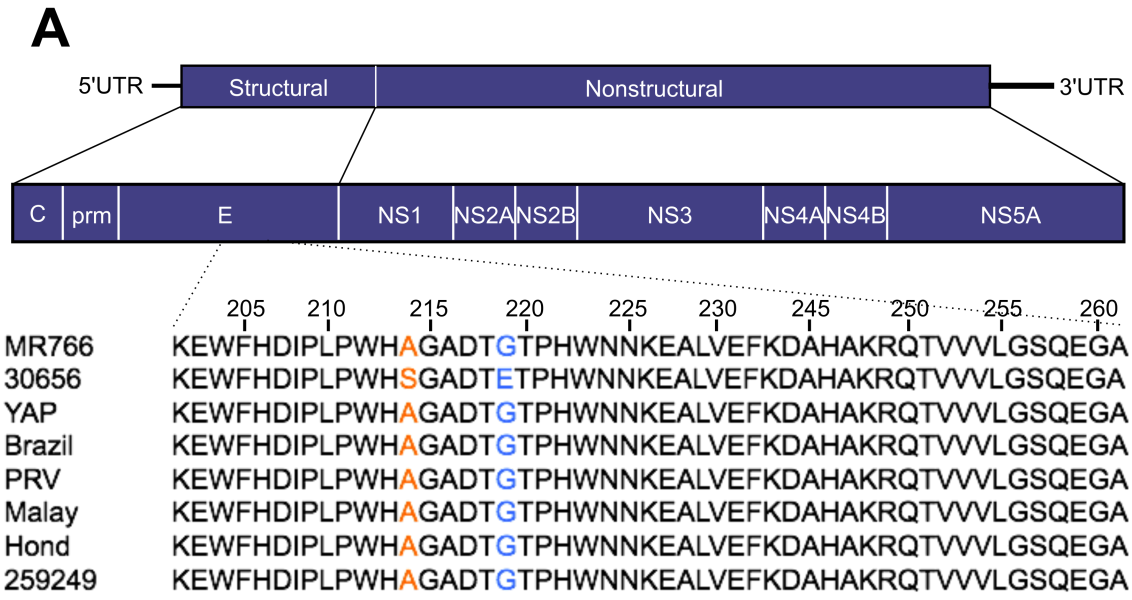

Figure 4.1: Amino Acid Alignment of the Envelope Protein Across Various Zika Virus Isolates: There are two notable substitutions unique to the envelope protein (E protein) of the Nigerian 30656 isolate, including an alanine to serine substitution at residue 214, and a glycine to glutamic acid at position 219. Other structural and nonstructural aspects of the Zika virus genome are displayed.

other isolates tested. Two of these amino acids are in close proximity to each other and involve changes from a hydrophobic to a polar residue (alanine to serine at 214) and a negative charge in place of a neutral residue (glycine to a glutamic acid at 219) (Figure 4.1). These all present targets at the amino acid level for better understanding the neurovirulence of ZIKV, and the relevance of these residues will be tested once infectious clones of the virus are generated. Additionally, if the necessity of these residues is confirmed by infectious clone studies, they present very attractive pharmacological targets for drug design meant to block ZIKV infection of neuronal tissue.

The Risk of Congenital Zika Virus Syndrome Based on Gestation Age

As the ZIKV epidemic has swept across the Western Hemisphere, a major concern has been at what stage of pregnancy are women at risk of having their fetus

develop microcephaly or other forms of CZVS from ZIKV infection. Early evidence suggested that the risk was only during the first and second trimester (Brasil et al., 2016). Additionally a large, prospective study across Colombia found that of 616 women who developed clinical symptoms of ZIKV during the third trimester, not a single patient gave birth or had a fetus with any intracranial abnormalities (Pacheco et al., 2016). Nonetheless, more recent reports have indicated that women infected with ZIKV as late as the 36th week of pregnancy gave birth to children with normal head circumference but intracranial abnormalities including subependymal cysts and lenticulostriate vasculopathy (Soares de Souza et al., 2016). The cysts could form as the consequence of cell death, while lenticulostriate vasculopathy results from damage to the blood vessels in the deep brain structures, and ZIKV is known to infect and damage blood vessels and the blood brain barrier (Shao et al., 2016).

Studies have examined intracranial injection of postnatal mice with ZIKV (Huang et al., 2016) or the postnatal outcomes in mice infected with ZIKV during early- or mid-gestation (Miner et al., 2016; Shao et al., 2016), but no one has investigated ZIKV exposure to late embryonic tissue corresponding to the third-trimester. We found that none of the isolates that we had tested earlier in Chapter 3 were able to infect or replicate in the E19 tissue, but as we were performing these experiments a new isolate became available, which was the only isolate from 2016 commercially available. This isolate was from a patient infected in Honduras, and it was able to efficiently replicate in E19 tissue over the course of 8 days post infection (8 DPI). Intriguingly, it only seemed to infect cells located in the neocortex, and the vast majority of these cells were neurons. This would represent a large divergence

from the behavior of other isolates of ZIKV which preferentially infect neural stem cells (Tang et al., 2016).

The fact that the most recently isolated ZIKV sample that we have diverged in its behavior from the other isolates suggests that the virus is mutating. Our preliminary analysis of the genome of the Honduran isolate did not show any overt candidates for genomic changes unique to this isolate. Additionally, it remains unknown if the other isolates are unable to infect and replicate because they are unable to get into the neuronal cells, or if the internal cellular environment does not support their replication. At this point *ex utero* electroporation studies of the ssRNA for these isolates into E19 brains remains inconclusive. Since our experimental model bypasses viral transport from the mother to the fetus, it also does not take into account any increased difficulty that may be present in crossing from the mother to the fetus during the third trimester. Nonetheless it does suggest that ZIKV may be mutating, that certain strains possess the ability to infect neurons, and that we should be vigilant about ZIKV infection leading to neurological sequelae such as encephalitis, which other flaviviruses such as West Nile and Japanese Encephalitis Virus are well associated with (Pierson and Diamond, 2012).

The Implications for Ongoing Vaccine Development

There is a great effort underway to develop an effective vaccine for ZIKV (Dowd et al., 2016). There exist successful vaccines for other Flaviviruses such as Japanese Encephalitis Virus and Yellow Fever (Larocca et al., 2016), and even as recently as last year a DENV vaccine was finally proven effective through a Phase-III clinical trial (Hadinegoro et al., 2015). These all provide hope that a ZIKV vaccine

can quickly proceed through development and gain approval. It should be noted that there are many difficulties with successful vaccine design for flaviviruses, exemplified in the development of the DENV vaccine (Hadinegoro et al., 2015). Because of the many different circulating serotypes of DENV, an adequate vaccine has long remained elusive. The current vaccine is a live attenuated vaccine designed to generate antibodies against four different forms of DENV (Olivera-Botello et al., 2016). Nonetheless, the vaccine only prevents DENV infection in roughly 60% of the patients, and is poorly effective in children under 9 years old, which represent one of the most vulnerable patient populations for DENV (Hadinegoro et al., 2015). Therefore the vaccine is only approved for use in patients ages 9-45, and it is only approved in the Philippines, Mexico, and Brazil at the time of writing.

While these represent obstacles to vaccine development, the progress made in developing vaccines to ZIKV in mice (Larocca et al., 2016) and in *Rhesus macque* monkeys (Abbink et al., 2016; Dowd et al., 2016) has been remarkable. Interestingly this has also represented an opportunity to test the utility of a DNA-based vaccine, where a DNA plasmid encoding the antigen is injected as opposed to a live-attenuated virus or a virus protein subunit (Abbink et al., 2016; Dowd et al., 2016). Due to the rapid success of the vaccine trials in monkeys and mice there are now three Phase I clinical trials underway to examine the vaccine potential in humans (ClinicalTrials.gov identifiers: NCT02963909, NCT02952833, NCT02840487)

Both trials that examined vaccine efficacy in monkeys demonstrated that animals vaccinated against Brazilian or Puerto Rican isolates had protection when challenged with the other isolate (Dowd et al., 2016; Hadinegoro et al., 2015). A

study in mice using neutralizing antibodies generated against the E protein found one antibody that protected against five isolates across the African, Asian, and American lineages (Sapparapu et al., 2016). Nonetheless, they only examined one isolate in the American lineage, and the vaccine studies were challenged only with older isolates from Brazil and Puerto Rico. Our studies do suggest that ZIKV is mutating, and that recent isolates are behaving differently from others, but they do not provide any cause for alarm with regards to vaccine testing. Merely, it suggests that ZIKV may have the capacity to evolve as it spreads, developing multiple serotypes similar to DENV, and that vaccine trials should encompass many isolates across a broad temporal and geographical spectrum.

REFERENCES:

Abbink, P., Larocca, R.A., La Barrera, De, R.A., Bricault, C.A., Moseley, E.T., Boyd, M., Kirilova, M., Li, Z., Ng'ang'a, D., Nanayakkara, O., et al. (2016). Protective efficacy of multiple vaccine platforms against Zika virus challenge in rhesus monkeys. Science *353*, 1129–1132.

Alkuraya, F.S., Cai, X., Emery, C., Mochida, G.H., Al-Dosari, M.S., Felie, J.M., Hill, R.S., Barry, B.J., Partlow, J.N., Gascon, G.G., et al. (2011). Human Mutations in NDE1 Cause Extreme Microcephaly with Lissencephaly. The American Journal of Human Genetics *88*, 536–547.

Baffet, A.D., Hu, D.J., and Vallee, R.B. (2015). Cdk1 Activates Pre-mitotic Nuclear Envelope Dynein Recruitment and Apical Nuclear Migration in Neural Stem Cells. Developmental Cell *33*, 703–716.

Bakircioglu, M., Carvalho, O.P., Khurshid, M., Cox, J.J., Tuysuz, B., Barak, T., Yilmaz, S., Caglayan, O., Dincer, A., Nicholas, A.K., et al. (2011). The Essential Role of Centrosomal NDE1 in Human Cerebral Cortex Neurogenesis. The American Journal of Human Genetics *88*, 523–535.

Bolhy, S., Bouhlel, I., Dultz, E., Nayak, T., Zuccolo, M., Gatti, X., Vallee, R., Ellenberg, J., and Doye, V. (2011). A Nup133-dependent NPC-anchored network tethers centrosomes to the nuclear envelope in prophase. The Journal of Cell Biology *192*, 855–871.

Brasil, P., Pereira, J.P., Raja Gabaglia, C., Damasceno, L., Wakimoto, M., Ribeiro Nogueira, R.M., Carvalho de Sequeira, P., Machado Siqueira, A., Abreu de Carvalho, L.M., Cotrim da Cunha, D., et al. (2016). Zika Virus Infection in Pregnant Women in Rio de Janeiro - Preliminary Report. N. Engl. J. Med.

Brault, A.C., Huang, C.Y.-H., Langevin, S.A., Kinney, R.M., Bowen, R.A., Ramey, W.N., Panella, N.A., Holmes, E.C., Powers, A.M., and Miller, B.R. (2007). A single positively selected West Nile viral mutation confers increased virogenesis in American crows. Nat Genet *39*, 1162–1166.

Cannon, T.D., Thompson, P.M., van Erp, T.G.M., Toga, A.W., Poutanen, V.-P., Huttunen, M., Lonnqvist, J., Standerskjold-Nordenstam, C.-G., Narr, K.L., Khaledy, M., et al. (2002). Cortex mapping reveals regionally specific patterns of genetic and disease-specific gray-matter deficits in twins discordant for schizophrenia. Proc. Natl. Acad. Sci. U.S.a. *99*, 3228–3233.

Cao-Lormeau, V.-M., Roche, C., Teissier, A., Robin, E., Berry, A.-L., Mallet, H.-P., Sall, A.A., and Musso, D. (2014). Zika virus, French polynesia, South pacific, 2013. Emerging Infect. Dis. *20*, 1085–1086.

Carabalona, A., Hu, D.J.-K., and Vallee, R.B. (2016). KIF1A inhibition immortalizes

brain stem cells but blocks BDNF-mediated neuronal migration. Nat Neurosci *19*, 253–262.

Cheng, J., Türkel, N., Hemati, N., Fuller, M.T., Hunt, A.J., and Yamashita, Y.M. (2008). Centrosome misorientation reduces stem cell division during ageing. Nature *456*, 599–604.

Chin, G.M., and Herbst, R. (2006). Induction of apoptosis by monastrol, an inhibitor of the mitotic kinesin Eg5, is independent of the spindle checkpoint. Mol. Cancer Ther. *5*, 2580–2591.

DAWBER, T.R., MEADORS, G.F., and MOORE, F.E. (1951). Epidemiological approaches to heart disease: the Framingham Study. Am J Public Health Nations Health *41*, 279–281.

Dejnirattisai, W., Supasa, P., Wongwiwat, W., Rouvinski, A., Barba-Spaeth, G., Duangchinda, T., Sakuntabhai, A., Cao-Lormeau, V.-M., Malasit, P., Rey, F.A., et al. (2016). Dengue virus sero-cross-reactivity drives antibody-dependent enhancement of infection with zika virus. Nature Immunology *17*, 1102–1108.

Doobin, D.J., Kemal, S., Dantas, T.J., and Vallee, R.B. (2016). Severe NDE1-mediated microcephaly results from neural progenitor cell cycle arrests at multiple specific stages. Nature Communications *7*, 12551.

Dowd, K.A., Ko, S.-Y., Morabito, K.M., Yang, E.S., Pelc, R.S., DeMaso, C.R., Castilho, L.R., Abbink, P., Boyd, M., Nityanandam, R., et al. (2016). Rapid development of a DNA vaccine for Zika virus. Science aai9137.

Duffy, M.R., Chen, T.-H., Hancock, W.T., Powers, A.M., Kool, J.L., Lanciotti, R.S., Pretrick, M., Marfel, M., Holzbauer, S., Dubray, C., et al. (2009). Zika virus outbreak on Yap Island, Federated States of Micronesia. N. Engl. J. Med. *360*, 2536–2543.

Ezratty, E.J., Stokes, N., Chai, S., Shah, A.S., Williams, S.E., and Fuchs, E. (2011). A Role for the Primary Cilium in Notch Signaling and Epidermal Differentiation during Skin Development. Cell *145*, 1129–1141.

Feng, Y., and Walsh, C.A. (2004). Mitotic spindle regulation by Nde1 controls cerebral cortical size. Neuron *44*, 279–293.

Firat-Karalar, E.N., and Stearns, T. (2015). Probing mammalian centrosome structure using BioID proximity-dependent biotinylation. Methods Cell Biol. *129*, 153–170.

Fischer, B.A., and Carpenter, W.T. (2009). Will the Kraepelinian dichotomy survive DSM-V? Neuropsychopharmacology *34*, 2081–2087.

Garey, L.J., Ong, W.Y., Patel, T.S., Kanani, M., Davis, A., Mortimer, A.M., Barnes, T.R.,

and Hirsch, S.R. (1998). Reduced dendritic spine density on cerebral cortical pyramidal neurons in schizophrenia. J. Neurol. Neurosurg. Psychiatr. *65*, 446–453.

Glantz, L.A., and Lewis, D.A. (2000). Decreased dendritic spine density on prefrontal cortical pyramidal neurons in schizophrenia. Arch. Gen. Psychiatry *57*, 65–73.

Guo, J., Higginbotham, H., Li, J., Nichols, J., Hirt, J., Ghukasyan, V., and Anton, E.S. (2015). Developmental disruptions underlying brain abnormalities in ciliopathies. Nature Communications *6*, 7857.

Guven, A., Gunduz, A., Bozoglu, T.M., Yalcinkaya, C., and Tolun, A. (2012). Novel NDE1 homozygous mutation resulting in microhydranencephaly and not microlyssencephaly. Neurogenetics *13*, 189–194.

Hadinegoro, S.R., Arredondo-García, J.L., Capeding, M.R., Deseda, C., Chotpitayasunondh, T., Dietze, R., Muhammad Ismail, H.I.H., Reynales, H., Limkittikul, K., Rivera-Medina, D.M., et al. (2015). Efficacy and Long-Term Safety of a Dengue Vaccine in Regions of Endemic Disease. N. Engl. J. Med. *373*, 1195–1206.

Han, Y.-G., and Alvarez-Buylla, A. (2010). Role of primary cilia in brain development and cancer. Current Opinion in Neurobiology *20*, 58–67.

Higginbotham, H., Guo, J., Yokota, Y., Umberger, N.L., Su, C.-Y., Li, J., Verma, N., Hirt, J., Ghukasyan, V., Caspary, T., et al. (2013). Arl13b-regulated cilia activities are essential for polarized radial glial scaffold formation. Nat Neuro *16*, 1000–1007.

Hu, D.J.-K., Baffet, A.D., Nayak, T., Akhmanova, A., Doye, V., and Vallee, R.B. (2013). Dynein recruitment to nuclear pores activates apical nuclear migration and mitotic entry in brain progenitor cells. Cell *154*, 1300–1313.

Huang, W.-C., Abraham, R., Shim, B.-S., Choe, H., and Page, D.T. (2016). Zika virus infection during the period of maximal brain growth causes microcephaly and corticospinal neuron apoptosis in wild type mice. Scientific Reports *6*, 34793.

Huangfu, D., Liu, A., Rakeman, A.S., Murcia, N.S., Niswander, L., and Anderson, K.V. (2003). Hedgehog signalling in the mouse requires intraflagellar transport proteins. Nature *426*, 83–87.

Inaba, M., Venkei, Z.G., and Yamashita, Y.M. (2015). The polarity protein Baz forms a platform for the centrosome orientation during asymmetric stem cell division in the Drosophila male germline. eLife *4*, 659.

Insolera, R., Bazzi, H., Shao, W., Anderson, K.V., and Shi, S.-H. (2014). Cortical neurogenesis in the absence of centrioles. Nat Neurosci *17*, 1528–1535.

Izawa, I., Goto, H., Kasahara, K., and Inagaki, M. (2015). Current topics of functional links between primary cilia and cell cycle. Cilia *4*, 12.

Kim, S., Zaghloul, N.A., Bubenshchikova, E., Oh, E.C., Rankin, S., Katsanis, N., Obara, T., and Tsiokas, L. (2011). Nde1-mediated inhibition of ciliogenesis affects cell cycle re-entry. Nature Cell Biology *13*, 351–360.

Kuepper, R., van Os, J., Lieb, R., Wittchen, H.-U., Höfler, M., and Henquet, C. (2011). Continued cannabis use and risk of incidence and persistence of psychotic symptoms: 10 year follow-up cohort study. Bmj *342*, d738.

Larocca, R.A., Abbink, P., Peron, J.P.S., Zanotto, P.M. de A., Iampietro, M.J., Badamchi-Zadeh, A., Boyd, M., Ng'ang'a, D., Kirilova, M., Nityanandam, R., et al. (2016). Vaccine protection against Zika virus from Brazil. Nature *536*, 474–478.

Lessler, J., Chaisson, L.H., Kucirka, L.M., Bi, Q., Grantz, K., Salje, H., Carcelen, A.C., Ott, C.T., Sheffield, J.S., Ferguson, N.M., et al. (2016). Assessing the global threat from Zika virus. Science *353*, aaf8160.

Lewis, D.A., Curley, A.A., Glausier, J.R., and Volk, D.W. (2012). Cortical parvalbumin interneurons and cognitive dysfunction in schizophrenia. Trends in Neurosciences *35*, 57–67.

Li, A., Saito, M., Chuang, J.-Z., Tseng, Y.-Y., Dedesma, C., Tomizawa, K., Kaitsuka, T., and Sung, C.-H. (2011). Ciliary transition zone activation of phosphorylated Tctex-1 controls ciliary resorption, S-phase entry and fate of neural progenitors. Nat Neuro *13*, 402–411.

Long, M.T., and Fox, C.S. (2016). The Framingham Heart Study--67 years of discovery in metabolic disease. Nat Neuro *12*, 177–183.

Marín, O., and Müller, U. (2014). Lineage origins of GABAergic versus glutamatergic neurons in the neocortex. Current Opinion in Neurobiology *26*, 132–141.

Maskey, D., Marlin, M.C., Kim, S., Kim, S., Ong, E.-C., Li, G., and Tsiokas, L. (2015). Cell cycle-dependent ubiquitylation and destruction of NDE1 by CDK5-FBW7 regulates ciliary length. The EMBO Journal *34*, 2424–2440.

May, S.R., Ashique, A.M., Karlen, M., Wang, B., Shen, Y., Zarbalis, K., Reiter, J., Ericson, J., and Peterson, A.S. (2005). Loss of the retrograde motor for IFT disrupts localization of Smo to cilia and prevents the expression of both activator and repressor functions of Gli. Developmental Biology *287*, 378–389.

McGrath, J., Welham, J., Scott, J., Varghese, D., Degenhardt, L., Hayatbakhsh, M.R., Alati, R., Williams, G.M., Bor, W., and Najman, J.M. (2010). Association between cannabis use and psychosis-related outcomes using sibling pair analysis in a cohort of young adults. Arch. Gen. Psychiatry *67*, 440–447.

McKenney, R.J., Huynh, W., Tanenbaum, M.E., Bhabha, G., and Vale, R.D. (2014). Activation of cytoplasmic dynein motility by dynactin-cargo adapter complexes.

Science *345*, 337–341.

Meyer, E.J., Ikmi, A., and Gibson, M.C. (2011). Interkinetic nuclear migration is a broadly conserved feature of cell division in pseudostratified epithelia. Curr. Biol. *21*, 485–491.

Miner, J.J., Bin Cao, Govero, J., Smith, A.M., Fernandez, E., Cabrera, O.H., Garber, C., Noll, M., Klein, R.S., Noguchi, K.K., et al. (2016). Zika Virus Infection during Pregnancy in Mice Causes Placental Damage and Fetal Demise. Cell 1–14.

Miyoshi, G., and Fishell, G. (2012). Dynamic FoxG1 expression coordinates the integration of multipolar pyramidal neuron precursors into the cortical plate. Neuron *74*, 1045–1058.

Muraki, K., and Tanigaki, K. (2015). Neuronal migration abnormalities and its possible implications for schizophrenia. Front Neurosci *9*.

Murphy, B.R., and Whitehead, S.S. (2011). Immune response to dengue virus and prospects for a vaccine. Annu. Rev. Immunol. *29*, 587–619.

Musso, D., and Gubler, D.J. (2016). Zika Virus. Clinical Microbiology Reviews *29*, 487–524.

Norden, C., Young, S., Link, B.A., and Harris, W.A. (2009). Actomyosin Is the Main Driver of Interkinetic Nuclear Migration in the Retina. Cell *138*, 1195–1208.

Olivera-Botello, G., Coudeville, L., Fanouillere, K., Guy, B., Chambonneau, L., Noriega, F., Jackson, N., CYD-TDV Vaccine Trial Group (2016). Tetravalent Dengue Vaccine Reduces Symptomatic and Asymptomatic Dengue Virus Infections in Healthy Children and Adolescents Aged 2-16 Years in Asia and Latin America. J. Infect. Dis. *214*, 994–1000.

Pacheco, O., Beltrán, M., Nelson, C.A., Valencia, D., Tolosa, N., Farr, S.L., Padilla, A.V., Tong, V.T., Cuevas, E.L., Espinosa-Bode, A., et al. (2016). Zika Virus Disease in Colombia - Preliminary Report. N. Engl. J. Med.

Paciorkowski, A.R., Keppler-Noreuil, K., Robinson, L., Sullivan, C., Sajan, S., Christian, S.L., Bukshpun, P., Gabriel, S.B., Gleeson, J.G., Sherr, E.H., et al. (2013). Deletion 16p13.11 uncovers NDE1 mutations on the non-deleted homolog and extends the spectrum of severe microcephaly to include fetal brain disruption. Am. J. Med. Genet. A *161A*, 1523–1530.

Paridaen, J.T.M.L., Wilsch-Bräuninger, M., and Huttner, W.B. (2013). Asymmetric inheritance of centrosome-associated primary cilium membrane directs ciliogenesis after cell division. Cell *155*, 333–344.

Pedersen, L.B., and Rosenbaum, J.L. (2008). Chapter Two Intraflagellar Transport

(IFT) (Elsevier).

Pettersson, J.H.-O., Eldholm, V., Seligman, S.J., Lundkvist, Å., Falconar, A.K., Gaunt, M.W., Musso, D., Nougairède, A., Charrel, R., Gould, E.A., et al. (2016). How Did Zika Virus Emerge in the Pacific Islands and Latin America? MBio *7*, e01239–16.

Pierson, T.C., and Diamond, M.S. (2012). Degrees of maturity: the complex structure and biology of flaviviruses. Curr Opin Virol *2*, 168–175.

Pierson, T.C., and Graham, B.S. (2016). Zika Virus: Immunity and Vaccine Development. Cell *167*, 625–631.

Pilaz, L.-J., and Silver, D.L. (2014). Live imaging of mitosis in the developing mouse embryonic cortex. J Vis Exp.

Sapparapu, G., Fernandez, E., Kose, N., Cao, B., Fox, J.M., Bombardi, R.G., Zhao, H., Nelson, C.A., Bryan, A.L., Barnes, T., et al. (2016). Neutralizing human antibodies prevent Zika virus replication and fetal disease in mice. Nature.

Schenk, J., Wilsch-Bräuninger, M., Calegari, F., and Huttner, W.B. (2009). Myosin II is required for interkinetic nuclear migration of neural progenitors. Proc. Natl. Acad. Sci. U.S.a. *106*, 16487–16492.

Sekar, A., Bialas, A.R., de Rivera, H., Davis, A., Hammond, T.R., Kamitaki, N., Tooley, K., Presumey, J., Baum, M., Van Doren, V., et al. (2016). Schizophrenia risk from complex variation of complement component 4. Nature *530*, 177–183.

Shao, Q., Herrlinger, S., Yang, S.-L., Lai, F., Moore, J.M., Brindley, M.A., and Chen, J.-F. (2016). Zika virus infection disrupts neurovascular development and results in postnatal microcephaly with brain damage. Development.

Soares de Souza, A., Moraes Dias, C., Braga, F.D.C.B., Terzian, A.C.B., Estofolete, C.F., Oliani, A.H., Oliveira, G.H., Brandão de Mattos, C.C., de Mattos, L.C., Nogueira, M.L., et al. (2016). Fetal Infection by Zika Virus in the Third Trimester: Report of 2 Cases. Clin. Infect. Dis. ciw613.

Spear, P.C., and Erickson, C.A. (2012). Apical movement during interkinetic nuclear migration is a two-step process. Developmental Biology *370*, 33–41.

Strzyz, P.J., Lee, H.O., Sidhaye, J., Weber, I.P., Leung, L.C., and Norden, C. (2015). Interkinetic nuclear migration is centrosome independent and ensures apical cell division to maintain tissue integrity. Developmental Cell *32*, 203–219.

Tang, H., Hammack, C., Ogden, S.C., Wen, Z., Qian, X., Li, Y., Yao, B., Shin, J., Zhang, F., Lee, E.M., et al. (2016). Zika Virus Infects Human Cortical Neural Progenitors and Attenuates Their Growth. Cell Stem Cell.

Tong, C.K., Han, Y.-G., Shah, J.K., Obernier, K., Guinto, C.D., and Alvarez-Buylla, A. (2014). Primary cilia are required in a unique subpopulation of neural progenitors. Proc. Natl. Acad. Sci. U.S.a. *111*, 12438–12443.

Troy, C.M., and Jean, Y.Y. (2015). Caspases: therapeutic targets in neurologic disease. Neurotherapeutics *12*, 42–48.

Tsai, J.W., Chen, Y., Kriegstein, A.R., and Vallee, R.B. (2005). LIS1 RNA interference blocks neural stem cell division, morphogenesis, and motility at multiple stages. The Journal of Cell Biology *170*, 935–945.

Tsai, J.-W., Bremner, K.H., and Vallee, R.B. (2007). Dual subcellular roles for LIS1 and dynein in radial neuronal migration in live brain tissue. Nat Neurosci *10*, 970–979.

Tsai, J.-W., Lian, W.-N., Kemal, S., Kriegstein, A.R., and Vallee, R.B. (2010). Kinesin 3 and cytoplasmic dynein mediate interkinetic nuclear migration in neural stem cells. Nat Neuro *13*, 1463–1471.

Tsetsarkin, K.A., Vanlandingham, D.L., McGee, C.E., and Higgs, S. (2007). A single mutation in chikungunya virus affects vector specificity and epidemic potential. PLoS Pathog. *3*, e201.

Unsain, N., and Barker, P.A. (2015). New Views on the Misconstrued: Executioner Caspases and Their Diverse Non-apoptotic Roles. Neuron *88*, 461–474.

Urnavicius, L., Zhang, K., Diamant, A.G., Motz, C., Schlager, M.A., Yu, M., Patel, N.A., Robinson, C.V., and Carter, A.P. (2015). The structure of the dynactin complex and its interaction with dynein. Science *347*, 1441–1446.

Venkei, Z.G., and Yamashita, Y.M. (2015). The centrosome orientation checkpoint is germline stem cell specific and operates prior to the spindle assembly checkpoint in Drosophila testis. Development *142*, 62–69.